COMPARING DIFFERENT SCANNING TECHNIQUES FOR THE DESIGN AND FABRICATION OF MAXILLOFACIAL PROSTHESES

by

Gustav Macklin Barnard

Dissertation submitted in fulfilment of the requirements for the degree Magister Technologiae: Design, Department of Design and Studio Art, Faculty of Humanities, Central University of Technology, Free State, Bloemfontein

Supervisor: Dr JG van der Walt (DTech)

Co-supervisor: Mr O Ojo (MTech)

November 2021

Declaration

DECLARATION WITH REGARD TO INDEPENDENT WORK

I, Gustav Macklin Barnard, identity number _____ and student number _____, do hereby declare that this research project submitted to Central University of Technology, Free State (CUT) for the MAGISTER TECHNOLOGIAE OF DESIGN degree, is my own independent work; and complies with the code of academic integrity, as well as other relevant policies, procedures, rules and regulations of Central University of Technology, Free State; and has not been submitted previously to any institution by myself or any other person in fulfilment of the requirements for the attainment of any qualification.

SIGNATURE OF STUDENT  DATE November 2021

Acknowledgements

I wish to express my sincere gratitude to Dr Kobus van der Walt, my research supervisor, for his patient guidance, enthusiastic encouragement, and valuable critiques of this research work. His willingness to give his time so generously is greatly appreciated. My thanks to Mr Olutunmise Ojo for providing much-needed support and guidance. I also want to express my great appreciation to Prof Annabel Fossey for her valuable and constructive suggestions during the planning and development of this research work. Sincere thanks to the Bloemfontein Hospital's Oncology Department staff, Stellenbosch University's Central Analytical Facilities (CAF), and The South African Nuclear Energy Corporation (*NECSA*) for providing access to instrumentation needed for conducting this research work. I would also like to thank Prof Gerrit Jordaan for his support and encouragement throughout this study. Finally, I would like to acknowledge the financial support provided by the Department of Science and Innovation funded Collaborative Programme in Additive Manufacturing, Central University of Technology, Free State, and the Centre for Rapid Prototyping and Manufacturing (CRPM).

Table of Contents

Declaration i

Acknowledgements ii

Table of Contents iii

List of Tables ix

List of Figures x

Abbreviations xv

Abstract xvii

Chapter 1 1

Introduction to the Study 1

1.1 Introduction 1

1.2 Problem statement 2

1.3 Aim and objectives of the study 2

1.4 Methodology and research design 2

1.5 Layout of dissertation 4

Chapter 2 5

Literature Review 5

2.1 Introduction 5

2.2 Historical developments of maxillofacial prosthetics 6

2.2.1 Traditional methods of maxillofacial prosthetic fabrication 6

2.3 Problems associated with traditional methods for fabricating facial prostheses 9

2.4 Advanced methods in maxillofacial prosthesis fabrication 10

2.4.1 Medical imaging 10

2.4.2 Computerized tomography 11

2.4.3 Digital Imaging and Communication in Medicine 12

2.4.4 Quality of a CT scan 13

2.4.5 Test models developed for determining the accuracy of CT scanning 15

2.5 Hand-held scanners 17

2.5.1 The clinical use of surface scanners first 18

2.5.2 Photogrammetry 20

2.6 Additive manufacturing 21

2.6.1 Classification of additive manufacturing processes 21

2.6.2 Laser sintering 22

2.6.3 Testing the accuracy of additive manufacturing 23

2.7 Fabricating a maxillofacial prosthesis using advanced manufacturing methods 28

2.7.1 Digital modelling of maxillofacial prosthesis 29

2.7.2 Additive manufacturing of maxillofacial prosthesis 29

2.7.3 Discussion on problems associated with advanced methods of prosthesis fabrication 31

Chapter 3 32

Methodology 32

3.1 Introduction 32

3.2 Creating a benchmark test model 32

3.2.1 Establishing a design criterion 32

3.2.2 Design of individual test geometries 34

3.2.3 Design of the First Test Model 40

3.3 Fabrication and evaluation of the First Test Model 41

3.4 Design and fabrication of a Second Test Model 42

3.4.1 Design of a Second Test Model 44

3.4.2 Fabrication of a Second Test Model 46

3.5 Hand-held scanning of the Second Test Model 46

3.5.1 Artec® Spider® hand-held scanner 47

3.5.2 Artec® Studio® software application 48

3.5.3 Conducting a hand-held scan of the Second Test Model 49

3.5.4 Processing of scan data using Artec® Studio® 49

3.6 CT scanning of the Second Test Model 56

3.6.1 Toshiba® Aquilion LB® CT scanner 56

3.6.2 Conducting the CT scanning procedure 57

3.6.3 Processing of CT data into 3D models 58

3.7 Micro-CT scanning of the Benchmark Test Model 63

3.7.1 Mediso® NanoScan® micro-CT scanner 63

3.7.2 Micro-CT 3D Model 64

Chapter 4 66

Results and Discussion 66

4.1 Introduction 66

4.2 Evaluation of the 3D model from hand-held scanning 66

4.3 Evaluation of 3D models produced by CT data translation 67

4.4 Results of comparing digital 3D models 72

4.4.1 MyVGL® software 72

4.4.2 Comparing CAD design and micro-CT model 72

4.4.3 Comparison between Artec® Spider® model and micro-CT model 74

4.4.4 Comparison between 3D Doctor® and micro-CT 75

4.4.5 Comparison between Invesalius® and micro-CT 77

4.4.6 Comparison between Materialise® Mimics® and micro-CT 78

Chapter 5 80

Conclusions and Future Work 80

5.1 Conclusion 80

5.2 Future Work 82

References 84

Annexure A 94

List of Tables

Table 2.1 Classification of AM processes. 21

Table 2.2 Characteristics of Moylan's test model design. 27

Table 3.1 Design criterion 33

Table 3.2 Description of criterion changes. 43

Table 3.3 Suggested additions to the design criterion. 43

Table 3.4 Specifications of the Artec® Spider® scanning device 48

Table 3.5 Specifications of the Artec® Studio® software application 48

Table 3.6 Specifications of the Toshiba® Aquilion® CT scanner 57

List of Figures

Figure 1.1 Layout of dissertation. 4

Figure 2.1 Workflow used in traditional maxillofacial prosthetic fabrication. 6

Figure 2.2 Taking an impression using polyvinyl siloxane. 7

Figure 2.3 Sculpting of an ear prosthesis out of wax. 8

Figure 2.4 Plaster mould for casting the prosthesis. 8

Figure 2.5 Final prosthesis with pigments added. 9

Figure 2.6 Diagram of a typical CT scanning device. 12

Figure 2.7 Hounsfield scale used to determine density in DICOM images. 12

Figure 2.8 Example of a DICOM image slice displaying various scanning information. 13

Figure 2.9 The TOR CDR phantom®. 15

Figure 2.10 CT scanning test model. 16

Figure 2.11 The ACR phantom. 16

Figure 2.12 Diagram illustrating the hand-held scanning process. 17

Figure 2.13 In photogrammetry multiple images are taken from various angles. 20

Figure 2.14 Hierarchy of AM according to material characteristics. 22

Figure 2.15 Principal diagram of LS AM process. 23

Figure 2.16 Test model by Kruth for determining material increase during AM. 23

Figure 2.17 Test model by Childs for testing various AM processes. 24

Figure 2.18 Test Model by Mahesh, Wong, Fuh, and Loh for evaluating AM processes. 25

Figure 2.19 Test Model by Sercombe and Hopkins for shrinkage and accuracy during laser sintering of aluminium. 25

Figure 2.20 Circular diamond test model by Cooke and Soons. 26

Figure 2.21 Design of Moylan's test model. 27

Figure 2.22 Workflow of advanced additive manufacturing a prosthesis. 28

Figure 3.1 Elevation Test Geometry design. 35

Figure 3. 2 Depth Test Geometry design. 36

Figure 3.3 Pattern Test Geometry design. 37

Figure 3.4 Wall Thickness Test Geometry design. 38

Figure 3.5 Spacing Test Geometry design. 39

Figure 3.6 Pattern Test Geometry design. 40

Figure 3.7 CAD images of individual test geometry designs and combined First Test Model. 41

Figure 3.8 EOSINT® P385 LS machine. 41

Figure 3.9 First Test Model produced through laser sintering. 42

Figure 3.10 Final design of the Second Test Model 45

Figure 3.11 Design modifications applied to the Second Test Model. 45

Figure 3.12 Second Test Model produced through laser sintering. 46

Figure 3.13 The Artec® Spider® scanning device. 47

Figure 3.14 Graphic representation of the hand-held scanning process 49

Figure 3.15 Fine serial registration 50

Figure 3.16 Erasing of unnecessary captured scan data. 51

Figure 3.17 Choosing of common points. 52

Figure 3.18 Scans aligned together. 52

Figure 3.19 Scans moved to a single coordinate system 53

Figure 3.20 Erasing of scan noise. 54

Figure 3.21 Various scans joined together. 55

Figure 3.22 Simplified digital 3D model. 55

Figure 3.23 Toshiba® Aquilion LB® CT scanner. 56

Figure 3.24 The Second Test Model positioned for CT scanning..... 57

Figure 3.25 Sample of the DICOM images produced through CT scanning. 58

Figure 3.26 DICOM images translated to a 3D model using Invesalius® 60

Figure 3.27 DICOM images translated to a 3D model using 3D Doctor® 61

Figure 3.28 DICOM images translated to a 3D model using Materialise® Mimics®. 63

Figure 3.29 The Mediso® NanoScan® micro-CT scanner. 64

Figure 3.30 Golden Standard 3D model produced through micro-CT scanning..... 65

Figure 4.1 The 3D model generated from the Artec® Spider® hand-held scanner..... 66

Figure 4.2 CT results of Anchor Point Test Geometry (A, B, C), Spherical Test Geometry (1, 2, 3), and Anatomical Test Geometries features (4, 5, 6). 68

Figure 4.3 Result of Depth Test Geometry features..... 69

Figure 4.4 Pattern Test Geometry features translated from DICOM data 70

Figure 4.5 Angulation Test Geometry features translated from DICOM data 70

Figure 4.6 Elevation and Anatomical Test Geometries translated from DICOM data..... 71

Figure 4.7 Thickness and Spacing Test Geometries translated from DICOM data. 71

Figure 4.8 Sizing difference between CAD of Second Test Model and micro-CT. 73

Figure 4.9 Deviation analysis map between CAD and micro-CT of Second Test Model. 73

Figure 4.10 Size difference between Artec® Spider® and micro-CT. 74

Figure 4.11 Deviation analysis map: Artec® Spider® and micro-CT. 75

Figure 4.12 Sizing difference between 3D Doctor® and micro-CT 76

Figure 4.13 Deviation analysis map: 3D Doctor® and micro-CT. 76

Figure 4.14 Sizing difference between Invesalius® and micro-CT. 77

Figure 4.15 Deviation analysis map: Invesalius® and micro-CT. 78

Figure 4.16 Sizing difference between Mimics® and micro-CT 79

Figure 4.17 Deviation analysis map: Materialise® Mimics® and micro-CT. 79

Abbreviations

2D	Two Dimensional
3D	Three Dimensional
AM	Additive Manufacturing
CAD	Computer-aided design.
CRPM	Centre for Rapid Prototyping and Manufacturing.
CT	Computerized Tomography
CUT	Central University of Technology, Free State.
DICOM	Digital Imaging and Communications in Medicine.
G-CODE	Geometry Code
NECSA	The South African Nuclear Energy Corporation
LS	Laser Sintering
STL	Standard Triangulation Language

Copyright and trademarks

Copyright and trademarks for the different software programs are indicated in this dissertation according to the copyright and trademark specifications of the respective developers.

Invesalius™	Developed by **CTI** (Renato Archer Information Technology Center)
3D Doctor®	Developed by Able Software Corporation®
Zbrush®	Developed by Pixologic®
Mimics®	Developed by Materialise®

Artec Studio®	Developed by Artec3D®
Solidworks®	Developed by Dassault Systèmes®
MyVGL®	Developed by Volume Graphics®

Abstract

Facial prosthetics can play a significant role in relieving the psychological impact of patients who have lost facial features due to various causes. Traditional manual techniques of fabricating these prostheses are now largely replaced with modern computer aided design/computer aided manufacturing techniques that utilizes computerized tomography (CT) scanning for determining facial features. The prosthesis is designed from the CT data and molds produced through additive manufacturing (AM) for casting the prosthesis in silicone. Despite CT scanning presenting considerable advantages in acquiring reliable dimensional form and sizes of affected areas, it is not without complications. Key drawbacks are the high costs involved in scanning patients and the availability of these machines, which excludes many patients requiring facial prosthetics from benefitting from this technology. This study aimed to investigate if a three-dimensional (3D) hand-held scanner used in healthcare and engineering industries (Artec® Spider®) can be used to generate facial digital data suitable for the fabrication of maxillofacial prostheses. A test model was designed to highlight the strong and weak points of both CT and hand-held scanners and the model was scanned with both. The 3D models generated from the hand-held and CT scanner were compared to the 3D model of the test model generated by a micro-CT scanner and compared to determine accuracy. The study showed that the hand-held scanner produced scans comparable in accuracy to CT scanner but at a much lower cost. This will enable a significant number of patients requiring maxillofacial prosthetic care to be helped.

Keywords: Maxillofacial prosthetics, Computerized tomography, Hand-held scanning devices, Computer-Aided Design, Additive manufacturing, Micro-CT scanning, Laser sintering

Chapter 1

Introduction to the Study

1.1 Introduction

The loss or absence of facial features can be devastating to the social wellbeing of a patient. This may result from several causes such as trauma, disease, or congenital disorders. Regardless of the causes, the psychological implications on the sufferer could be as debilitating as the physical, leading to lower self-esteem and a diminished quality of life. A maxillofacial prosthesis can provide some cosmetic and psychological relief to these patients (Bocchialini et al., 2018; Keys et al., 2021).

The traditional process of fabricating a facial prosthesis such as an ear, involved taking a negative impression of the opposite ear using an impression material such as water-based alginate. The impression was then used to cast a positive of the ear in plaster and this was then used as example to sculpt the missing ear in wax. The wax model was next invested in plaster, the wax was melted out, and bio-compatible silicone was cast into the plaster mould to create the prosthesis. This was a time-consuming process and required significant skill to sculpt the prosthesis in wax.

In recent times, emerging computer aided design/computer aided manufacturing (CAD/CAM) technologies have begun to establish a presence in maxillofacial prosthetic fabrication. This is made possible through combinations of computerized tomography (CT), CAD and various additive manufacturing (AM) processes (Dincă, Banu, and Vişan, 2017). In the case of a missing ear, the healthy opposite ear can easily be mirrored about the mid-plane of the patient's head in the virtual environment from CT scan data. A negative mold can then be designed and printed using various AM technologies to cast of a silicone prosthesis. CT imaging, most commonly used to determine facial geometry, presents the advantage of non-contact with the patient. Therefore, the patient experiences less trauma, and the geometry is determined accurately without the risks and problems associated with impression material.

1.2 Problem statement

Despite CAD/CAM techniques having considerable advantages in producing maxillofacial prostheses, it is not without drawbacks. Key concerns are the high costs involved in having a CT scan taken to acquire the geometry of the affected area and access to these machines. They are only available in large hospitals necessitating patients in rural areas to travel long distances for a scan. This is especially the case in South Africa, where a large proportion of the population is dependent on the government for health care assistance (Mduzana, Tiwari, Lieketseng and Chikte, 2020; Tetteh, Bibb and Martin, 2017). A significant number of patients requiring maxillofacial prostheses are therefore excluded from benefitting from this technology.

1.3 Aim and objectives of the study

The aim of this study was to investigate if a 3D hand-held scanner can generate sufficiently accurate digital data to make it suitable for the fabrication of maxillofacial prostheses. The use of such a portable 3D scanner should generate digital facial data that is more cost-effective than CT scanning. By contributing to the lower cost for the generation of such digital data, it can potentially provide access to a significant number of patients who require maxillofacial prosthetic care.

The following objectives were set to achieve the aim of the study:

- Undertake a comprehensive review of literature to determine what research has been performed in this field of study.
- Design and fabricate a Test Model that will be used to compare the accuracy of the digital data generated by a 3D hand-held scanner with the digital data generated by a CT scanner.
- Scan the Test Model with the 3D hand-held scanner and CT scanner and compare it to a scan of the same Test Model taken with a micro-CT scanner to determine accuracy and suitability for maxillofacial prosthesis fabrication.

1.4 Methodology and research design

The study utilized a practise led research approach that incorporated various interdisciplinary fields including engineering, medicine and art. The Test Model designed to compare the available hand-held scanner (Artec® Spider®) and CT scanner was developed using various software and hardware

provided by the various departments and institutions associated with Central University of Technology, Free State (CUT). The study also formed part of a larger research initiative undertaken by CUT's Centre for Rapid Prototyping and Manufacturing (CRPM) and Product Development Technology Station (PDTS) to identify prosthetic assistance measures that could be offered at a lower cost.

The following research approach was followed in the study:

- A literature study was performed to determine traditional approaches to maxillofacial prosthetic fabrication and how modern technologies are utilized to improve this. Secondly, existing test models to assess the accuracy of AM processes and CT scanning techniques were investigated.

- A set of guidelines was established, and a criterion was formed that guided the development of the Test Model. After the Test Model was fabricated, an initial evaluation led to a Second Test Model with additional test features to extend the scope for comparing accuracy between the scanning modalities.

- The fabricated Second Test Model was subjected to the Artec® Spider® hand-held scanner, which produced geometric scan data. Using the Artec® Studio® software application, the scan data was processed into a digital 3D model.

- The Second Test Model was then subjected to a CT scanning process that produced Digital Imaging and Communications in Medicine (DICOM) scan data. This data was uploaded to three different DICOM image translation software applications from where a 3D model was generated from each.

- The Second Test Model was next subjected to a micro-CT scanning procedure. The digital 3D model produced from this process represented the most optimal and accurate digital representation of the Second Test Model available. This "Golden Standard" 3D model acted as the basis for comparing the digital 3D models produced from the Artec® Spider® scanner and 3D models translated from the CT scans.

1.5 Layout of dissertation

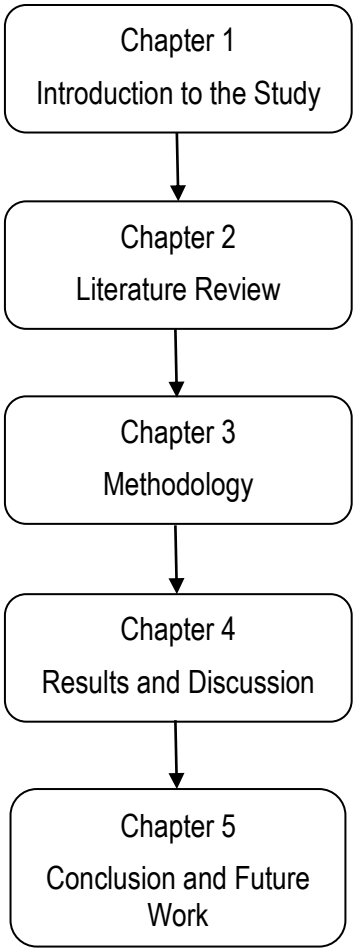

Figure 1.1 Layout of dissertation.

Chapter 2

Literature Review

2.1 Introduction

The earliest evidence of prosthetic development can be traced back to ancient China, India, and Egypt. It is here where raw materials were crafted into the first reported prosthetics using rudimentary experimental techniques. In ancient China, the first artificial limbs were constructed from combinations of wooden planks and horse hooves to aid lower limb amputees. In ancient India, the nose carried a sense of societal trust, and in some cases, it may have been severed as a form of corporal punishment. An early physician named Sushruta developed one of the first known surgical rhinoplasty techniques known as the "Indian technique". In Egypt, prosthetics carried a more profound spiritual significance, with various prosthetics produced to replace missing facial features. These were deemed as necessities for a complete rebirth in the afterlife. Although these three cultures' approaches were unique in their expressions, the need to address the debilitating effects of disease and trauma through prosthetic aid was a sentiment shared by all. Although the general population today is more well informed on various medical conditions and treatments, the psychological complications coupled with injuries sustained to one's appearance can still create hesitation and ultimately ostracization from society (Alqutaibi, 2015; Li *et al.,* 2013; Champaneria, Workman and Gupta, 2016).

The need for facial prosthetics can arise as a consequence of various factors. Some can be attributed to trauma, removing tumours around the facial area, or congenital disorders. Humanity's appetite for warfare has also contributed considerably to the demand for prosthetics, with consequences extending beyond the battlefield and influencing lives on emotional and physical levels. The great Greek physician Hippocrates alluded to this, saying that: "War is the only proper school for a surgeon." Due to the severity of many cases and the fact that prosthetic care was still in its infancy, the task of prosthetic improvisation fell mostly on local physicians and field doctors. Even though these early methods and techniques were crude compared to today and, in many cases, the prosthetics themselves impractical for everyday use, they created a framework for understanding the intricacies demanded from such a specialized discipline (Ott, Serlin and Mihm, 2002).

The face carries a profound psychological significance as a tool for communicating emotions and needs, helping us shape our sense of identity. Restoring an affected person's appearance to a more

normalized and acceptable level may soften traumatic psychological aftermaths and help ease reintegration into society (Jack and Schyns, 2015).

2.2 Historical developments of maxillofacial prosthetics

Although there are many prior instances of historic contributions towards prosthetic and facial prosthetic fabrication, the literature layout in this study aims to illustrate contributions made from the early 20th century to currently used technologies.

2.2.1 Traditional methods of maxillofacial prosthetic fabrication

Traditional facial prosthesis fabrication methods fall between art and orthodontic fields to create prosthetics that strive to provide some form of physical and psychological relief while remaining as inconspicuous as possible. The creation process entails several steps that first acquire a geometric recording of the area where the prosthesis would be attached. Afterwards, a sculpting method is employed to manipulate and shape wax material into what resembles the missing facial features. To allow for the reproduction of the sculpted model, a mould is made, whereafter pigments approximating the patient's skin tone, are added to silicone-based material and cast to produce the prosthesis (Figure 2.1).

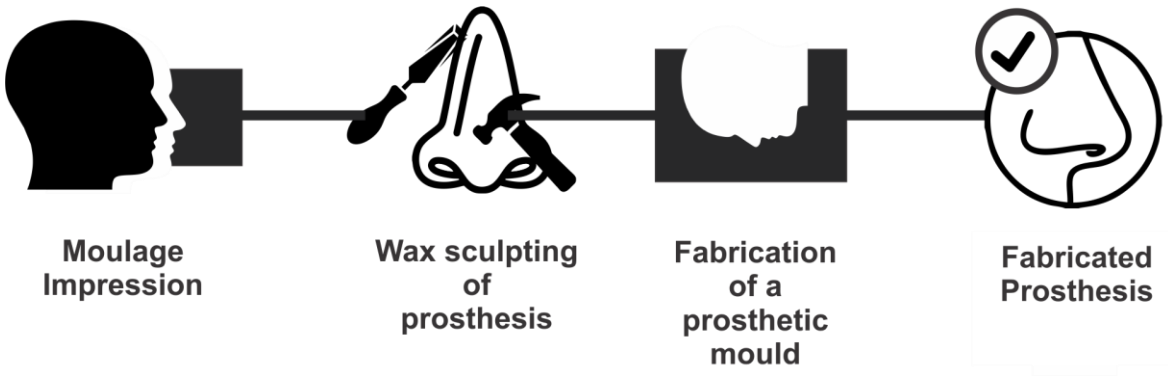

Figure 2.1 Workflow used in traditional maxillofacial prosthetic fabrication.

Facial moulage

Creating a facial prosthesis that conforms to a patient's unique profile typically requires an impression of the affected areas to be made first. The materials used for capturing such details usually range from polyvinyl siloxane and polyether to impression plasters, hydrocolloids, and elastomeric materials. In applying these materials, specialized syringes are often used to extrude the material into cavities or around protrusions. Often, impression trays and tong depressors are later added to help keep the material in the correct position while still setting. In some cases, rigid material such as dental stone plaster is layered on top to help retain form. Typically, the impression-making process varies between 3-15 minutes, depending on factors like moisture, heat, the presence of bodily fluids, or material properties (Alsiyabi and Minsley, 2006; Malard *et al*., 2015; Taicher *et al*, 1983) (Figure 2.2).

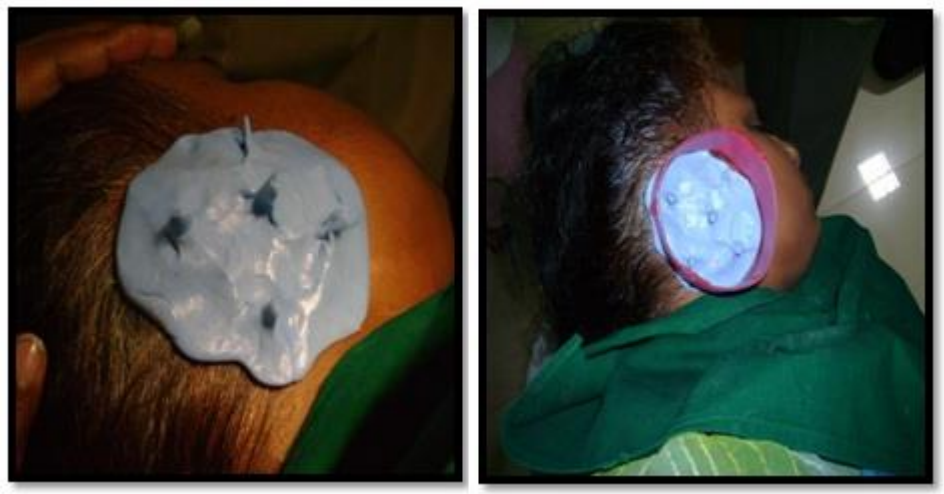

Figure 2.2 Taking an impression using polyvinyl siloxane. (Source: Ravuri *et al*., 2014)

Wax pattern fabrication

After removing, the settled impression material, it is boxed and filled with dental stone plaster to produce a positive impression containing the affected area's landmarks. Wax is then added on top of the positive plaster impression, where it is sculpted and carved using delicate tools to the correct size and proportion needed (Figure 2.3). The wax model is usually fitted several times on the actual

patient from where modifications could be made to ensure a proper fit. In dealing with bilateral facial features such as the ears, the donor method could be applied where an impression is made from a person with similar geometric sizing to the area required. This may lessen the required amount of sculpting but may still need to be modified to ensure proper fitment to the recipient (Demir *et al*., 2019; Veerareddy, Nair and Reddy, 2018).

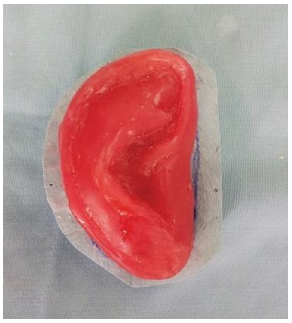

Figure 2.3 Sculpting of an ear prosthesis out of wax. (Source: Demir *et al*., 2019)

Fabrication of prosthetic mould

After the wax model has been sculpted, it is sealed onto the dental stone impression, with all visible separation edges lightly feathered. Then a negative/inverted mould is made by casting dental stone plaster over the wax carving. Location marks are added during this stage to ensure proper realignment of mould parts afterwards. In some cases, due to various geometric intricacies such as overhangs and undercuts, the mould may be split into several parts. After the mould material has been set, the wax is removed from the model by applying heat, leaving a cavity representing the sculpted wax prosthesis (Padmanabhan, Mohamed and Parameswari, 2012) (Figure 2.4).

Figure 2.4 Plaster mould for casting the prosthesis. (Source: Mohammed *et al*., 2018)

Fabrication of a final prosthesis

In the last step, a colourless silicone and catalyst material are weighed out and mixed on a glass plate to minimize bubbles that lead to porosity in the cast model. Small amounts of pigments are added to the mix and continuously compared to the patient to obtain an appropriate skin tone. The mould cavity is then coated with a thin layer of silicone, whereafter the rest of the material is poured into the cavity and clamped. It is placed in a dry heat oven for curing at a recommended time and temperature indicated by the manufacturer. After polymerization, the mould can be removed from the oven and allowed to cool at room temperature. The casting is removed from the mould and trimmed to produce the final prosthesis (Prasad, Swaminathan and Prasad, 2016) (Figure 2.5).

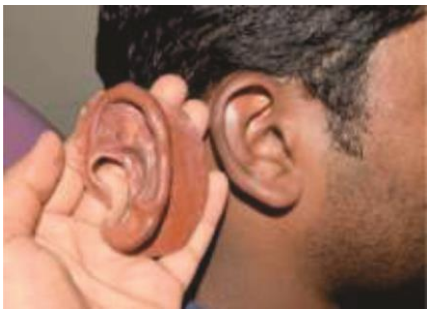

Figure 2.5 Final prosthesis with pigments added. (Source: Prasad, Swaminathan and Prasad, 2016)

2.3 Problems associated with traditional methods for fabricating facial prostheses

Traditional techniques for fabricating facial prosthetics require significant skill from the technologist to first sculpt the prosthesis in wax, which can turn into a time-consuming process. Taking an impression to produce a nose prosthesis is a risky undertaking since the impression material may enter the patient's airways, leading to suffocation. Many patients experience taking an impression of the facial area as traumatic, and some may furthermore experience an allergic reaction to the impression material. It is, therefore, vital to select the suitable impression material for the specific application. Facial silicone prosthetics have a limited lifespan and need to be replaced regularly. Therefore, a new impression would need to be taken of the patient each time due to morphological changes that facial features undergo over time. The weight of the impression material further

deforms the patient's soft facial tissue during the impression-taking procedure. This often results in a less than ideal fit of the final silicone prosthesis.

2.4 Advanced methods in maxillofacial prosthesis fabrication

The start of the twenty-first century has delivered many new developments and standardisations across various medical fields. Constant improvement, implementation, and expansion of treatments have significantly impacted on extending patients' life expectancy. The birth and evolution of diagnostic imaging tools such as the X-ray to more recent technologies as MRI and CT scans have been instrumental in many discoveries while providing more detailed and reliable diagnoses. The image data produced through these medical diagnostic tools, combined with the growing possibilities that AM can offer, has resulted in many promising firsts for patient-specific implants and prosthetic care (Srivatsan and Sudarshan, 2015).

What makes AM such an appealing process for creating prosthetics is the reduced manufacturing time, higher accuracy, and the ability to create intricate features repetitively. The ever-developing biocompatible AM material industry reinforces its implementation, making it possible to fabricate end-use parts directly. The ever-increasing capabilities at lowering purchase costs have resulted in AM becoming more accessible to the general public. This has produced many successful "do-it-yourself" initiatives and collaborations in prosthetic design (Hofmann *et al*., 2016; Sing *et al*., 2016).

In addition to this, numerous new software applications have been developed to strengthen collaborations between AM and medical practices. Some of these include software used for converting raw medical scan data into digital models, which could be digitally modified and fabricated into tangible objects.

2.4.1 Medical imaging

The primary objective of medical imaging is to produce a visual representation of the human body's inner workings in a non-intrusive, low-risk manner. Physicians can use this to create a diagnosis without the threat of worsening a condition and help plan workflows for medical procedures. Medical imaging comprises a wide variety of imaging modalities, namely X-ray, CT, MRI, and ultrasound. Although these technologies have distinct functions and branches of applications, they collectively contribute to a fuller visual understanding of human anatomy (Schramek *et al.,* 2013).

First identified in 1895 by a German professor, Wilhelm Roentgen, the X-ray would become the early catalyst for demonstrating the potential benefits medical imaging could contribute to public health care. It provided an increase in the current body of medical knowledge and the development of cancer treatments as radiation therapy (Krupinski, 2000).

Similarly, significant to the discovery of the X-ray, CT would represent a new generation of medical scanning technology, helping to display even higher detailed images revealing many new anatomical anomalies. Its capabilities extended beyond observing and determining the extent of bone fractures to include visual distinctions between hard and soft tissues. This enabled doctors to monitor and track conditions to a higher degree and perform better diagnoses at a lower risk of radiation exposure to patients (Ter-Pogossian, 1977).

By the late 70s, medical imaging would make another technological stride. Based on the discovery and research on nuclear magnetic resonance (NMR) phenomenon by Felix Bloch and Edward Purcell in 1946, Magnetic resonance imaging (MRI) was developed. In 1971 an American physician Raymond Damadian theorized that NMR could be useful in detecting internal tumours in their early stages. By 1977, Damadian and a group of researchers built a prototype device nicknamed the “Indomitable” and were able to make full-body scans of patients. The most significant difference between CT and MRI scanning is the underlying principle in which each function. Computerized tomography scanning exposes patients to ionizing radiation, whereas MRI uses magnetic fields and computer-generated radio waves to obtain images. Today MRI is commonly used for diagnosing tears in ligaments to tumours. The technology has also been advantageous for examining brain and spinal cord injuries (Hayden and Nacher, 2016).

2.4.2 Computerized tomography

During a standard CT scanning procedure, a narrow X-ray beam is projected through a body. In a series of short pauses, the X-ray source rotates around the body from where more X-rays are projected from various angles. After passing through the object, the X-rays are detected by a series of sensors located directly across from the projection source (Figure 2.6). The generated data is afterwards processed with the help of various computing algorithms into a series of cross-sectional 2D images known as Digital Imaging and Communications in Medicine (DICOM) image slices. The scanned object's structural density is displayed in each DICOM image through a range of greyscale

tonal values. These are based on the Hounsfield Unit scale value, which uses known densities of water and air to assign darker or lighter values to an object or area in each image slice (Figure 2.7).

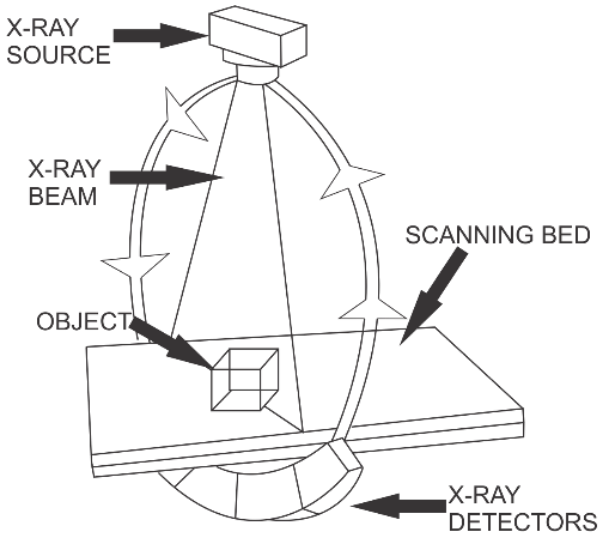

Figure 2.6 Diagram of a typical CT scanning device.

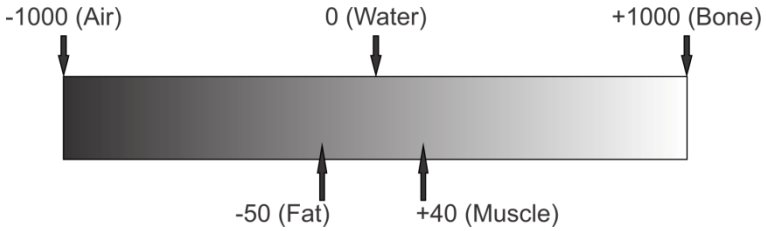

Figure 2.7 Hounsfield scale used to determine density in DICOM images.

2.4.3 Digital Imaging and Communication in Medicine

Digital Imaging and Communications in Medicine (DICOM) standard was first created by the American College of Radiology and the National Electrical Manufacturers Association in 1985. It was created to exchange, store, and view medical images data more efficiently regardless of which medical scanning modality it originated from. By 1993 it had revolutionized medical imaging by replacing traditional X-ray film and gaining recognition by the International Organization of Standardization as the new global medical standard for managing various medical scanning information.

DICOM creates a communication protocol using TCP/IP (internet protocol suite) with multiple systems. Simultaneously, its file format allows for viewing data on any monitor that interprets the DICOM format. In some circumstances, TCP optimization can be applied, which reduces network time by dividing the bandwidth connection between a subscriber's network and an Internet network, leading to better network efficiency, improved transfer speeds, and lower retransmission times. This optimization can be applied in two ways, referred to simply as the "one-box" or "two-box" approach. In the one-box approach, the optimization solution is deployed between two TCP endpoint users. In contrast, the two-box solution is deployed at two endpoints and is managed by the service provider (Golubev, Bogatencov and Secrieru, 2018).

In addition, the DICOM format also stores additional information such as the patient's name, ID number, sex, and date of the scanning procedure. It typically also stores data on specific hardware settings and calibrations that may have been used during the scanning procedure (Mildenberger, 2002) (Figure 2.8).

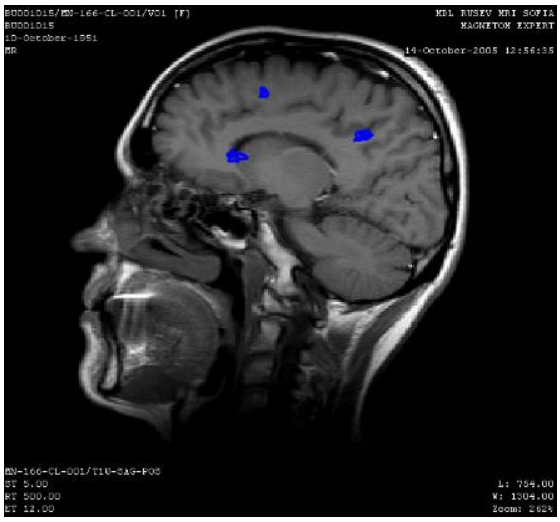

Figure 2.8 Example of a DICOM image slice displaying various scanning information. Source: (https://www.riversideimagingspecialists.com/mri-ct-scans/)

2.4.4 Quality of a CT scan

In CT scanning, various factors interact to determine the quality of a CT image. This may entail the scanning process itself and the processing of data through medical image translation software applications. As a test subject for determining this, numerous test models have been designed through studies to help evaluate CT accuracies and limitations.

Factors determining the quality of a CT scan

- The slice thickness determines the resolution at which structures are displayed three-dimensionally. This is set by the operator depending on scan requirements and usually ranges from 1 to 10 mm. The capturing of thinner slices may provide better diagnostic content but usually increases image noise (Ford and Decker, 2016).

- Noise in a CT image may appear due to various factors, including acquisition, computation errors, and variations in reduction numbers between voxels. The dose of exposure in the CT process can also greatly influence the image quality, reducing the radiation dose, inevitably leading to higher noise levels and lower contrast in images. In a recent study to determine CT image reconstruction based on edge-preserving noise reduction filters, Punwani *et al*. concluded that these filters could serve as an advantage to help detect lesions in lower-dose CT images (Wang, 2013; Ehman, 2014; Winkler, 1999).

- The spatial resolution in a CT image refers to the number of pixels needed to generate structures and features. In a digital display, this distinction is achieved by generating pixels of various sizes through computing algorithms. A large pixel size will be unable to resolve two nearby structures as compared to small pixel sizes. Also, spatial resolution can be influenced by the X-ray focal spot's size, the distance between source and object, and the size of the detectors found in the CT scanning device model. Modern CT scanners have a spatial resolution from around 0.5 - 0.625 mm in the Z-axis and roughly 0.5 mm in both the X and Y -axes (Wang and Fleischmann, 2018).

- Contrast is used to display various densities between neighbouring regions in a CT image through the Hounsfield scale. High contrasts can be observed in areas with notable differences in densities ranging from black to white tones of colour. Lower contrast areas can be observed in areas where a lesser density is displayed through colours ranging from black to grey (Goldman, 2007).

2.4.5 Test models developed for determining the accuracy of CT scanning

For quality assurance, phantoms are used to check that CT image quality and parameters are acceptable. One such phantom object commonly used in South Africa, namely the TOR CDR® (Figure 2.9), assesses image quality based on bar patterns and numbers. The ability to verify sensitometry is made possible through 10 designed inserts measuring 5.6 mm in diameter. Low contrast image details are determined through 17 elements of 11 mm diameter and contrast range between 0.002 to 0.075 at 70 kVp. High contrasts are determined through 17 inserts with a contrast range between 0.39 to 0.954 at 70 kVp and a diameter of 0.5 mm (Groenewald, 2017).

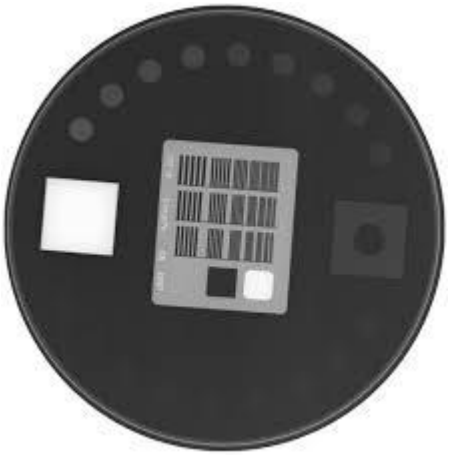

Figure 2.9 The TOR CDR phantom®. (Source: Groenewald, 2017)

In a recent study to determine the dimensional accuracy of CT scanning, a test model was designed consisting of a 15.24 mm diameter aluminium disc, with simple geometric shapes cut out. The design intended to display accuracies in capturing various wall thicknesses, radii, and various slice thicknesses. This study found that a hole measuring 3.175 mm had a difference of 0.014 mm. It was also found that the accuracy of dimensional data increased slightly with increased levels of contrast sensitivity. The noise level also significantly impacted accuracy and should generally be kept lower than 5% (Neel *et al.,* 1998) (Figure 2.10).

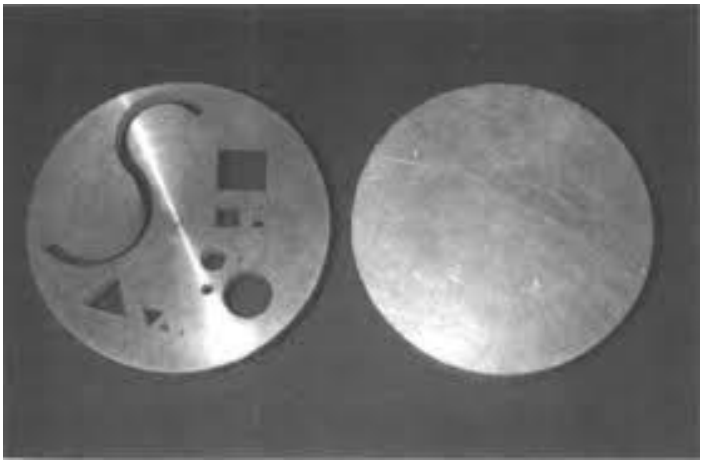

Figure 2.10 CT scanning test model. (Source: Neel and Klosterman, 1998)

The ACR phantom was created with the intent of being an integral part of the American College of Radiology CT accreditation programme in helping physicians assess their CT facility, personnel qualifications, image quality, and quality assurance. The ACR CT Phantom attempts to help illustrate several scanning parameters, including accuracy of positioning, CT number accuracy, image noise, high and low contrast, and slice thickness. The phantom is constructed out of a material with a density similar to water to ensure uniform density. In its design, four disc-shaped objects, each with a diameter of 20 cm and a thickness of 4 cm, were aligned next to one another. Each disc contained markings to help align the phantom in the X, Y, and Z axes (Hobson *et al.,* 2014) (Figure 2.11).

Figure 2.11 The ACR phantom. (Source: Hobson, 2014)

2.5 Hand-held scanners

Three-dimensional hand-held scanners provide a quick method for digitally capturing high-resolution geometric data of an object in a non-contact manner. Because of their usual compact design, they are frequently used in industrial projects such as the reverse engineering of parts, quality control of manufactured parts, and archaeological scanning of artefacts (Kersten, Lindstaedt and Starosta, 2018).

In most cases, these 3D scanners rely either on a passive triangulation or active principle. In a passive triangulation-based scanning system, multiple cameras record an object's surface from various views. Image optimization software the allows for prominent landmarks in each scan to be identified, isolated and combined through the use of varies software algorithms into a single digital 3D model (Figure 2.12) (Eder *et al.,* 2012).

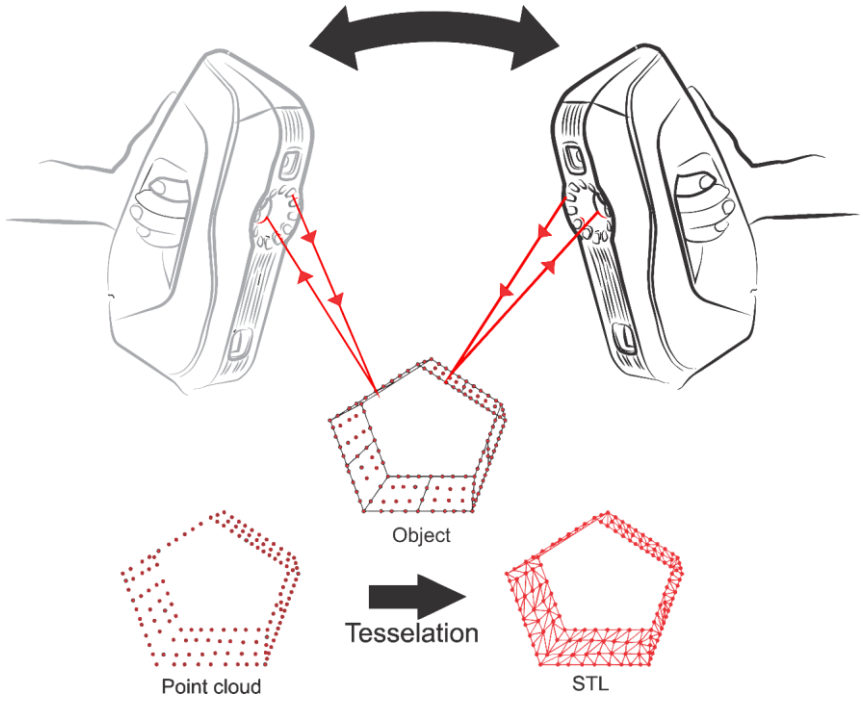

Figure 2.12 Diagram illustrating the hand-held scanning process.

In an active triangulation-based scanner, the light or laser source and detectors are fixed at a known distance from one another. The light projected onto the object is partly reflected and recorded by a charge-coupled device (CCD) sensor. Each time this happens, a digital data point is created, and its

position stored. As the scanner passes over the object, the process is repeated, creating several points representing the object's surface, commonly referred to as a point cloud. Afterwards, a computing algorithm combines the various points through tessellation to produce a digital surface geometry (Kuzminsky and Gardiner, 2012).

After several digital 3D surfaces have been generated, they are linked together to form a single digital 3D model using specialized software. The resulting digitally re-constructed 3D models can then be exported into several digital formats that enable further modifications through CAD software applications for AM or other rapid prototyping processes.

2.5.1 The clinical use of surface scanners first

Due to lower cost and ease of use, surface scanning has gained increasing interest from various medical fields in looking for faster and more reliable methods of obtaining 3D data for preoperative planning in craniofacial and plastic surgery. As with all other forms of 3D scanning, surface scanning aims to be a non-contact method of capturing data without causing any shape deformation. 3D scanning creates the opportunity to capture a person's unique profile to create better custom medical products. In the dental field, it is used to assess oral health, while for burn victims, it contributes to creating facial masks and various other prosthetics, not to mention preoperative assessments. 3D scanning allows for measuring organic shapes in a way that may not be possible through traditional devices and methods.

In a study by Seminati *et al.* to determine the potential scanning accuracy of hand-held scanners, the Artec® Eva® structured light scanner's accuracy was compared against a high precision laser scanner to capture limb shape and volume accurately. This particular scanner was chosen due to its wide range of applications and has been linked to similar studies associated with orthognathic and breast surgery. The scanner can capture multiple surfaces ranging from black to shiny without the need to place any scan markers. In addition, this scanner has an accuracy of up to 0.1 mm. It can process up to 2 million data points per second with a full colour resolution at a field of view of 214 mm x 148 mm, making it well suited for capturing larger surface areas. Ten prosthetic limbs were scanned by three different observers, with each using both the Artec® Eva® and laser scanners on each occasion. The prosthetic limbs were from both transtibial and transfemoral amputees. The results showed significant volumetric differences on some occasions ranging from 885 to 4399 ml in volume. In comparing the scans, it was found that the average deviation between the prostheses

was less than 1 mm or 0.6% across a diameter of 160 mm, with the most differences noted at the prominences of the residual limb prostheses. The study concluded that although the scanning device showed promise, actual scanning of patients could further validate its clinical application viability (Seminati *et al.,* 2017).

In a study to determine several surface scanning devices' abilities to scan and reconstruct virtual organs, three surface scanning systems, namely laser scanning, Artec® Eva® structured light scanning, and photogrammetry, were compared against each other. For scanning, the chosen objects consisted of porcine and ovine material obtained from a butcher, a plastic human skull, a rubber liver model, and a plastinated human heart. The results showed that all scanning devices could capture surface scan data; however, all scanning systems experienced difficulty acquiring data from biological specimens due to sub-surface reflections. It was found that the application of dark-coloured sprays improved scanning from which topology could be extracted. The study found that the laser scanning device performed best but highlighted that this might not be suitable for all applications. The study also concluded that scanned materials should ideally contain rigid and deformable elements for more extensive testing between various surface scanning technologies (Avis, Kleinermann, and Mcclure, 2004).

In another study, the Artec® Eva® was used to determine the dimensional accuracy of surface scanning techniques by scanning a human hand model. The study's first steps evaluated two image data acquisition methods referred to as the one or two-step scanning processes. The model was scanned in a single continuous 360-degree rotational movement around the model for the one-step data acquisition. For the two-step method, a front scan and a separate back scan were taken of the model. It was concluded that the one-step process yielded better results, with errors more likely to occur in combing scans than with the two-step method. In certain areas, especially where scanned areas may overlap, or the scanning process may not have captured the model surface adequately, the difference between the one-step and two-step methods was more prominent. The first discrepancy was about a 10% difference between the one-step and two-step approaches, with the latter appearing smaller. Secondly, areas of missing geometry were automatically filled and aligned using prominent features in the one-step scanning process, which yielded better results. This study also highlighted the importance of post-processing for generating reliable 3D models from data (Geierlehner, Malferrari, and Kalaskar, 2019).

2.5.2 Photogrammetry

Another less expensive method of recording the geometry of a model is through photogrammetry. In contrast to typical hand-held scanning devices that use projected and reflected light patterns, photogrammetry works by taking 2-dimensional images of an object from various angles and matching textures found across the captured images to create data points similar to that of a hand-held scanner (Figure 2.13). These digital points, in turn, are then combined through the triangulation principle to generate a digital surface of a captured 3D model.

One major advantage of this technology is low cost since almost any digital camera can be used. However, the results may vary since the cost and quality of cameras on the market also vary widely. Another notable drawback is the difficulty in capturing smoothed surfaces, which in some cases could require that powder or colour be added to the scanned model to help improve texture mapping to generate digital 3D models (Ciobanu and Rotariu, 2014).

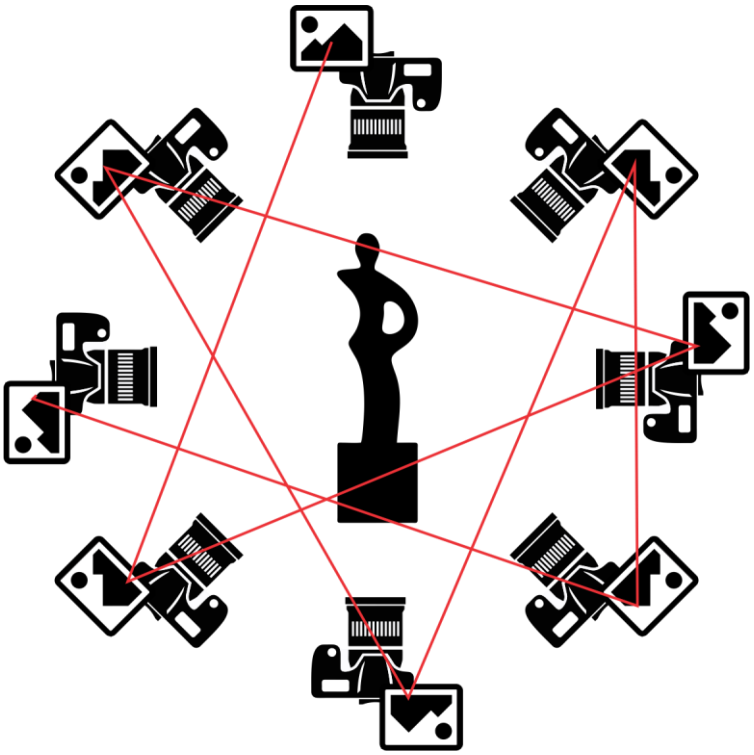

Figure 2.13 In photogrammetry multiple images are taken from various angles.

2.6 Additive manufacturing

The American Society for Testing and Materials (ASTM) defines AM in their F2792-12a standard as a collection of processes that involve developing objects from 3D model data files by joining materials, layers upon layers, contrary to subtractive manufacturing strategies. Since its initial development, this technology has been used extensively in the early phases of prototyping, with later processes allowing for the direct production of fully functional end-use parts and components (Wang *et al*. 2020).

In preparing a digital three-dimensional CAD model for fabrication, the model must first be divided into a series of 2D profiles. This is done through software known as “digital slicers,” which produces a computer numerically controlled programming language that is referred to as G-code. The G-code is a set of operational instructions or toolpath that can be interpreted by an AM machine to commence the fabrication process. Adjusting the thickness of each deposited layer of material will influence the resolution at which a model is fabricated and affect the amount of finer visible details (Brown, Conradie and De Beer, 2014).

2.6.1 Classification of additive manufacturing processes

AM processes can be categorized by the type of material used, the deposition technique, or how the material is fused or solidified. According to the ASTM 52900:2015 standard, AM can be categorized into seven processes and applications, as listed in Table 2.1. AM can also be classified according to the materials being used, with the materials either being liquid, solid, or powder-based (Figure 2.14) (Schmid and Wegener, 2016).

Table 2.1 **Classification of AM processes.** (Source: Schmid and Wegener, 2016)

Process	Application
Material extrusion	Plastic prototyping
Vat polymerization	Prototyping and high surface finish parts
Binder jetting	Prototyping and investment casting

Material jetting	Visual prototyping
Powder bed fusion	Functional prototyping and engineering functional parts
Sheet lamination	Prototyping
Direct energy deposition	Prototyping, functional parts, and repairing metal parts and fixtures

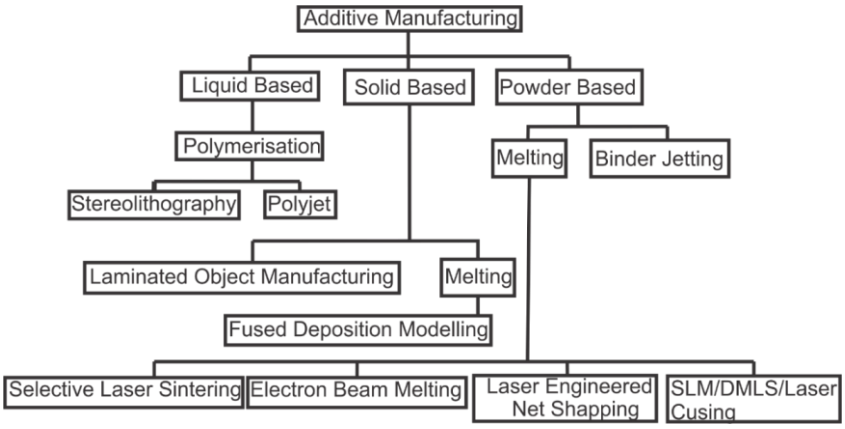

Figure 2.14 Hierarchy of AM according to material characteristics.

2.6.2 Laser sintering

Although there are many types of AM, only the powder bed laser sintering process will be described here since it is relevant to this study. Laser sintering (LS) is a fabrication process that uses thermal energy from a laser beam to sinter (bind) powdered material particles together to form a tangible 3D model. The method uses a mirror deflection system to scan consecutive cross-sections of a part calculated from a CAD model onto a powder bed (Figure 2.15). First developed in the 1980s at the University of Texas by a PhD student Carl Deckard, it would grow into one of the most advanced and promising manufacturing methods still in use today. Unlike other AM processes such as fused deposition modelling, LS creates more durable, accurate, and intricately detailed models without requiring any additional support structure in the design to aid the fabrication process. Although significant amounts of heat are involved in this process, problems like the warping of fabricated parts are minimal due to excess heat quickly being dissipated by the material surrounding the fabricated model (Bakshi, 2016).

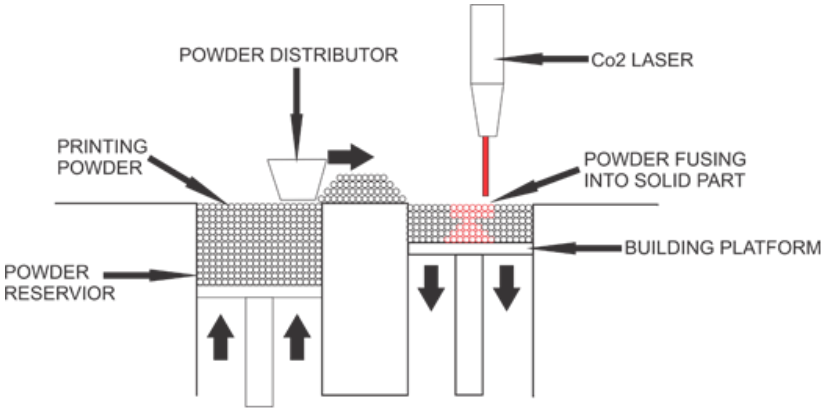

Figure 2.15 Principal diagram of LS AM process.

2.6.3 Testing the accuracy of additive manufacturing

The assessment of the performance of a particular AM device can be done through two methods. The first includes directly measuring parts produced through the device or, secondly, by measuring a clearly defined standardized artifact produced through different devices. Such an artifact should strive to evaluate the performance of an AM device quantitatively. The advantage of using a standardized artifact is that a wide range of AM technologies can be compared with one another. This could potentially highlight limitations and provide a means for demonstrating improvements in a specific field of AM technology.

Kruth (1991) made one of the earliest attempts in designing a benchmark model for studying layer manufacturing technologies. In his design, he used squares, embossed letters, cylinders, inclines, overhangs, and an inverted U-frame to create an artifact capable of being measurable in all three directions (Figure 2.16).

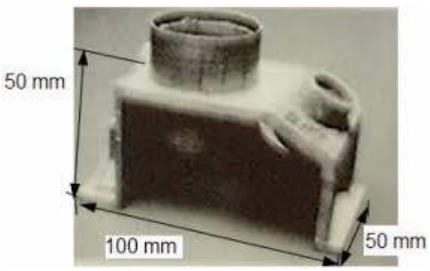

Figure 2.16 Test model by Kruth for determining material increase during AM. (Source: Kruth, 1991)

The most significant dimensions of the model were, however, relatively small compared to most AM device's building platforms. Furthermore, the artifact possessed no repeated features and was initially intended to determine the accuracy of a particular AM device over a series of repeated copies. He further remarked that the orientation of the artifact is based on conserving production time. This would undoubtedly be determined by the CAD dimension and chosen AM resolution, indicating the number of layers needed to produce the artifact (Kruth, 1991).

An artifact produced by Childs and Juster (1994) consisted of a squared base of 240 mm and a thickness of 10 mm. Nine identical squares measuring 25 mm x 20 mm were evenly spaced on the base for linear accuracy and repeatability to be measured. Each square contained a cylindrical hole with seven orientated along the Z-direction and two along the Y-direction. These allow for the accuracy and repeatability of radius, roundness, and cylindrical shapes to be determined. The artifact also contains several thin-walled features ranging from 1 - 5 mm, allowing for measuring wall thicknesses (Figure 2.17) (Childs and Juster, 1994).

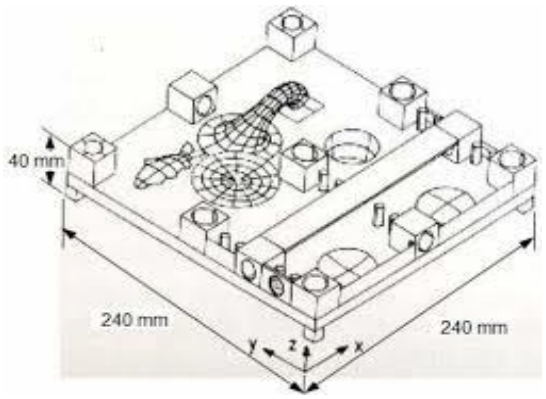

Figure 2.17 Test model by Childs for testing various AM processes. (Source: Childs and Juster, 1994)

Through their design, Mahesh, Wong, Fuh, and Loh (2004) sought to compare the accuracy between four AM processes, namely laser sintering, fused deposition modelling, laminated object manufacturing, and stereolithography. Their design incorporated slots, spheres, cylindrical holes, and thin walls based on existing ISO standards. In their study, the artifact also helped highlight how shrinkage levels may vary across numerous AM processes (Figure 2.18) (Mahesh *et al*., 2004).

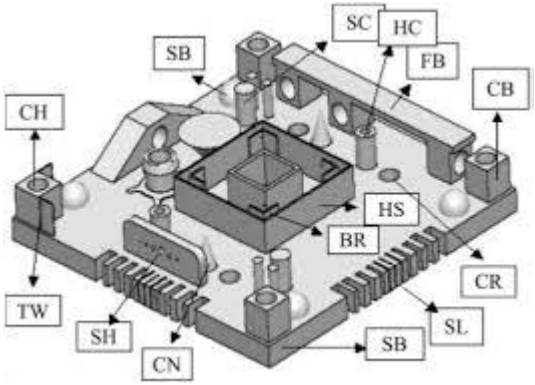

Figure 2.18 Test Model by Mahesh, Wong, Fuh, and Loh for evaluating AM processes. (Source: Mahesh, *et al.* 2004)

To observe the shrinkage process and accuracy changes during the laser sintering of aluminium and understand the underlying factors that affect tolerances inspired the artifact design by Sercombe and Hopkinson (2006). Their design used a square base with two staircases with uniform thickness, orientated along the X and Y axes. One drawback of this design was that it could only determine linear accuracy and required numerous manufactured copies to conclude accuracy (Figure 2.19) (Sercombe and Hopkinson, 2006).

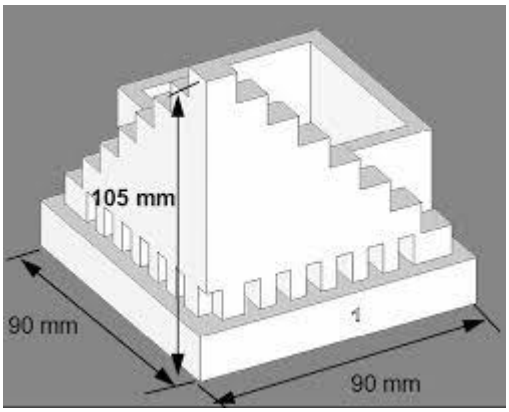

Figure 2.19 Test Model by Sercombe and Hopkins for shrinkage and accuracy during laser sintering of aluminium. (Source: Sercombe and Hopkinson, 2006)

In their research to determine the accuracy of machine parts, Cooke and Soons (2010) used a circle-diamond-square test part with an inverted cone that is commonly used to evaluate the performance of five-axis milling machines. The test model was based on the classic Aerospace Industries Association (AIA), National Aerospace Standard, NAS 979 circle-diamond-square with an

inverted cone. The test model's features were intended for measuring size, flatness, squareness, parallelism, and surface finishes. The design consisted of a squared shape rotated at 45° and intended for measuring size. A ramping feature with a 5° incline was included for determining angular deviation. The centre circle was designed for determining circularity, size, and surface finish. (Figure 2.20) (Cooke and Soons, 2010).

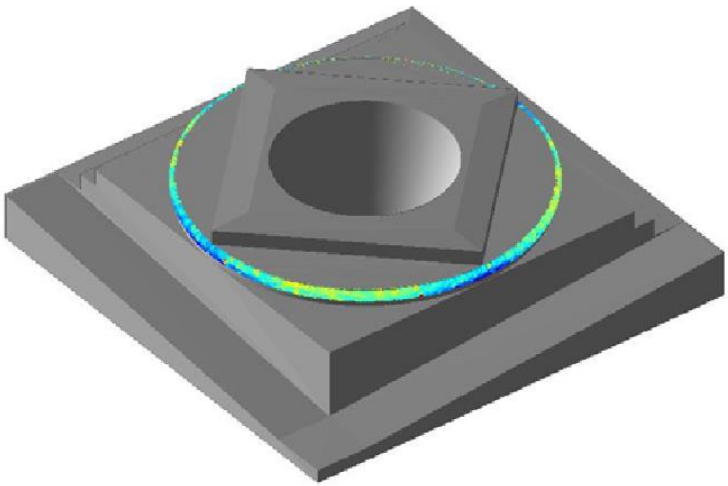

Figure 2.20 Circular diamond test model by Cooke and Soons. (Source: Cooke and Soons, 2010)

In attempting to produce a standardized artifact for evaluating AM processes, Moylan, Slotwinski, Cooke, Jurrens and Donmez (2014) suggested that several factors be considered in the design. Firstly, the artifact should be large enough to measure the AM technology's performance near the model's edges and centred areas. Secondly, the artifact should possess numerous small, medium, and large features. Thirdly holes and bosses (protruding features) should be present to help verify beam width compensation. Lastly, the artifact's fabrication should not consume a large quantity of material or time and be easily measurable. His design showed numerous influences from other research with corresponding features (Figure 2.21).

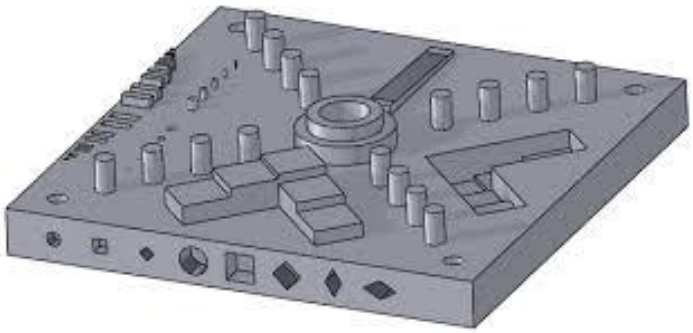

Figure 2.21 Design of Moylan's test model. (Source: Moylan *et al.,* 2014)

His artifact's design was based on a set of "rules" to govern his design process. These guidelines helped establish a criterion identifying the intent behind each test feature's design (Moylan *et al*. 2014). The features and their intended purposes in the design are displayed in Table 2.2.

Table 2.2 Characteristics of Moylan's test model design. (Source: Moylan *et al*. 2014)

Characteristics Investigated	Feature(s) used to Demonstrate
Straight features	Vertical walls of staircases; outer edges
Parallel or perpendicular features	Vertical walls of staircases; outer edges
Circular or arced features	Centre hole; central cylinders
Concentric circles or arcs	Central cylinders
3D or freeform features	Ramp; lateral features
Holes and bosses	4 mm pins and holes; centre holes and central cylinders; staircases; fine features
Multiple planes	Lateral features
Location	4 mm pins and holes
Geometric errors of laser positioning axes	4 mm pins and holes
Geometric errors of the build platform	Staircases; centre hole; ramp

Alignment errors between axes	The top surface and centre hole
Errors in beam size	4 mm holes and pins
Fine features	Delicate features, holes, and pins

2.7 Fabricating a maxillofacial prosthesis using advanced manufacturing methods

Although divided in terms of technology, both advanced and traditional methods of maxillofacial prosthesis fabrication share similar goals. In both approaches, the first goal is to acquire the geometry of the affected area. In modern methods, this is done through 3D scanning to produce a digital copy of the area. This is followed by a digital creation process, which, unlike traditional hand carving and shaping, is performed through CAD or other polygonal-based freeform modelling software applications. The next step is to produce a mould of the designed prosthesis through AM. As in the more traditional approach, such mould could comprise multiple parts to accommodate intricate designs to ease removal after curing. This last stage may not be necessary with some emerging AM technologies since some emerging processes directly fabricate silicone-based prosthetics (Figure 2.22).

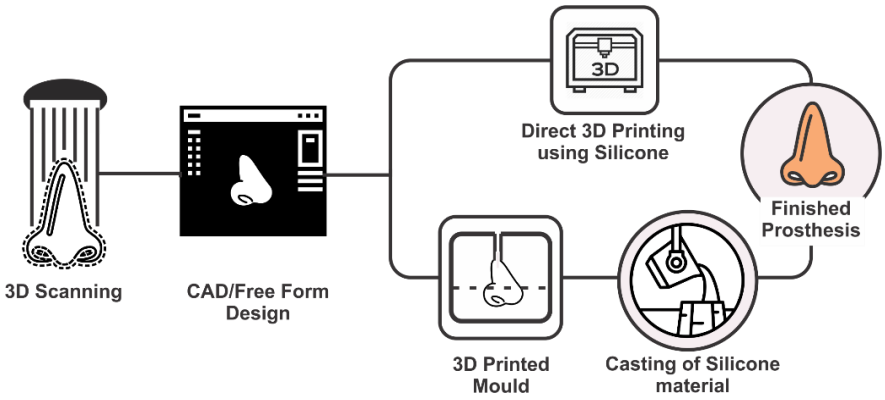

Figure 2.22 Workflow of advanced additive manufacturing a prosthesis.

2.7.1 Digital modelling of maxillofacial prosthesis

After scans have been captured and converted into digital polygonal models, a CAD software application is typically used to make adjustments by editing or deleting geometries, smoothing surfaces, scaling to the correct proportions, filling holes, or simplifying geometries. In some cases, software capabilities allow for digitally mirroring scanned surfaces to gain an inverted copy, such as for a missing ear prosthesis. In doing so, scans from unaffected healthy anatomical features from either the patient or somebody with similar anatomical proportions can be scanned and digitally modified to create prosthetics with appropriate proportions. Many modern medical CAD software applications have integrated digital collections of prior modelled facial features that allow changes to be made to fit a patient's profile (He *et al*., 2017).

2.7.2 Additive manufacturing of maxillofacial prosthesis

The use of AM in the advanced method of creating a facial prosthesis falls into either a direct or indirect approach. The first approach implies fabricating a final complete prosthesis directly from a specialized AM device using pigmented silicone and a catalyst material to produce the prosthesis based on the layer-by-layer principle. The indirect method involves fabricating a mould in which silicone-based materials can be cast, polymerized, and the prosthesis later extracted.

Direct additive manufacturing

In recent times there has been an increasing interest in the possibility of manufacturing finished silicon prostheses directly from AM devices. Not only could this lead to shortened manufacturing times but also be vastly less costly and labour-intensive. Although this possibility may be on the near horizon, the technology is still in its early stages, with some promising headway by manufacturers to develop specialized and reliable AM devices for this task (Unkovskiy *et al.,* 2018).

One such device developed by the Frip Design group, namely the Picsima®, uses technology that enables control over the amount of polymerization of silicone materials. In the process, small amounts of catalysing material are extruded through a syringe-like printing head on a layer-by-layer basis into a vat of unpolymerized silicon material. The silicone and catalyst materials can also be coloured to match the patient's surrounding facial features. The device can produce models with a resolution as fine as 40 microns and material shore hardness of up to 10A (Liravi and Toyserkani, 2018).

The ACEO® Imagine® is a liquid silicone-based 3D printer that dispenses tiny droplets of silicone to fabricate designed models. Its technology was developed, taking the silicone material's high viscosity into account. It was designed so that the printing head never comes into contact with the printed model, thus enabling precise geometries to be constructed. A UV light source is incorporated into the printing head to enable the curing of each layer before another is deposited. This AM device allows for multi-material printing, allowing various silicone materials to be incorporated into a single model. Generated support structures can be removed afterwards by washing in water. The final prosthesis needs to be vacuum post-cured for several hours (Porter *et al.,* 2017).

Indirect additive manufacturing

A more common method in which AM is used in the advanced maxillofacial prosthetic fabrication approach is to manufacture a mould into which silicone materials can be cast. The designed prosthesis is digitally subtracted from a larger 3D body in the virtual environment to create a cavity that represents its shape. The resulting digital model can be split into several parts to accommodate a geometry's undercuts, overhangs, and intricacies. In many cases, these moulds are fabricated using high-end AM technologies like material jetting or vat photopolymerization technologies, which typically produce higher resolutions. The printed parts of the mould are then UV cured to ensure greater material strength and grit blasted for a matt surface finish (Cruz *et al.,* 2020).

Advantages and Disadvantages of Direct and Indirect additive manufacturing

Direct Additive Manufacturing allows for the intended prosthesis/part to be manufactured directly, leading to quicker turnaround times. In addition, this process allows for the fabrication of complex geometries, which may not always be possible through a moulding process. However, silicone materials for manufacturing soft prosthetics are still in their initial stages, meaning that many trials would have to be done to deem certain materials biocompatible. In addition, colour pigments could be added to silicone materials which may be limited in their ability to match exact skin tones or may even discolour over time.

Indirect Additive manufacturing is a traditional method AM that is a highly cost-effective method for producing high volumes of products at a high level of detail. In addition to this, the process allows for the feedstock of various materials, including thermoplastic polymers, thermoplastic elastomers, and several other non-plastic materials. Some IM machines have recently been developed to use more

than one material in their fabrication process. However, some disadvantages of this process include limitations of designs since the part would need to be ejected from the rigid mould. In addition, warpages, bubbles, sink marks, crack and burn marks may occur.

2.7.3 Discussion on problems associated with advanced methods of prosthesis fabrication

Despite the advantages that advanced CAD/CAM methods of facial prosthetic fabrication present, it is not without drawbacks. One key concern is the high costs of having a CT scan taken and how this excludes many patients from gaining access to this technology. Unfortunately, this is especially the case in South Africa, where a large proportion of the population is dependent on the government for health care assistance. It is difficult to pin an exact number on the requirement for facial prosthetics, but the incidence of facial trauma has shown a constant increase in recent years since it is strongly associated with burns, assaults, traffic accidents and cancer (Yadav and Shrestha 2017). According to a 2016 study that investigated clinical predictors of abnormal findings in CT head scans of non-trauma patients, it was found that a typical CT scan could cost between $200 and $400. Adding to this dilemma is the availability of resources evident in a recent study set to determine the available radiology resources in South Africa, with a primary focus on the Western Cape rural and metropolitan areas. Out of 349 provincially equipped units, less than 5% were equipped with CT scanners (van Zyl *et al.,* 2021; Bennimahadeo and Maharajh, 2016).

Traditional impression-making methods are therefore still widely in use. Although much cheaper compared to CT or any other scanning technology, it can create unfavourable results in accurately capturing the geometry of an area or creating an unpleasant experience for a patient. It is therefore believed that the use of alternative, inexpensive digital data capturing methods can be implemented to deliver lower-cost assistance for maxillofacial prosthetic fabrication (Mothopi *et al.,* 2012; Voros, 2009; Yadav and Balakrishna, 2017).

Chapter 3

Methodology

3.1 Introduction

To appropriately address the problems associated with CT scanning in producing maxillofacial prosthetics, scanning with a 3D hand-held scanner was proposed. These scanners require less technical expertise to operate, are vastly less expensive compared to CT scanners and are also portable, which makes it convenient to scan patients in rural areas. However, the question was if these scanners could produce sufficiently accurate scan data to make it suitable for the intended application. This was determined through a practise led research approach through the design of a custom-made test model which drew inspiration from elements derived from engineering, medicine and art. The intention with the test model was to compare the scanning accuracy of the 3D model generated by an Artec® Spider® hand-held scanner to 3D models of CT scans generated through different translation software packages. Access to the software and hardware used in this research project was made possible through the various departments and institutions associated with Central University of Technology, Free State (CUT). The study also formed part of a larger research initiative undertaken by CUT's Centre for Rapid Prototyping and Manufacturing (CRPM) and Product Development Technology Station (PDTS) to identify prosthetic assistance measures that can be offered at lower cost.

3.2 Creating a benchmark test model

During the initial part of the experimental phase of the study, the focus was first on the design and fabrication of geometrical test models. Although no scan data of actual patients were used to design any test geometries, the researcher created features that strived to provide similar data capturing assessments to determine accuracy.

3.2.1 Establishing a design criterion

To create a test model that could compare the accuracy between hand-held and CT scanning, a set of guidelines had to be developed to help guide the design process. This relied on examining previous research where test geometries were used to determine the accuracy of AM processes and

scanning techniques as described in Chapter 2. The elements derived from the review of these literary works were then structured into a design criterion with a scope that identifies each element's purpose and limitation.

Ten distinct criteria elements were identified within five overarching categories. These categories covered design aspects such as size, shape, AM considerations, and design intention (Table 3.1).

Table 3.1 Design criterion

Number	Category	Criterion name	Description	Limitations of design	Visual explanation
1	Size	Size	The design element size should range from small to large.	The feature should be no smaller than 0.65 mm or larger than 30 mm.	
2	Size	Elevation and depth	Design elements should display elevations and depths.	Each elevation or depth should differ in increments.	
3	Type	Texture	The pattern design element should be included on one of the surfaces.	Texture patterns should be depicted in various sizes.	
4	Size	Wall thickness	Protruding rectangular design elements should have a range of wall thicknesses.	The thinnest feature must be greater than 0.5 mm.	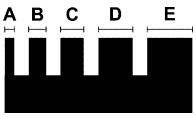
5	Arrangement	Spacing	Protruding elements of similar design should be of various distances apart.	The minimum spacing between structures should be no smaller than 2 mm.	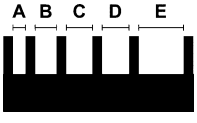

6	Utilisation feature	Anchoring points	Anchoring points that simulate prosthetic attachment sites should be included.	Anchoring points should be arranged in a similar configuration as an actual prosthetic attachment.	
7	Type	Spherical dimensions	Positive (p) and negative (n) half-spheres should be included.	Spherical dimensions should have identical diameters.	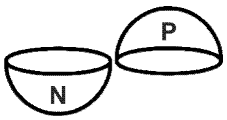
8	Manufacturing	AM features	The minimum size of features must be greater than 0.5 mm to ensure the design is manufacturable using an AM process.	The size and shape of the model should allow it to be manufactured.	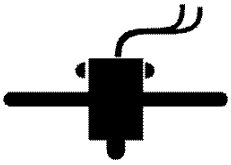
9	Size	Measurement	The sizes of features should be measurable to determine if any deviation had occurred.	Any sizes used for the design of test models should be measurable using a Vernier caliper.	
10	Type	3D geometric shapes	All design elements should have geometric shapes	Basic geometric shape structures should be used for easier measurability.	

3.2.2 Design of individual test geometries

Six individually developed geometric test models were produced from the design criteria, each depicting an element's required attributes and limitations. Their design's geometric sizes and shapes were intended to be easily measurable to indicate dimensional deviation that may have occurred due

to the AM process or because of limitations of the specific scanning process used. The six individually developed geometric test models are described below:

Elevation Test Geometry

The Elevation Test Geometry attempts to determine the scanning devices' ability to distinguish between areas of elevation. In its design, five raised platforms were created on top of one another, with differing height increments assigned to each. The horizontal and vertical surfaces join perpendicular, resembling a stepped pyramid (Figure 3.1).

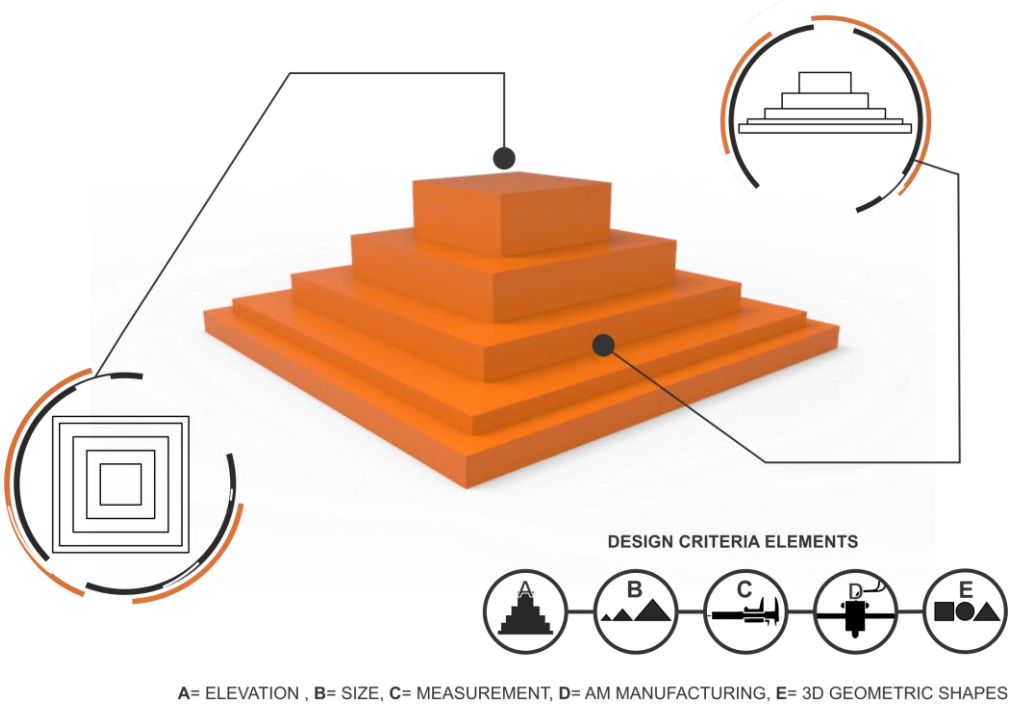

Figure 3.1 Elevation Test Geometry design.

Depth Test Geometry

The Depth Test Geometry's design aimed to determine the correlation between the radius of a particular hole and the depth at which a hand-held scanner can image it. This feature is specifically aimed to point out the weakness of handheld scanners that work on the line-of-sight scanning principle. Since the camera captures images projected by the device's light at a set angle there is a

limit to deep narrow features that can be scanned into. This is not a problem for CT scanners which take slices through the object, thus easily revealing features of deep holes. Four rows with four holes, each having a different depth and radius were designed. The depths of each varied in increments of 20 mm, with the uppermost holes situated at the top of each row having a depth of 80 mm. The diameters of the holes increased in even increments from top to bottom with the smallest having a diameter of 5 mm and the largest 17 mm (Figure 3.2).

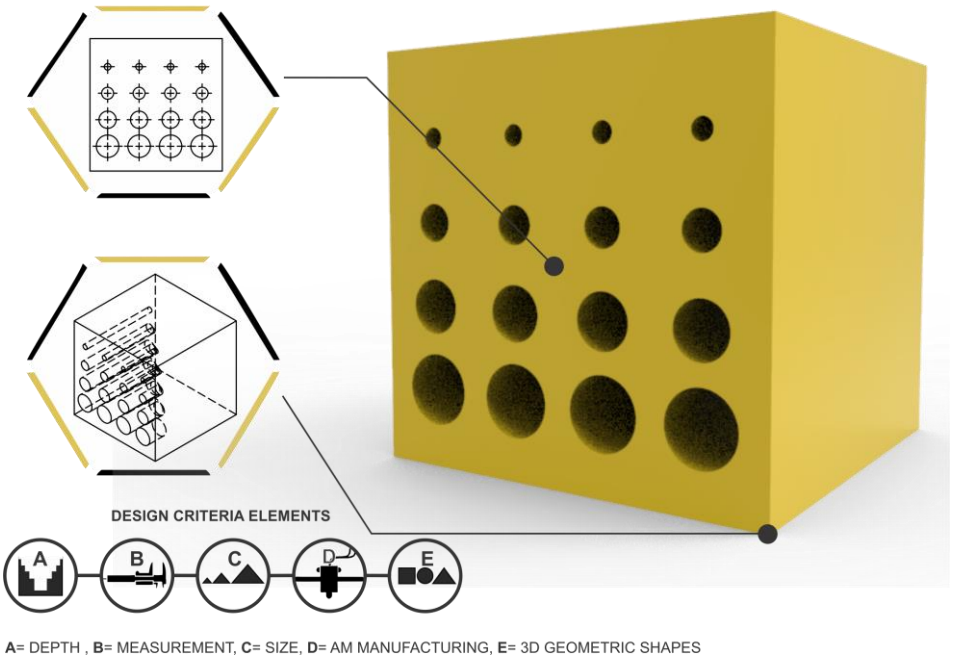

Figure 3. 2 Depth Test Geometry design.

Pattern Test Geometry

The Pattern Test Geometry was designed to determine the scanning device's ability to capture a series of dimensional structures that make up a textured surface. Aesthetics can play a vital role in deciding whether a prosthesis can pass off as being convincingly real. By accurately capturing finer details and textured surfaces, prosthetics can be developed that visually blend in better and more closely resemble healthy surrounding tissue. Thus, this test model consisted of four squares next to one another, each containing different sizes of the same pattern formations. Their grid dimensions vary from 5 mm x 5 mm, 4 mm x 4 mm, 3 mm x 3 mm, and 2 mm x 2 mm, all with 60 degreed tapered protruding prism shapes (Figure 3.3). This feature also highlighted the CT scanner's limitation in scanning fine features in the direction of the X-ray beam where scans are spaced a

minimum of 0.5 mm apart. Since the 2 mm x 2 mm prism shapes were only 1 mm heigh, the CT scanner should not have been able to accurately reproduce it at its minimum slice thickness of 0.5 mm. Accurately scanning these features with the hand-held scanner should not have presented any problems.

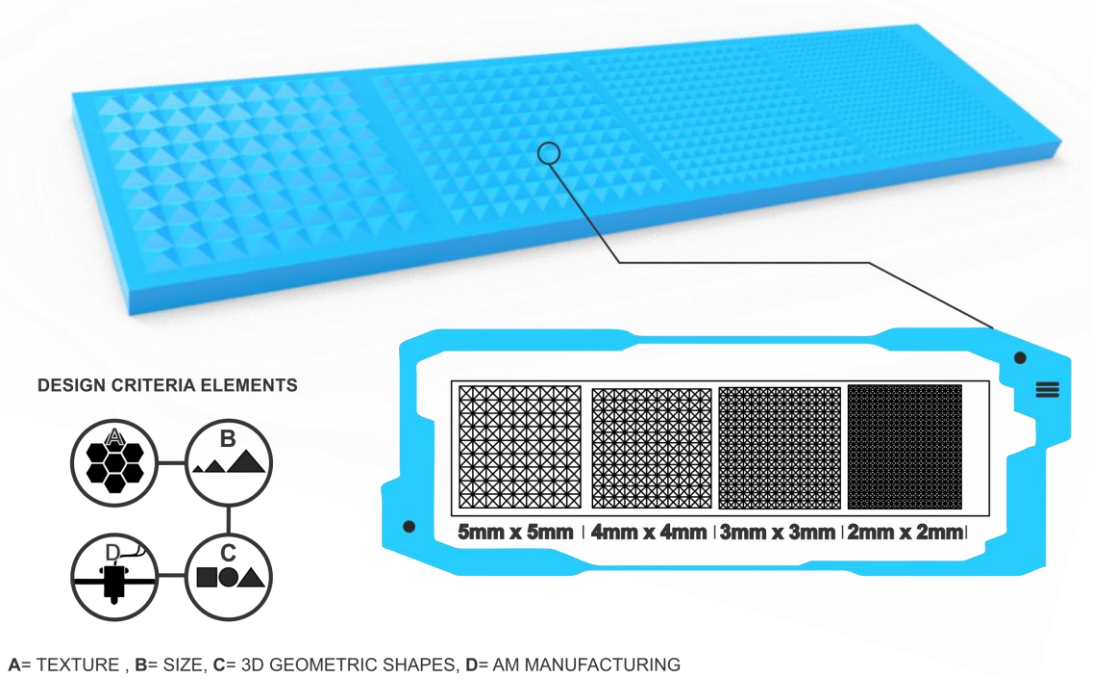

Figure 3.3 Pattern Test Geometry design.

Wall Thickness Test Geometry

The design intention behind the Wall Thickness Test Geometry was to determine the scanner's ability to detect the thicknesses of various geometric features. This was done by creating eleven fin-like structures with varying sizes of thicknesses assigned to each. The thickness of each structure differed in increments of 0.5 mm, with the thinnest feature starting at 0.65 mm. This compensated for the CT scanner only being able to capture slice data at thicknesses of 0.5 mm, thus making the thinnest designed structure detectable. Inaccuracy was, however, expected because of the 0.5 mm slice spacing while scanning across the width of the walls. The structures were designed not to extend more than 10 mm in height to provide adequate strength and stability while avoiding possible warping or breaking during the AM process (Figure 3.4).

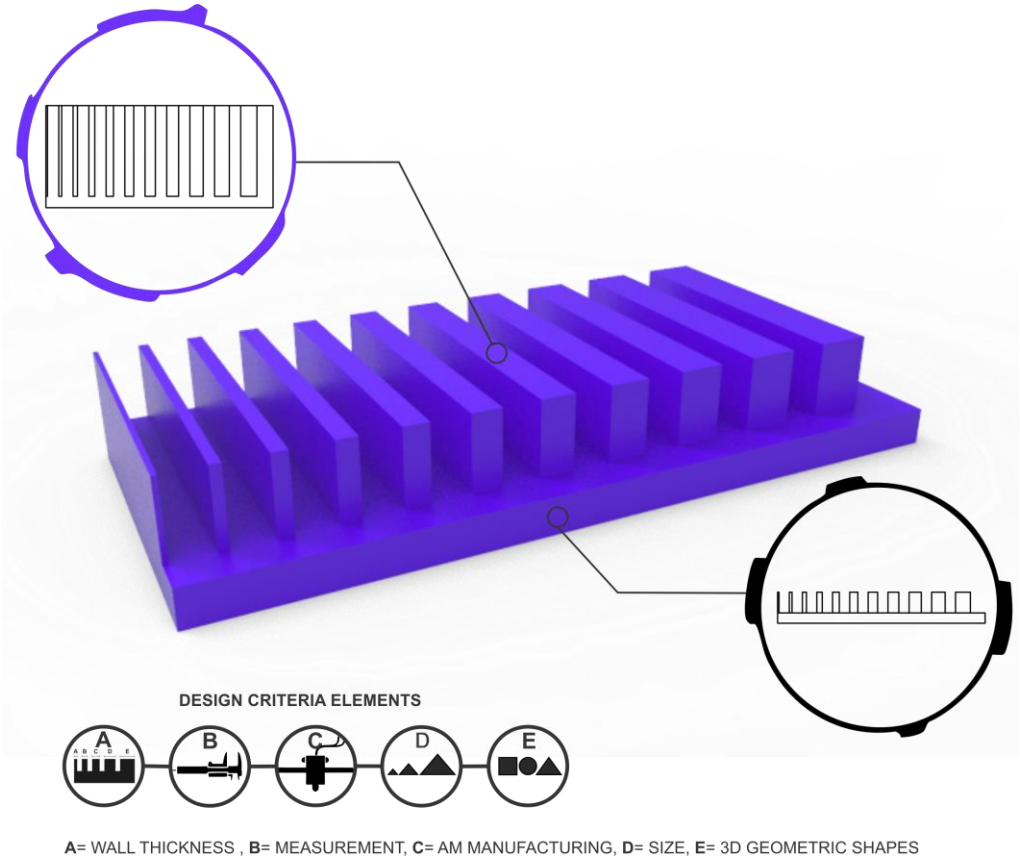

Figure 3.4 Wall Thickness Test Geometry design.

Spacing Test Geometry

The aim of the Spacing Test Geometry was to highlight the hand-held scanner's inability to scan into narrow crevices. This is similar to the limitation that was described under the Depth Test Geometry for the hand-held scanner. The width of the eight fins in the design was kept the same but the spacing between the fins increased in 2.5 mm increments (Figure 3.5).

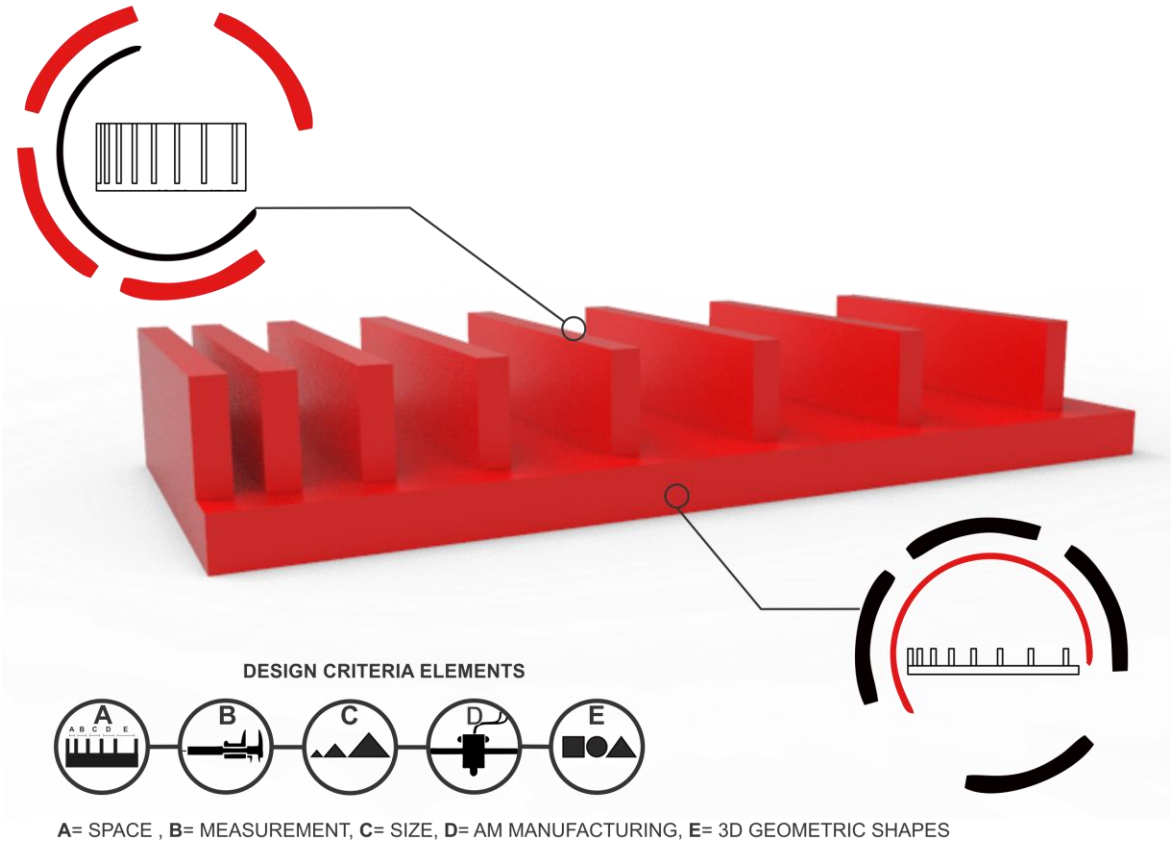

Figure 3.5 Spacing Test Geometry design.

Anchor Point and Spherical Test Geometries

Prosthetic materials can degrade and become discoloured over time, meaning that a new prosthesis will have to be manufactured several times during a patient's lifetime. In many of these instances, particularly nasal and auricular prosthetics, magnetic components will be surgically implanted into the bone in the position of the prosthesis. The silicone prosthesis is then retained through magnets which are embedded into the prosthesis. Each time a new prosthesis needs to be made; the facial geometry of the patient will need to be re-determined since the facial features change with time. If a CT scan is used to scan the area, metallic implants will be problematic since metal in the scanning field causes artifacts in the scanned image. To demonstrate this, three 2.5 mm radius holes were designed into a cube roughly orientated in the same orientation as auricular prosthetic attachment points (Figure 3.6). Metal pins can then be placed in the holes to represent the implants.

The Spherical Test Geometry's design attempted to highlight how accurately curved surfaces can be scanned. For this test geometry, various half-spherical shapes with varying radiuses were designed

and positioned, with one protruding outwards (positive) and another protruding inwards (negative). (Figure 3.6).

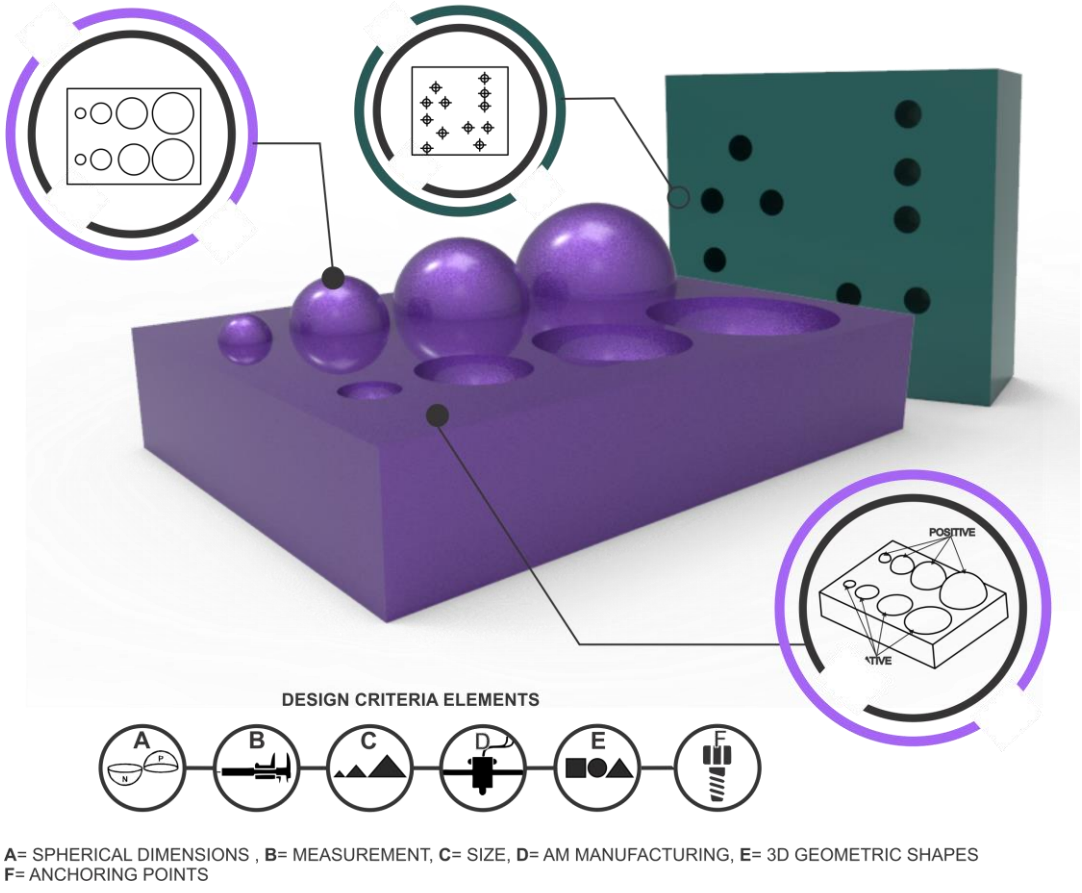

Figure 3.6 Pattern Test Geometry design.

3.2.3 Design of the First Test Model

In creating the First Test Model, the researcher attempted to combine all the individually developed geometric test geometries into a single digital prototype model design. Therefore, a 3D cube was chosen for a base geometry with the different sides housing the various individual developmental geometric test models. The layout of the test geometries was also taken into consideration to potentially allow the prototype model to be tilted on its side if scanning from various angles is needed. The SolidWorks® software application was the only software used to design all the individual developmental geometric test models associated with the First Test Model (Figure 3.7).

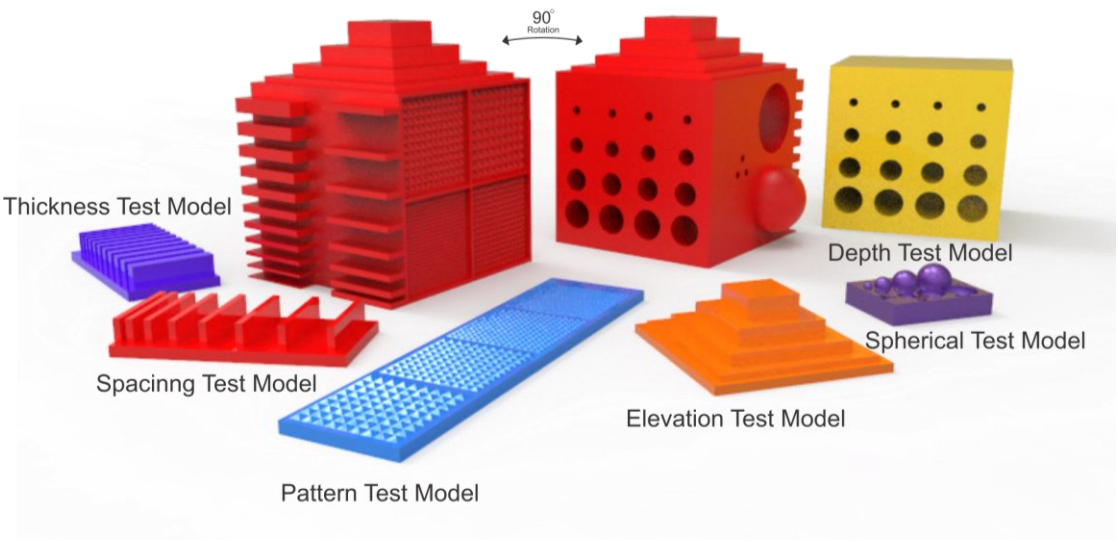

Figure 3.7 CAD images of individual test geometry designs and combined First Test Model.

3.3 Fabrication and evaluation of the First Test Model

Several different AM devices are available at the CRPM at CUT. These include machines that can process both metals and polymers through AM. Polymer laser sintering was selected to produce the First Test Model. Although more expensive compared to many other AM processes, LS presents the advantage that no supports are required which would have been difficult to remove from the hole features of the test model. The First Test Model was prepared for the AM process by translating its digital file format into STL. The digital STL model was then uploaded into dedicated software from Electro-Optical Systems® (EOS), where it was correctly orientated, and the design sliced in preparation for the AM process. An EOSINT® P385 polymer laser sintering machine from EOS was employed to produce the test model from nylon PA12 powder (Figure 3.8).

Figure 3.8 EOSINT® P385 LS machine. (Source: <https://www.eos.info/en>)

The machine operates by sintering the nylon powder together layer-by-layer using a CO2 laser according to the model's slice file. The model was "thin-walled", meaning that the walls were printed solid to a thickness of 5 mm, while the remaining powder inside the model was left unsintered. This reduces the sintering time and reduces the chances of warping during the production process. After fabrication, the model was cleaned by removing excess nylon powder material using brush tools and compressed air (Figure 3.9).

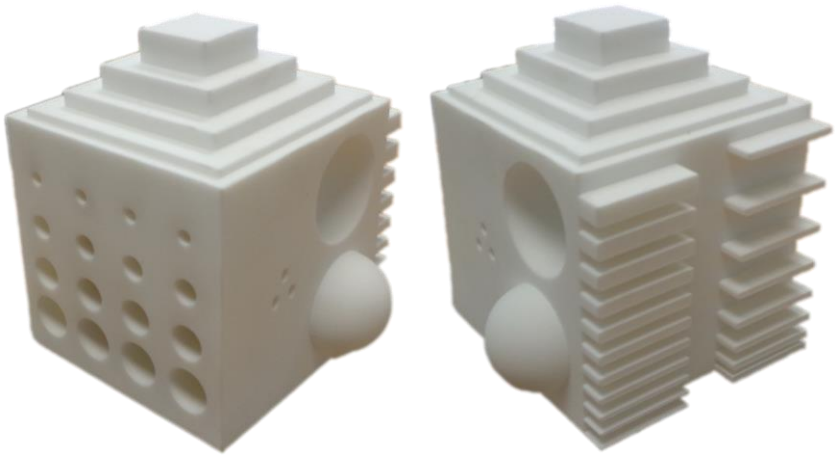

Figure 3.9 First Test Model produced through laser sintering.

After fabrication, a preliminary scan of the First Test Model was conducted using an Artec® Spider® hand-held scanner. This revealed that certain features were obstructing the scanner from fully capturing others. A focus group was put together from the staff of the Department of Mechanical and Mechatronics Engineering and the Department of Studio Art and Design at CUT. The results of the scans were presented to them, and suggestions were made to improve the design of the First Test Model. It was put forward that certain features would have to be modified, while others would need to be added to widen the model's initial scope. These suggestions were incorporated into a second design iteration known as the Second Test Model.

3.4 Design and fabrication of a Second Test Model

The focus group suggested several changes to the existing design criteria. These aimed to improve the design of the proposed second model through modifications of already present criteria elements by simplifying, creating additional space, compensation for triangulation, or re-positioning features to more accurately resemble areas for prosthetic attachment (Table 3.2).

Table 3.2 Description of criterion changes.

Original number	Criterion name	Original description	Revised description
2	Elevation and Depth Test Geometries	Design elements should display elevations and depths.	The focus group suggested that certain features in the Depth Test should be changed to compensate for the angle of the scanning triangulation of the hand-held scanner.
4	Wall-Thickness Test Geometry	Protruding rectangular design elements should have a range of wall thicknesses.	The focus group suggested that the number of fin structures is reduced to create space for additional features.
6	Anchor Point Test Geometry	Anchoring points that simulate prosthetic attachment sites should be included.	The focus group suggested that the holes used to keep metallic anchoring inserts in place should be re-arranged to resemble an area where a prosthetic ear could be attached.

Table 3.3 Suggested additions to the design criterion.

Additional number	Criterion name	Description	Limitations of design	Visual explanation
11	Anatomical structures	3D Model of a nose	The focus group suggested the addition of organic shapes in the test model.	
12	Addition of angulation structures	3D Model showing four different corners of angulation.	The focus group suggested the addition of structures that allow for the testing of varying angles.	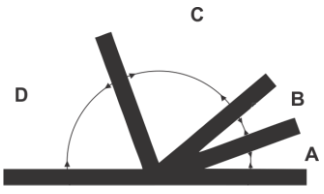

3.4.1 Design of a Second Test Model

Some of the design elements proposed by the focus group were simple and could be designed using CAD modelling software (SolidWorks®), such as was used with the First Test Model. However, other design elements were more organically based, and it was realized that this would be challenging to design using a traditional CAD modelling approach. Digital sculpting software (Zbrush®) was therefore chosen to create additional anatomical test features more closely associated with maxillofacial prosthetics.

The following changes were made to the First Test Model using the SolidWorks® CAD software:

- The Elevation Test Geometry was simplified to free up extra space for additional test features.
- The depths of the holes in the Depth Test Geometry top two rows were incrementally decreased and diameters increased while the walls of the bottom two rows were incrementally angled.
- The number of fin-structures in the Spacing and Thickness Test Geometries was reduced to allow for additional test features.
- The layout of the holes that housed the metallic inserts for attaching a prosthesis in the Anchor Point Geometry, was re-arranged to resemble more closely the layout associated with an auricular prosthesis.
- Structures that allow for scanning at varying angles were added to evaluate the hand-held scanner's ability to scan behind the ear.

The following additions were made using the Zbrush® digital sculpting software (Figure 3.11):

- A Nasal Test Geometry was digitally sculpted and added.
- An Auricular Test Geometry was digitally sculpted and positioned at the top of the Second Test Model.

Figure 3.10 shows the design of the Second Test Model, and Figure 3.11 highlights the specific design changes that were made. The dimensions of the model are shown in Annexure A.

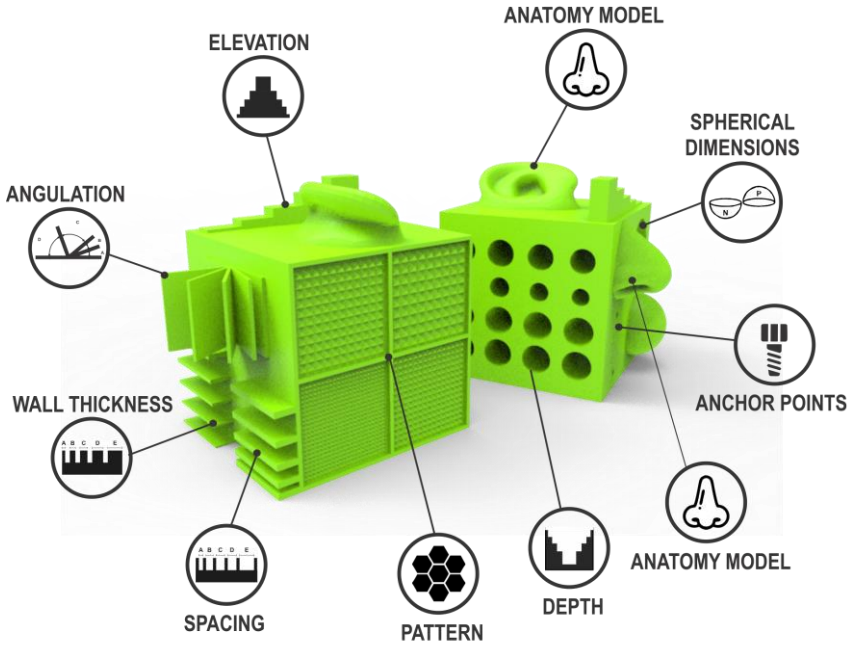

Figure 3.10 Final design of the Second Test Model

Modification: Wall thickness and Spacing developmental geometry test models features were reduced.
Addition: Angulation developmental geometric test model were added.

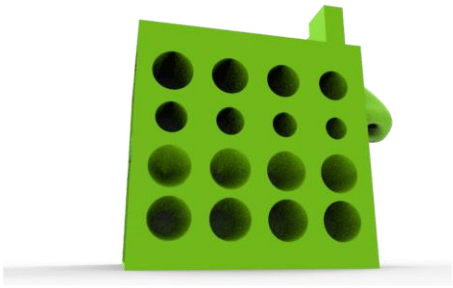

Modification: Depth developmental geometric test model was altered to compensate for triangulation.

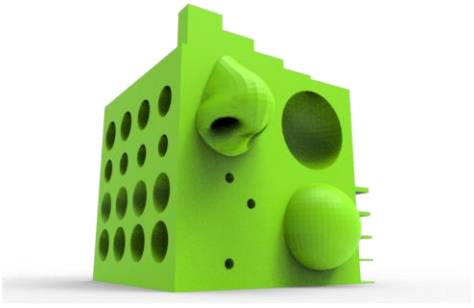

Modification: Anchor points developmental geometric test model were repositioned.
Addition: Anatomical developmental geometric test model of an nose was added.

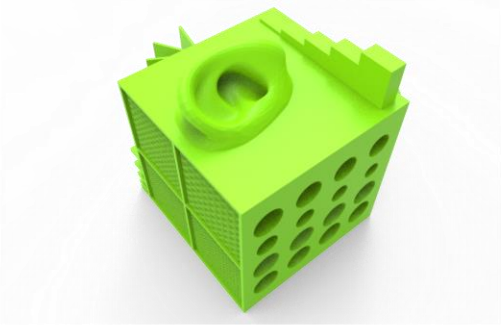

Modification: Elevation developmental geometric test model's positioning and dimensions were altered.
Addition: Anatomical developmental geometric test model of an ear was added.

Figure 3.11 Design modifications applied to the Second Test Model.

3.4.2 Fabrication of a Second Test Model

Upon finalizing all the additional and modified design features of the Second Test Model, the digital file format was converted to STL. As with the First Test Model, the Second Test Model was also produced in nylon PA12 on an EOSINT P385 laser sintering machine at the CRPM. Some post finishing was applied to the Second Test Model, which included changing its colour to grey by applying a thin layer of spray paint. Grey surfaces are well suited to scanning with a structured light hand-held scanner. Metallic inserts were also placed in the holes created for the Anchor Point Test to more accurately imitate the metallic pins used for attaching a prosthetic ear (Figure 3.12).

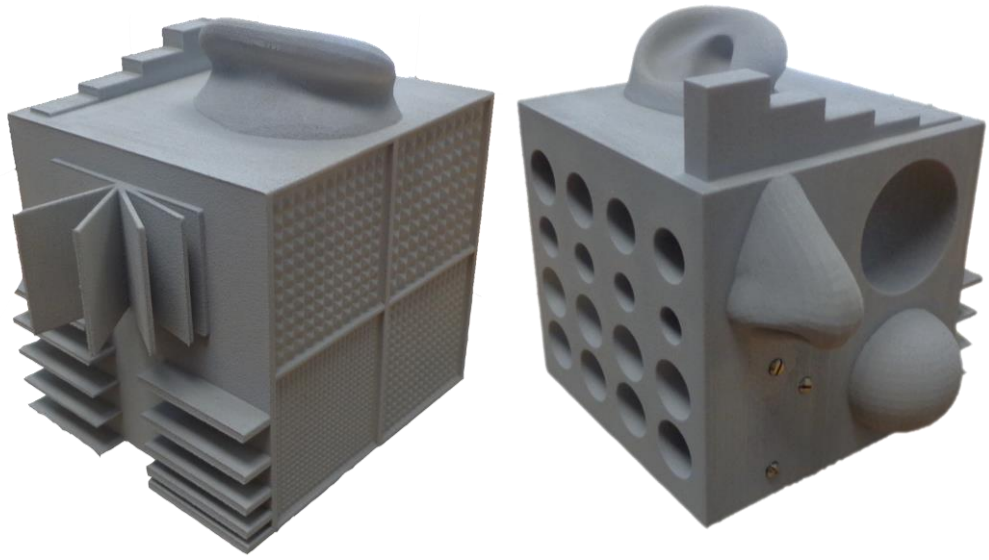

Figure 3.12 Second Test Model produced through laser sintering.

3.5 Hand-held scanning of the Second Test Model

In the second phase of the experimental stage, the research shifted towards geometric data capturing of the revised Second Test Model created in the design process using the available Artec® Spider®, hand-held scanner. The scanning process took place in a standard office cubicle with the model positioned on a rotational platform. First, several test scans were performed to get familiarized with the scan process. This entailed learning to manually operate the scanning device to obtain an appropriate scan quality and, secondly, the various post-processing steps required for converting raw scan data into a digital 3D model.

3.5.1 Artec® Spider® hand-held scanner

The Artec® Spider® is a structured light scanner that uses projected light formations to capture 3D geometric data from objects. The scanner was primarily developed with CAD users in mind but has since been adopted for several other technological applications such as automotive design, museum preservations, reverse engineering, and quality control. In addition, the Artec® Spider® has a short working distance of between 20 cm - 30 cm, making it well suited for targeting smaller and restricted areas. This is in contrast to the earlier mentioned Artec® Eva® scanner, which has a working distance of between 40 cm – 100 cm, making it more appropriate for large, full-body scans. The Artec® Spider® scanner is capable of capturing data at 7.5 frames per second at a resolution of 100 microns. It can also process one million data points per second without the need for placing tracking markers on a model. Six light-emitting diodes (LEDs) are arranged in a circular formation and used to emit pulsating light patterns onto an object. Then scan data relating to the scanned object's colour, surface texture, and geometric sizing are reflected and captured by three 3D cameras and a texture camera in the front of the scanning device. The scanning device weighs 850 grams and can work with a battery or a permanent power outlet source. Due to its relatively small size, this scanning device is highly compact and capable of working in most indoor and outdoor settings (Figure 3.13). Table 3.4 shows the scanner's specifications.

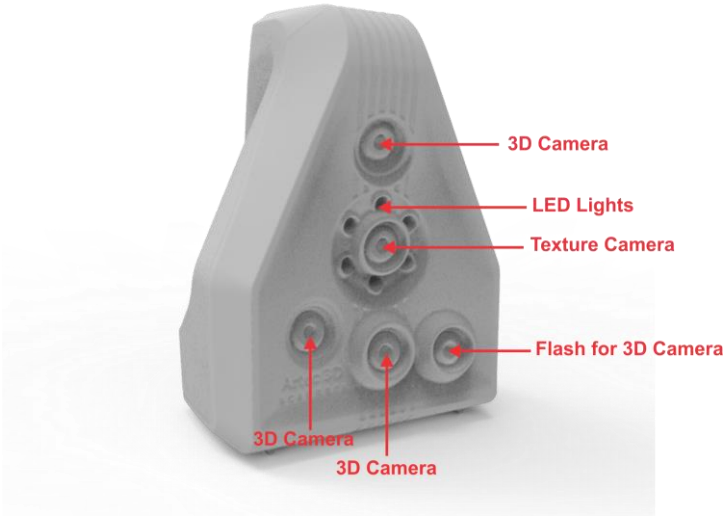

Figure 3.13 The Artec® Spider® scanning device.

Table 3.4 Specifications of the Artec® Spider® scanning device

Hardware details	Artec® Spider®
Developer	Artec 3D®
3D Resolution up to	0.1 mm
3D Accuracy up to	0.05 mm
Data acquisition speed	1 million points/sec
Angular field of view	30x21°
Cost	+/- US$ 25 000

3.5.2 Artec® Studio® software application

In addition to being a producer of scanning devices, Artec 3D® is also a developer of the renowned scan data processing software, Artec® Studio®. The software functions best when applied in combination with Artec's® range of hand-held scanners, although it can also be used with other third-party devices. This software serves a dual role during the scanning procedure. Foremost, it helps indicate the ideal distance between the scanning device and the object being scanned to create a field of view that captures adequate surface data. Secondly, it allows for the preparation, aligning, and fusing of multiple captured scans using numerous complex algorithms to create a single digital 3D polygonal model. In the Artec® Studio® software application, most processes could either be done automatically or manually. In most instances, when working with a complex geometry such as the Second Test Model, a more manual approach is required to obtain better results. The specifications of this software package are described in Table 3.5.

Table 3.5 Specifications of the Artec® Studio® software application

Software details:	Artec® Studio®
Developer	Artec® 3D®
Version	12
Year	2017
Characteristics	Processing of hand-held scan data into 3D STL models

3.5.3 Conducting a hand-held scan of the Second Test Model

During the hand-held scanning process, the Second Test Model was subjected to the Artec® Spider® structured light scanner. First, the test model was positioned on a raised platform that enables 360-degree rotation allowing scans from various angles. Because of the considerations taken earlier in the layout of test model features in the design, the prototype could easily be positioned on its sides to allow greater scanning access. The scanner was manually guided perpendicularly along the prototype model's surface. The linked Artec® Studio® application helped indicate the required optimal distance between the scanner and the scanned object to achieve the device's optimal focus (Figure 3.14).

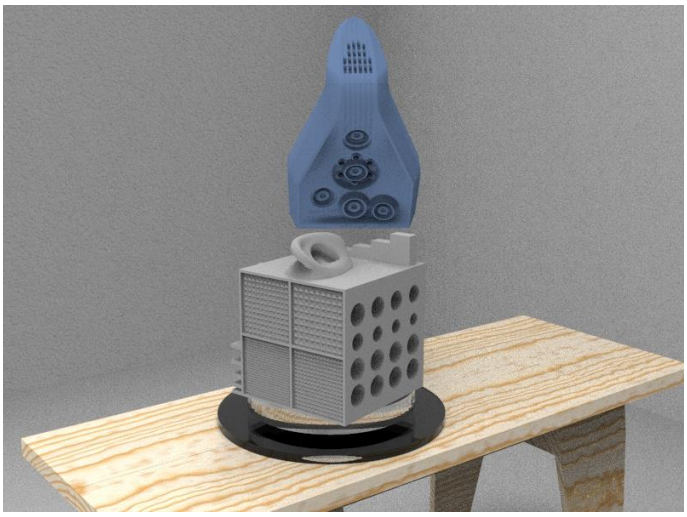

Figure 3.14 Graphic representation of the hand-held scanning process

3.5.4 Processing of scan data using Artec® Studio®

In total, 71 scans were captured using the hand-held scanning device. Afterward, the raw scan data was scrutinized, resulting in eliminations based on scan quality or for not possessing sufficient geometric features in more than one scan. The scans were subsequently reduced to 37, which were imported into the Artec® Studio® software application for further processing. The following steps attempt to illustrate the various functions and features of the Artec® Studio® software in generating a digital 3D model using raw scan data from the scanner. These features represent various algorithms that aim to clean, align, and simplify scan data into a single polygonal STL model:

Fine serial registration

Fine Serial Registration is an algorithm used to align frames generated each time a scanning procedure occurs. This is usually performed automatically upon completion or could be applied manually at a later stage. There are two methods in which this alignment could be applied, namely using the “geometry” or “geometry + texture” algorithm. When an object possesses prominent and unique features, such as the Final Test Model, it was found that using the “geometry” only algorithm produced better alignment results and was less taxing on computing due to capturing less scan data (Figure 3.15).

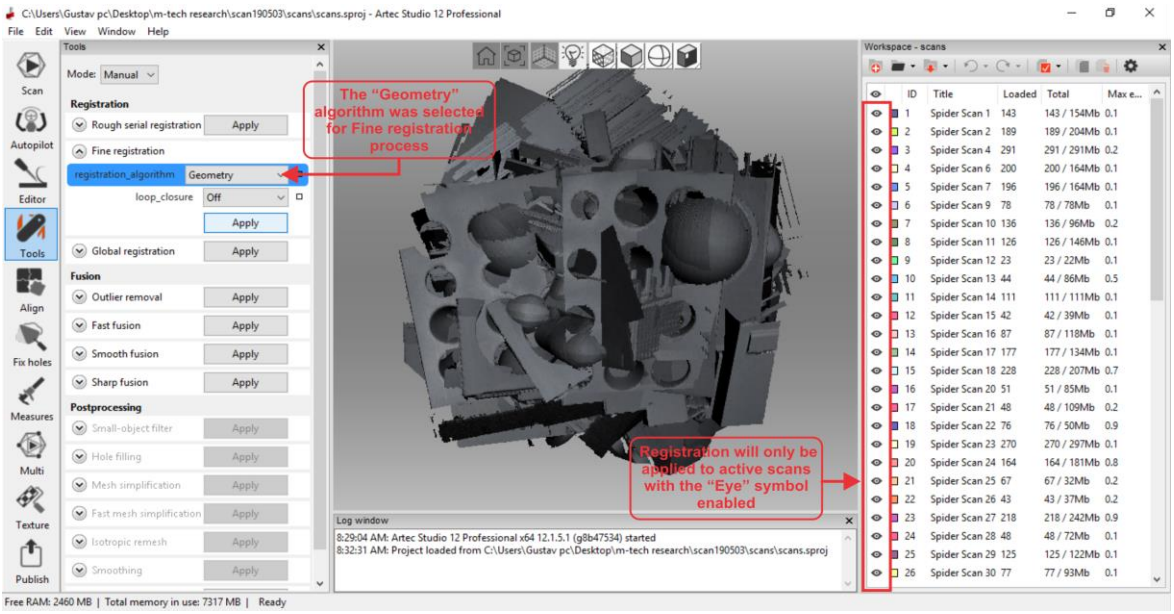

Figure 3.15 Fine serial registration

Erasing of unwanted data

In scanning the Second Test Model, some areas of the base on which the model was positioned and other random scattered points from the surrounding environment were also captured. These anomalies were eliminated using several erasing tools similar to painting features found in many modern 2D image editing software applications. By "painting" these features, they were isolated and erased from the scan by enabling the "delete" function. This was done for all scans used for generating a digital 3D model (Figure 3.16).

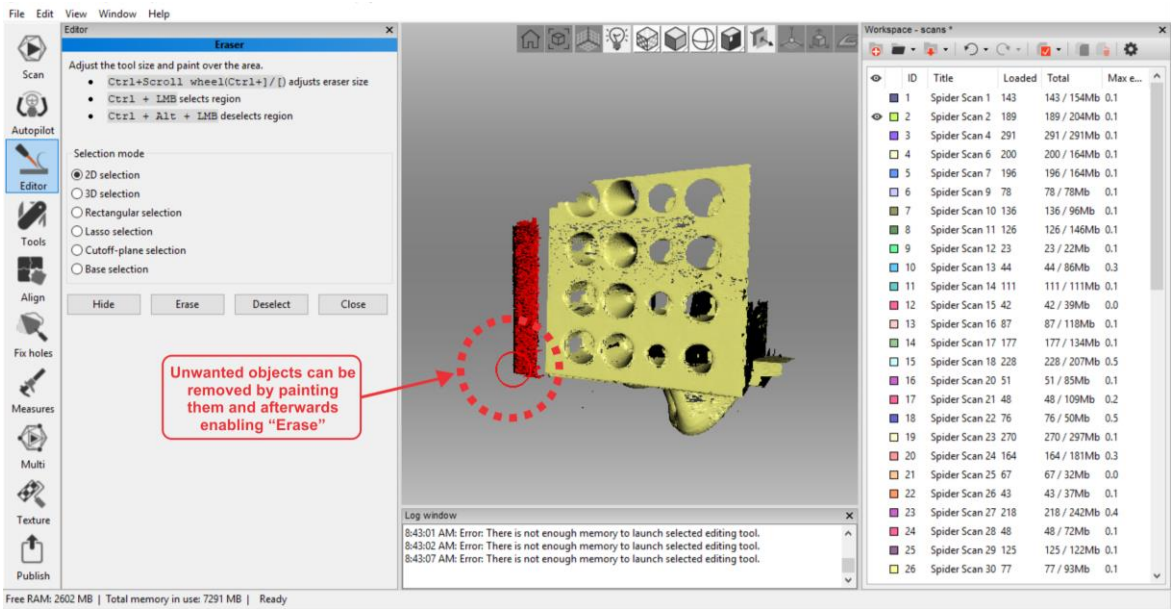

Figure 3.16 Erasing of unnecessary captured scan data.

Alignment of scans

After ridding the various scans of most anomalies, the alignment function was used to align all the multiple scans. First, the scans were visually positioned next to each other and by choosing three or more unique points found in both scans, paired together, giving it a more complete overlaid appearance. Sharp corners and depressions were most often favoured as common points since they are unique in shape and easily distinguishable throughout multiple scans. After pairing, the scans could be rotated and moved in unison (Figure 3.17, 3.18).

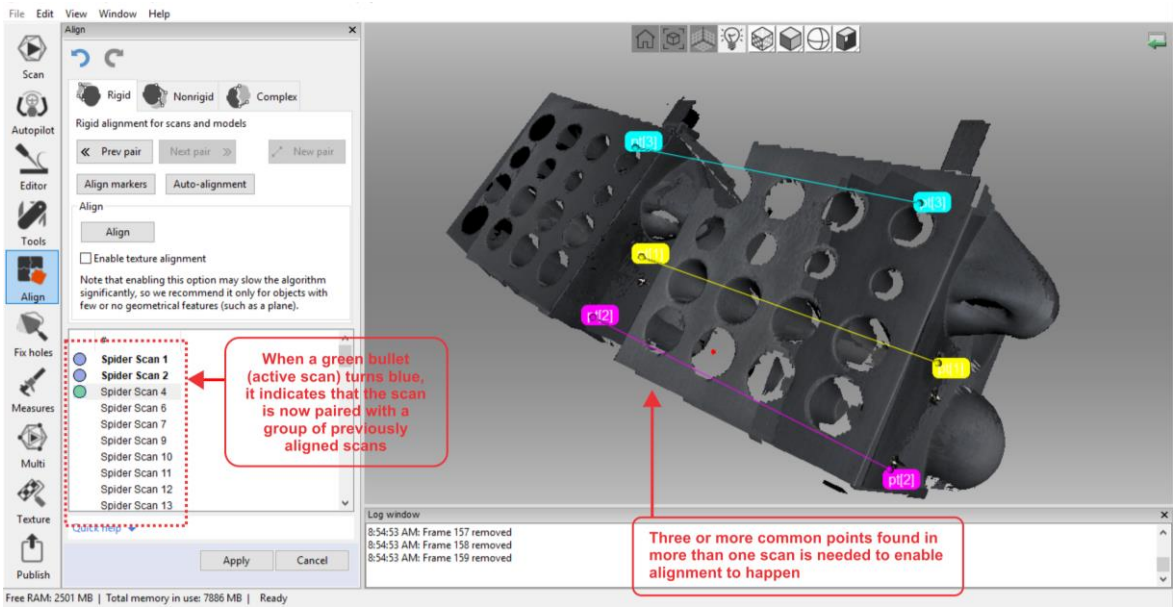

Figure 3.17 Choosing of common points.

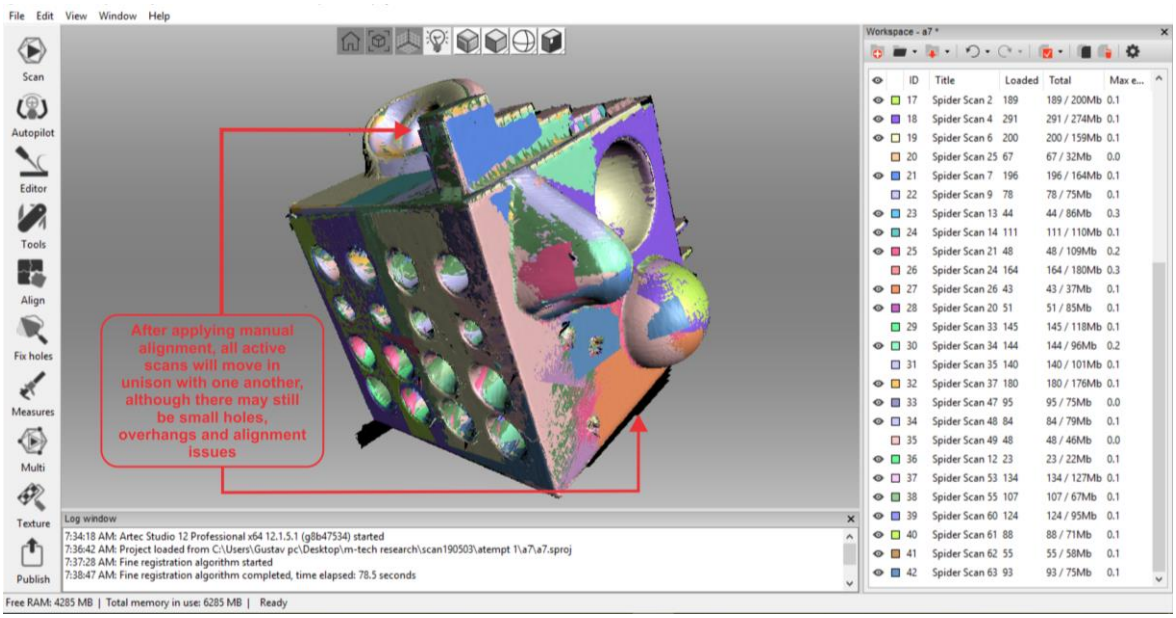

Figure 3.18 Scans aligned together.

Global registration

The Global Registration algorithm feature moved all the frames generated throughout the scanning procedure into a single coordinate system. The software does this by analysing geometrically similar features found throughout a set of scans and pairing them together. This allows for alignments to be more refined and could be applied numerous times over, which, in some instances producing better results (Figure 3.19).

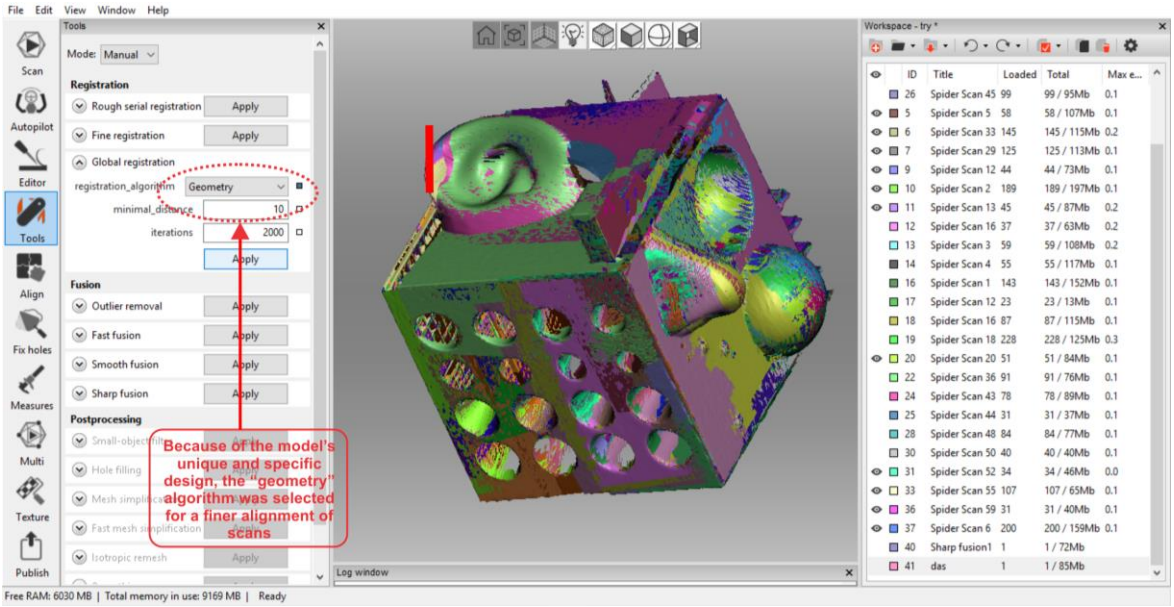

Figure 3.19 Scans moved to a single coordinate system

Outlier removal

Although most irrelevant scan data were removed using the erasing functions earlier, some small unattached geometries, known as noise, were still present in some. The outlier removal function was used to eliminate these by determining the most significant objects in a digital 3D scene and removing everything not attached to it. For this, the resolution at which the algorithm was applied was kept at 0.3% of the lowest scan quality number (Figure 3.20).

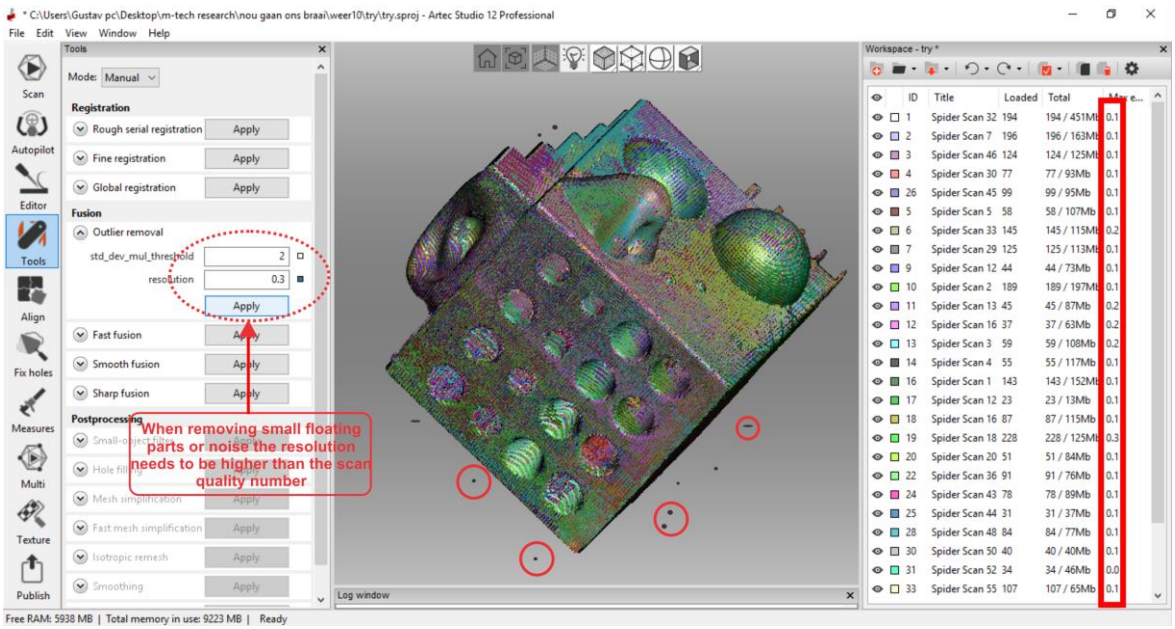

Figure 3.20 Erasing of scan noise.

Fusion

All the active scan layers that were aligned and globally registered were joined into a single digital polygonal 3D model through the fusion algorithm. Artec® Studio® provides three different methods of applying the fusion process; however, "sharp fusion" was the recommended method for working with the Artec® Spider® device. To ensure the resulting digital 3D model was without any missing geometries, the "watertight" function was chosen to automatically fill any holes or gaps that may be missing in the model's surface geometry (Figure 3.21).

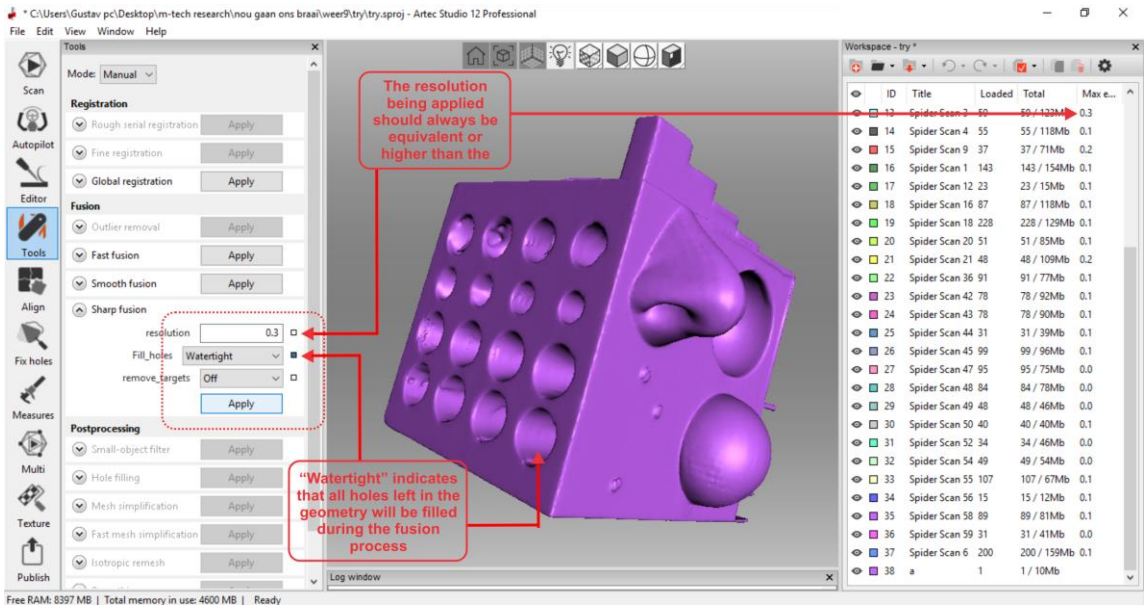

Figure 3.21 Various scans joined together.

Mesh simplification

Mesh simplification allows for the number of digital polygons that make up the digitally produced 3D model to be reduced. This algorithm feature re-arranges and eliminates excess polygons that have been duplicated or may overlap one another. This results in a reduced digital file size that is easier to transfer to other software applications for either viewing or further modifications (Figure 3.22).

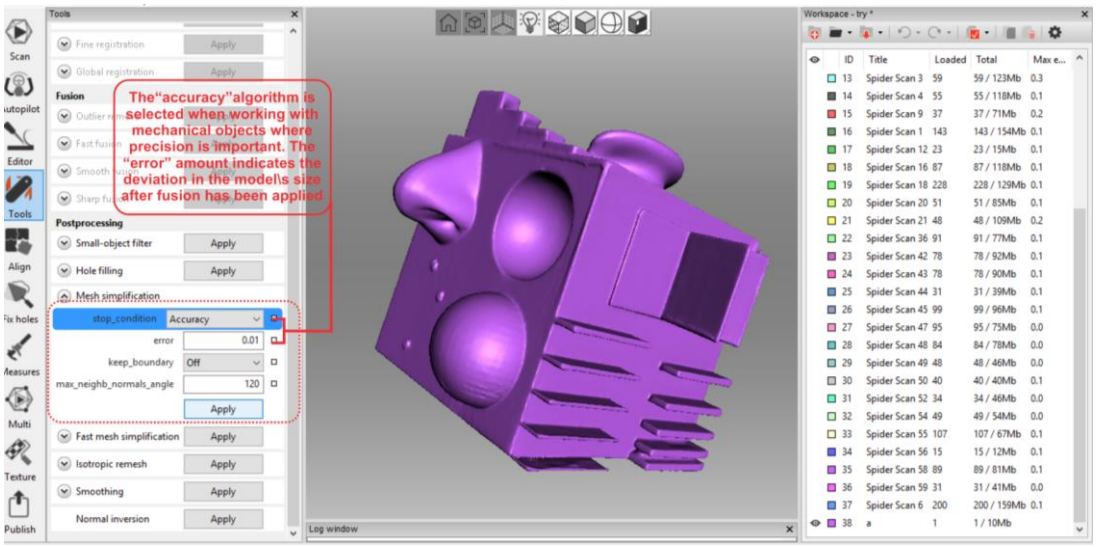

Figure 3.22 Simplified digital 3D model.

3.6 CT scanning of the Second Test Model

This study phase aimed to generate digital STL models from DICOM scan data using three selected medical image translation software applications. To perform this, the Bloemfontein National Hospital's Oncology department was approached to conduct a CT scan of the Second Test Model. The generated data was then uploaded, and through each software's unique procedural workflow, a digital 3D model was produced from each. After completion, the digital models were visually examined to determine how the test model features corresponded or deviated from one another in terms of accuracy and form.

3.6.1 Toshiba® Aquilion LB® CT scanner

The Toshiba® Aquilion LB® is a low-bed CT scanning device that has been specially designed to address diverse challenges in oncology (Figure 3.24). The scanner is currently one of the largest on the market, with an aperture of 90 cm and a scanning field of 70 cm. This enables full-body scans of patients to be performed regardless of their size or positioning while ensuring a higher picture quality across the entire image. The scanner has a row of 16 detectors that can identify various levels of radiation passing through a patient's body emitted from the X-ray source. This allows the scanning device to capture and produce DICOM images with different slice widths, resulting in various levels of detail when generating a 3D model from the scan data. The specifications of this CT scanner are stated in Table 3.6.

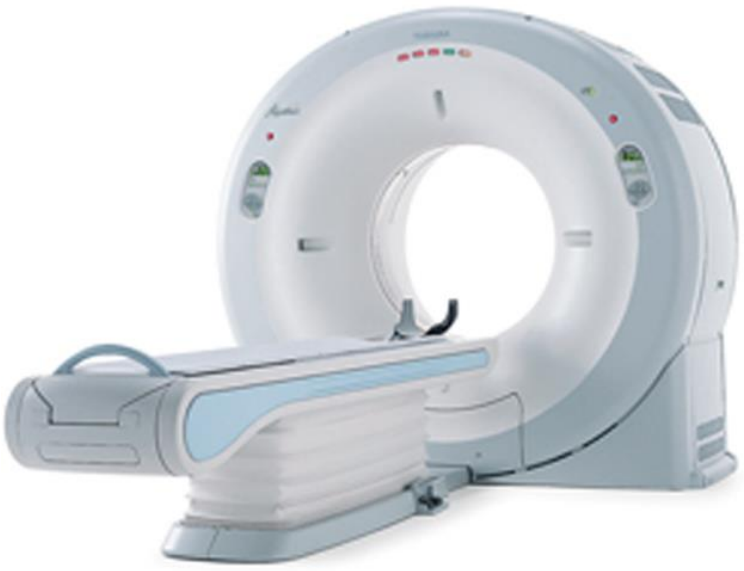

Figure 3.23 Toshiba® Aquilion LB® CT scanner.

Table 3.6 Specifications of the Toshiba® Aquilion® CT scanner.

Specification	Description
General description	90-cm large-bore CT scanner with a 16 x 0.5-mm detector architecture
Scanning mode	Multi-slice
Maximum scanning range	150 cm
Minimum temporal resolution	320 msec

3.6.2 Conducting the CT scanning procedure

The CT scanning process took place at National Hospital's Oncology Department according to the following steps: First, the Second Test Model was positioned by radiographers on the Toshiba® Aquilion® CT scanner's bed in the middle of the gantry opening (Figure 3.24). Various sets of cross-sectional DICOM image slices were scanned next, all with a thickness of 0.5 mm (Figure 3.25). Using the smallest DICOM image slice width ensured that all 3D models were generated from the highest scan quality available from the device. Afterward, the various DICOM images were evaluated, and the most suitable set was selected to generate 3D models. The chosen set consisted of 384 DICOM images slices.

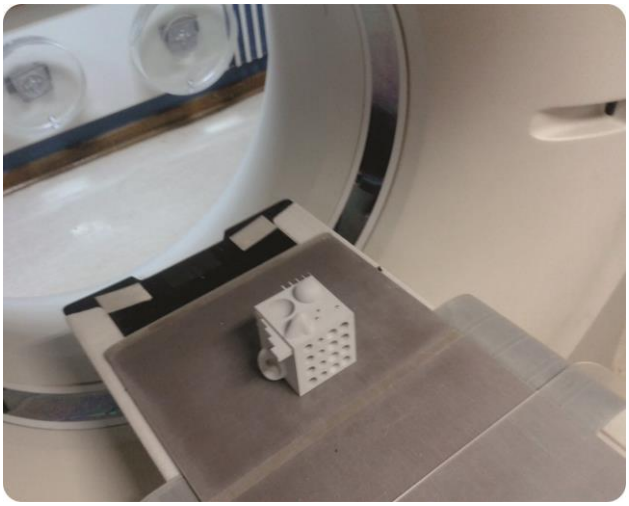

Figure 3.24 The Second Test Model positioned for CT scanning.

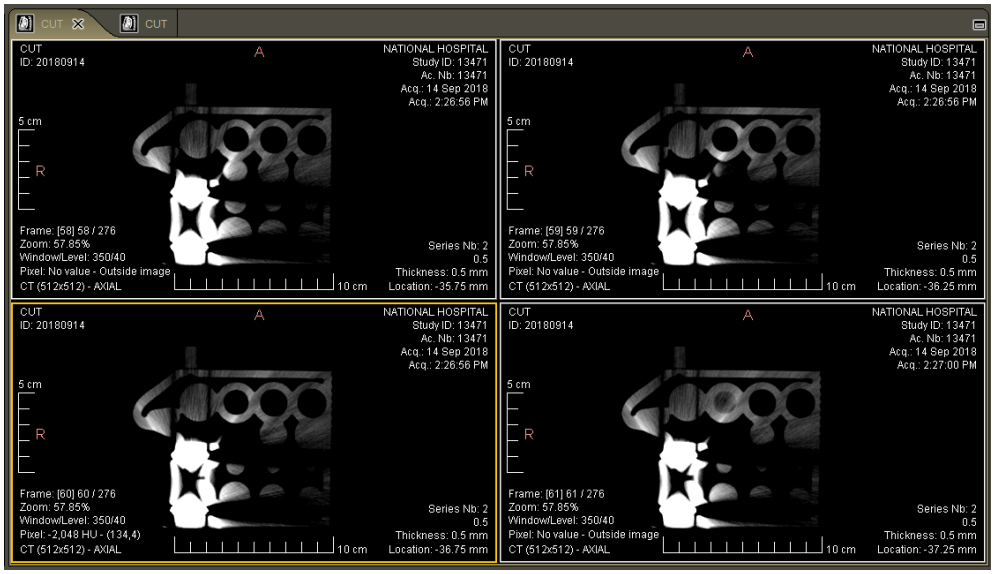

Figure 3.25 Sample of the DICOM images produced through CT scanning.

In addition to determining how hand-held and CT scanning differ in terms of accuracy, a sub-objective was to gauge how variously priced software used to translate DICOM data compared to one another in terms of accuracy. In this phase, three different medical image translation software applications were selected for processing the DICOM image data acquired from the CT scanning the Second Test Model into 3D models. The first software application selected was an open-source-based software named Invesalius®. The rationale behind choosing this software was to gauge the technological differences between commercially available and free-of-cost software applications. The second selected software application was a commercially available software application known as 3D Doctor®. The basis for choosing this software was to ascertain how similar, less expensive mid-level commercially available software compared against the well-recognized standards. The third selected software application, namely Mimics® by Belgium company Materialise®, has a well-proven track record and is generally regarded as a world leader in generating high-quality 3D models from various medical scanning modalities.

3.6.3 Processing of CT data into 3D models

3.6.3.1 Invesalius®

Invesalius® is an open-source medical image translation software that converts raw CT or MRI medical scan data into digital 3D models. Named after the famous Belgium physician Andreas

Vesalius it was initially developed by the Brazilian Ministry of Science and Technology and Renato Archer, Information Technology Centre, to digitally reconstruct 3D models from severe facial defects. Since then, it has been utilized in various areas where 3D imaging is becoming a standardized requirement such as in dentistry, veterinary, palaeontology, and anthropology practices. The 3D models generated from the raw DICOM data can be exported to numerous CAD software applications where further design modifications can be made. It has been utilized to create more than 5000 medical models since its development in 2001 up to 2017 (Amorim *et al.,* 2015).

Translation of DICOM data using Invesalius®

After uploading the selected DICOM images, the software indicated the scanning modality used, settings applied, and DICOM slice thickness. After verifying that all information was correct, the DICOM images were arranged in a 2D orthographic layout. This orientation is the axial, sagittal, and coronal slice planes, representing hypothetical planes used to identify the structures within a DICOM image slice. The next step was to isolate the relevant data in each DICOM slice by increasing the contrast between the test model's outer silhouette and darker surrounding background. For this, a colour mask was applied by adjusting the current image's "threshold" parameters to between -755 to 3071 HU (Hounsfield scale unit). Afterwards, the "generate 3D surface" function was enabled, which generated the model's digital surface using colour masks that have been automatically applied to each DICOM slice in the set. The "select largest body" function was enabled to remove any irrelevant geometries that may have been generated along with the primary 3D model. This identified the most significant object in the digital 3D scene and eliminated any anomalies that may not have been attached. The 3D model's digital file format was then converted to STL for later use in comparisons (Figure 3.26).

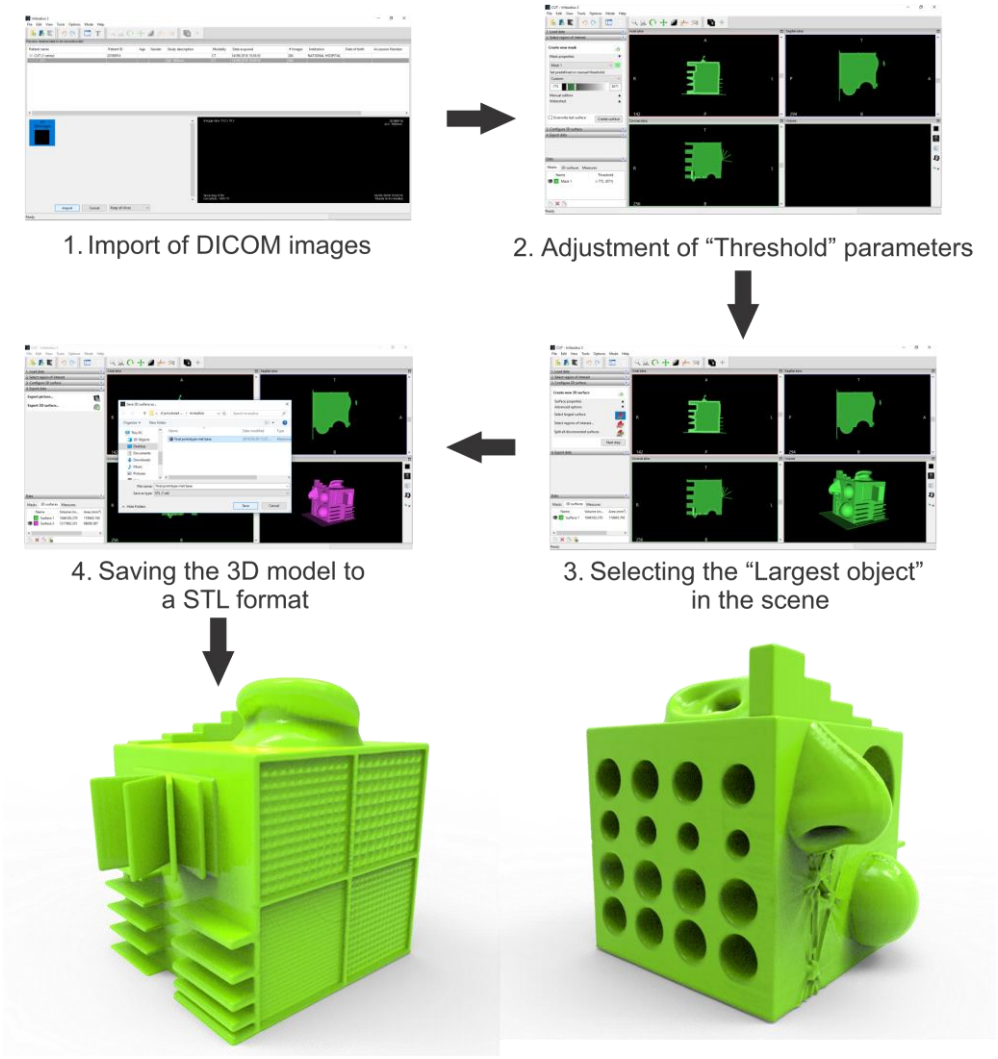

Figure 3.26 DICOM images translated to a 3D model using Invesalius®

3.6.3.2 3D Doctor®

3D Doctor® is a commercially available medical image translation software application developed by the Able Software Corporation, founded in 1993 in Lexington, Massachusetts, USA. The software application allows for 3D modelling, image processing, and measurement of anatomical data retrieved from either MRI, CT, PET, or microscopy. The software also supports colour and greyscale 2D image formats such as DICOM, TIFF, and JPEG as a raw input mediums. The generated 3D models can then be exported into various file formats such as STL, DXF, and IGES, allowing further development through CAD software or rapid prototyping methods. The software is one of few to have been assessed by the American Food and Drug Administration (FDA) and approved for medical imagery and 3D visualization applications (www.ablesw.com/3d-doctor/news.html).

Translation of DICOM data using 3D Doctor®

Upon opening the DICOM data in 3D Doctor®, the "image calibration editor" requested the confirmation of scanning information as the scanning modality used as well as the slice thickness at which the DICOM images were captured. First, a "region of interest" had to be selected, which functions to isolate relevant scan data from "noise" or other scattered geometries. This was done using the software's design tools to draw a rectangular shape as narrowly as possible around the 2D image of the model, eliminating any loose pixels falling outside this boundary. Afterwards, the "threshold" feature was enabled to project a colour mask with parameters of between 31774 and 32919 HU. Then, the "segment all" feature was enabled, which applied the colour mask to all the DICOM images within the set. Lastly, the "generate complex model" feature was enabled to produce the 3D model, which was later converted to an STL format (Figure 3.27).

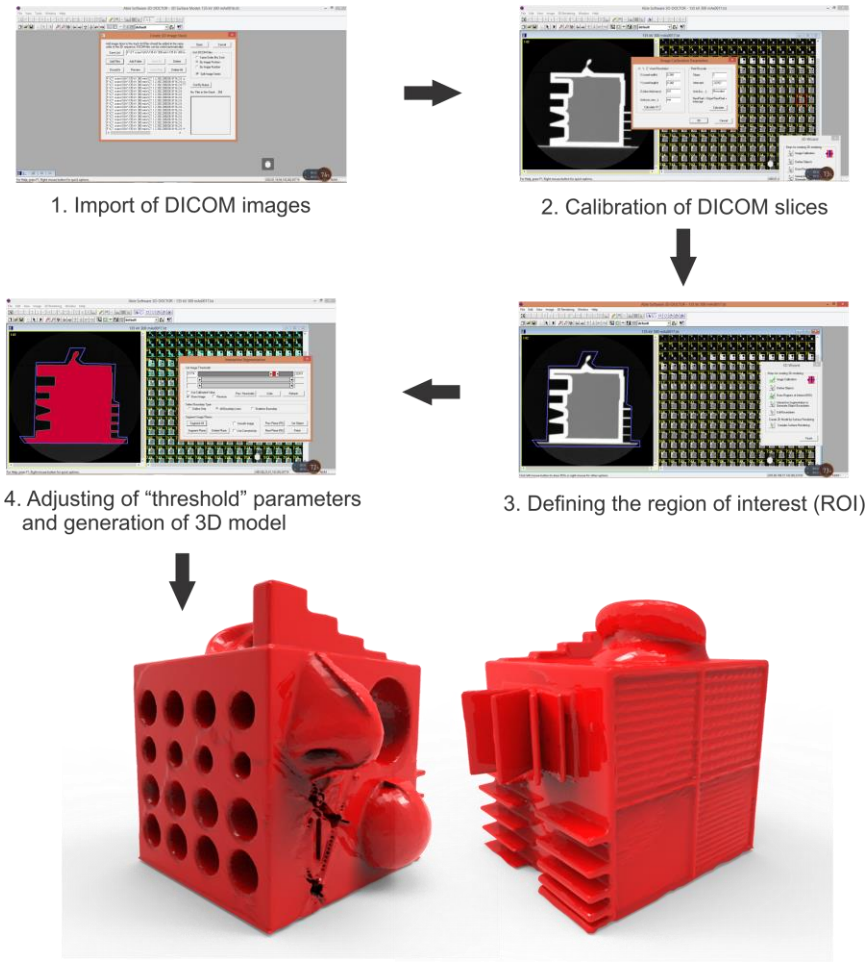

Figure 3.27 DICOM images translated to a 3D model using 3D Doctor®

3.6.3.3 Materialise® Mimics®

Materialise® is a world-renowned 3D software company started in 1990 in Belgium, specializing in developing image processing software for design purposes in various medical, dental, automotive, aeronautics, and AM fields. One particular application, namely the Mimics® innovation suite, was the first software in the world to receive clearance by the FDA to aid in providing visualizations and making diagnoses of patients through digital 3D viewing. As with most medical image translation software, the software supports a wide range of scan data inputs ranging from CT, MRI, X-ray, or ultrasound. In processing scanned data into digital 3D models, software features known as “thresholding” and “regions of interest” are further applied to refine the 3D model’s geometry. The software also supports numerous output digital formats allowing further developments through other CAD applications.

Translation of DICOM data using Materialise® Mimics®

After uploading the DICOM set to Mimics®, the scan data was displayed in a similar configuration as with Invesalius®, namely the axial, sagittal, and coronal planes. As previously, a colour mask was generated to extract relevant data from the DICOM set by adjusting the "threshold" parameters to between -934 HU to 23561 HU. Following this, the "regional growing" feature was enabled, further removing any unattached pixels falling outside the edges of the generated colour mask. The "calculate 3D" function was then activated, producing the digital model, which was converted to an STL format for later comparisons (Figure 3.28).

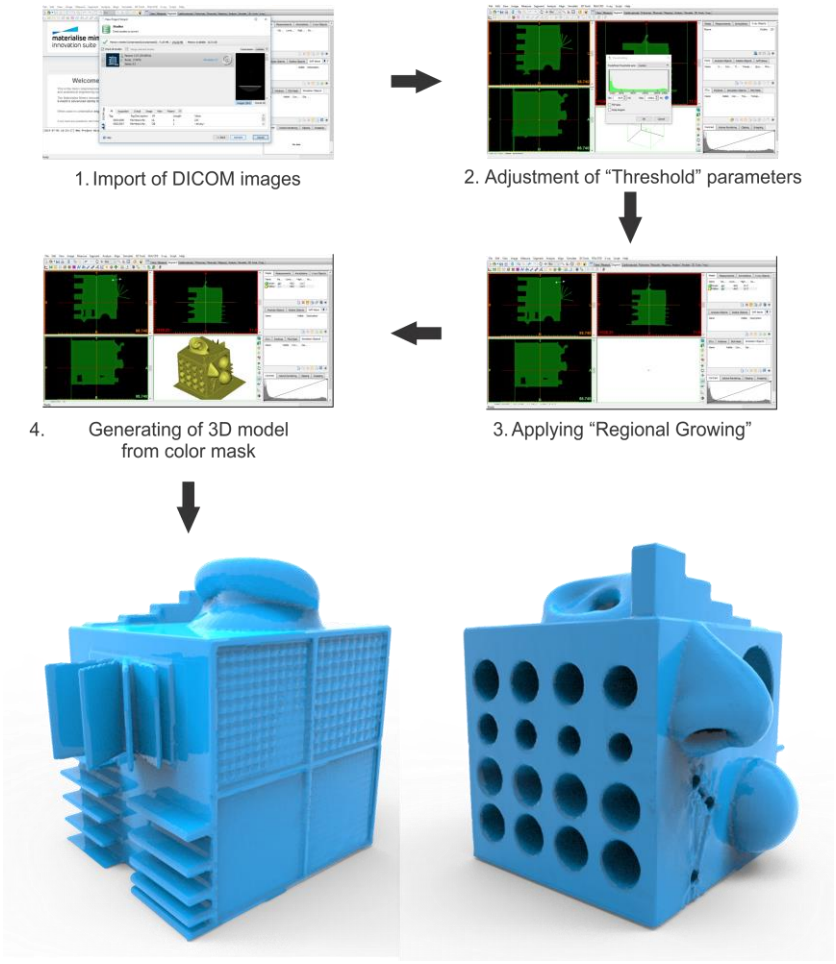

Figure 3.28 DICOM images translated to a 3D model using Materialise® Mimics®.

3.7 Micro-CT scanning of the Benchmark Test Model

In the last scanning phase of the study, the Second Test Model was subjected to a micro-CT procedure. This was done to generate an optimal digital 3D model or "Gold Standard" that represented the truest dimensional sizing of the designed test model. The South African Nuclear Energy Corporation (NECSA) produced the micro-CT STL model, specializing in non-destructive 3D X-ray scanning. Here the Mediso® NanoScan® micro-CT scanning device was utilized, which possesses a 250 mm transaxial field of view and 300 µm spatial resolution and was carried out by trained professionals.

3.7.1 Mediso® NanoScan® micro-CT scanner

The Mediso® NanoScan® micro-CT scanning device allows for functional and molecular imaging using positron-emitting radiotracers. The scanner is equipped with state-of-the-art Positron Emission

Tomography (PET) and CT detectors and data processing and reconstruction algorithms, making it one of the most accurate scanning devices on the market. The scanner is currently the only PET scanner globally with a sub-half 3 mm volumetric resolution creating high-resolution whole-body scans**.** Its Tera-Tomo reconstruction algorithm offers attenuation correction to create highly accurate 3D models through its patented Monte Carlo simulations, which removes the parallax error from scan data (Figure 3.29).

Figure 3.29 The Mediso® NanoScan® micro-CT scanner. Source: https://mediso.com/global/en/product/pre-clinical-products/nanoscanr-petct)

3.7.2 Micro-CT 3D Model

For scanning the Second Test Model, the metallic inserts used in the Anchor Point Test Geometry were removed to prevent any distortion or missing surface areas, which was apparent in all three 3D models produced from the earlier CT scanning process. The Pattern Test Geometry feature appears to have been captured fully with no visible distortion or "fading" for any of the different sized grid patterns. Factors like undercuts and overhangs in the geometry did not play a factor in translation from scan data into a 3D model. However, this was somewhat expected due to the ability of CT scanning to scan through objects. Unlike some of the other 3D models produced through CT scanning, there also does not appear to be an addition or thickness of surfaces which was apparent with the Anatomical Test feature (nose model) and upper top of the Spherical Test Geometry features (Figure 3.30).

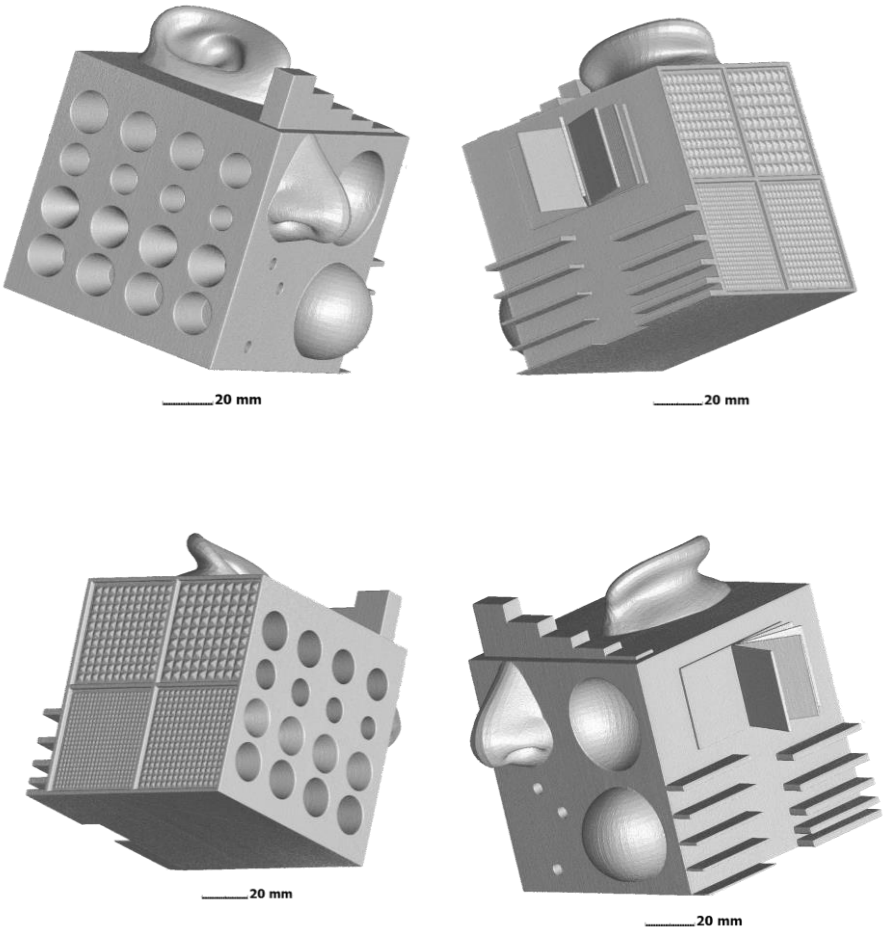

Figure 3.30 Golden Standard 3D model produced through micro-CT scanning.

Chapter 4

Results and Discussion

4.1 Introduction

This chapter presents results and discussions of the experimental work presented in Chapter 3. This includes a discussion of visual observations of the hand-held and CT scanning results of the Second Test Model and quantitative results of the scanned models compared to a micro-CT scanned model.

4.2 Evaluation of the 3D model from hand-held scanning

After finishing the scan data processing into a digital STL model using Artec® Studio®, the model was uploaded into a 3D viewing software where the following visual observations were made:

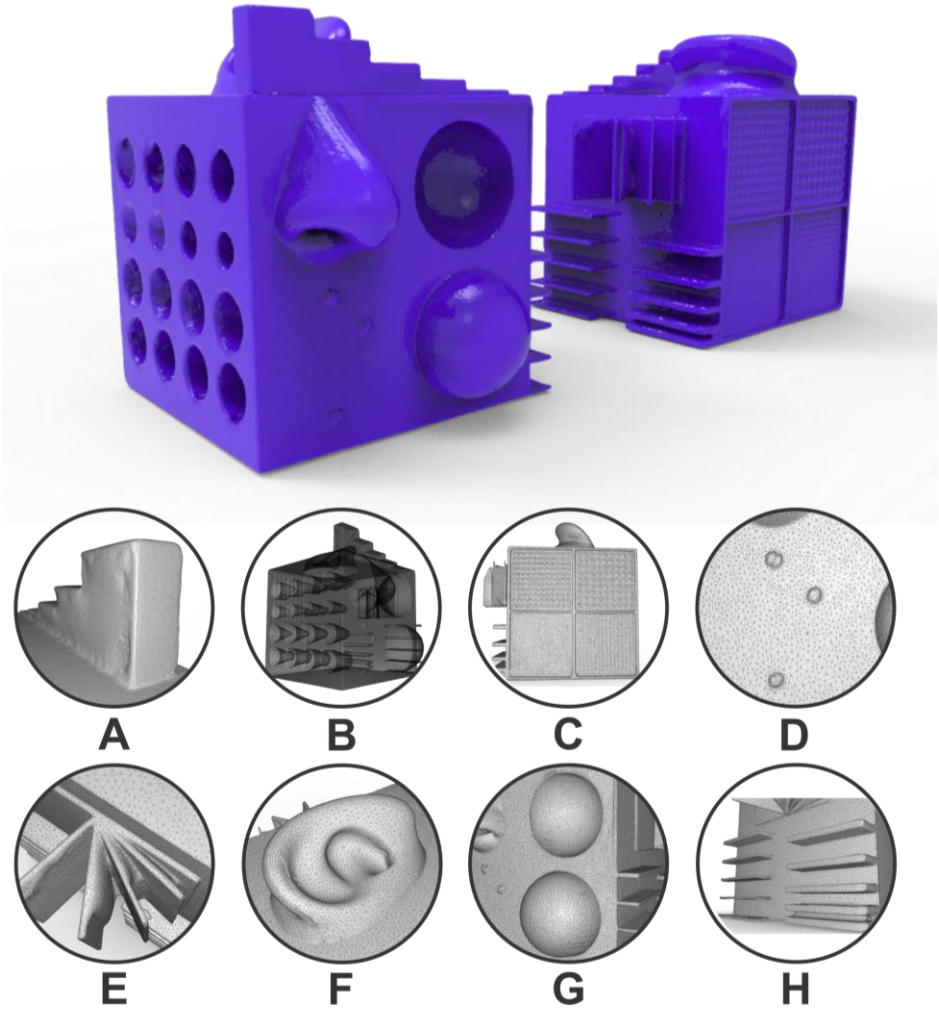

Figure 4.1 The 3D model generated from the Artec® Spider® hand-held scanner.

- The Elevation Test Geometry showed no visible difference in geometry on all five elevations, except the top elevation, which showed a small sign of misalignment at its side (Figure 4.1 A).
- In the Depth Test Geometry, the holes with their walls tapered at various angles were captured better than those angled at a straight 90-degree angle. The best feature captured in the depth test was one of the holes with a tapered pitch of precisely 21 degrees. (Figure 4.1 B).
- In the Pattern Test Geometry's scanning, it appeared that the four squares housing the variously grid-sized patterns have been captured accurately, showing no areas of missing or fading geometries in the overall patterns (Figure 4.1 C).
- For the Anchor Point Test Geometry's scanning, all metallic inserts/studs embedded into the arranged holes were captured and generated without any sign of distortion to surrounding surface areas (Figure 4.1 D).
- In scanning the Angulation Test Geometry, all features positioned at various degrees were all captured sufficiently except for the corners with a pitch of 10 and 20 degrees, which seems to have been fused towards the centre in an attempt by the software to create a “watertight” mesh (Figure 4.1 E).
- The Anatomical Test Geometry features appear to have been captured and generated successfully without any holes of missing surface geometry caused by obstructions such as intricate overhangs or undercuts in the test model's design (Figure 4.1 F).
- The Spherical Test Geometry feature displayed no visual deformation on either positive or negative geometry (Figure 4.1 G).
- The Spacing and Distance Test Geometry features presented some minor distortion. Some edges of the elements in the Spacing Test Geometry model seem to twist upwards, while the smallest spacing in the Distance Test Geometry appears to have been closed, which is very similar to the results from the Angulation Test Geometry's results (Figure 4.1 H).

4.3 Evaluation of 3D models produced by CT data translation

Upon completing the translation of the DICOM images using the three translation software applications, a visual inspection was carried out, and the following was observed with reference to Figure 4.2:

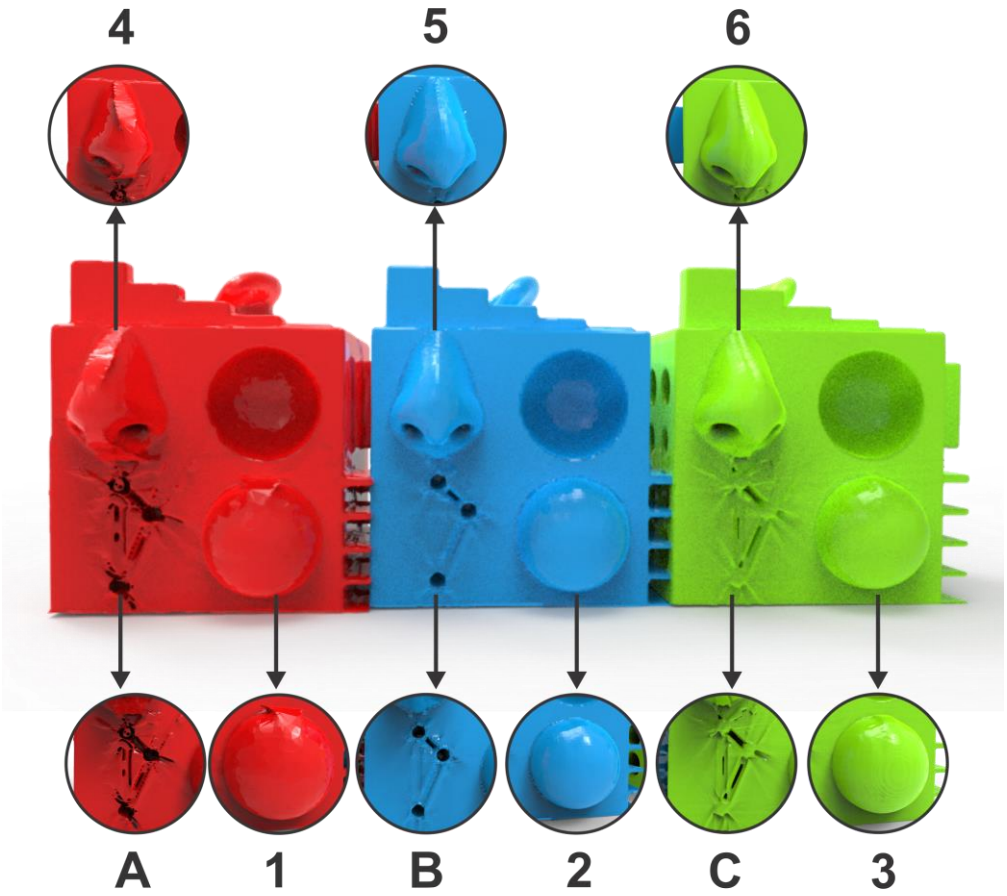

Figure 4.2 CT results of Anchor Point Test Geometry (A, B, C), Spherical Test Geometry (1, 2, 3), and Anatomical Test Geometries features (4, 5, 6).

- The Anchor Point Test Geometry, which housed three metallic inserts representing an area where a prosthesis could be attached, showed distortion and missing surface geometry in all three STL models. In this regard, it appears that the Mimics® (B) produced a better result followed closely by Invesalius® (C) and, lastly, 3D Doctor® (A).
- The Anatomical Test Geometry of the nose appeared to have a slight deviation present in all 3D models to varying degrees. The nose's bridge seems to have acquired some additional thickness, stretching from the nose's tip to connect to the main body. The Mimics® digital model (5) had the least amount of deviation, followed closely by Invesalius® (6) and lastly, 3D Doctor® (4).
- The Spherical Test Geometry feature showed no visible deviation in the positive feature; however, the negative feature did show some flaws in the models from Invesalius® and 3D Doctor®. In both these models, additional surface geometry was observed stretching from the centre of the positive sphere to the top, where it attaches to the main body. This appears to be similar to the results from the anatomical test feature. Regarding performance, the

Spherical Test Geometry features derived from the Mimics® (2) processing performed best followed closely by Invesalius® and, lastly, 3D Doctor®.

- The Depth Test Geometry feature seemed to have been translated correctly across all three software applications. The various depth, radius, and diagonal pitch of individual holes were displayed without any visual deviations. This was anticipated since the CT scanning is not restricted by undercuts or overhangs in test models when scanning (Figure 4.3).

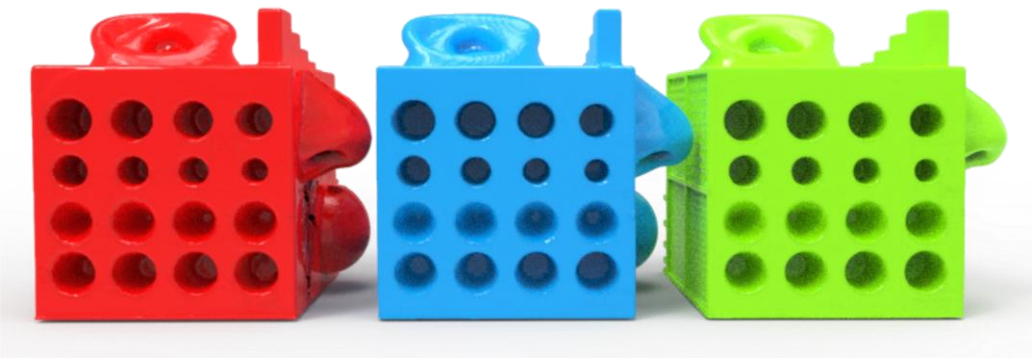

Figure 4.3 Result of Depth Test Geometry features

- One of the more noticeable differences between the various 3D models was observed in the Pattern Test Geometry feature, which is explained with reference to Figure 4.4. The 3D model produced through the Invesalius® (C) software application seemed to have performed the best, preserving all four pattern grid sizes more clearly. However, it slightly faded with showing the minor grid pattern of 2 mm x 2 mm in size. The second-best result was from the Mimics® (B) software application, which accurately displayed the two larger grid patterns sizes but struggled with producing the smaller 3 mm x 3 mm and 2 mm x 2 mm sized patterns. This 3D Doctor® (A) model's result was similar to that of the Mimics®, with the larger two grid patterns displayed more prominently while the smallest grid patterns appeared faded.

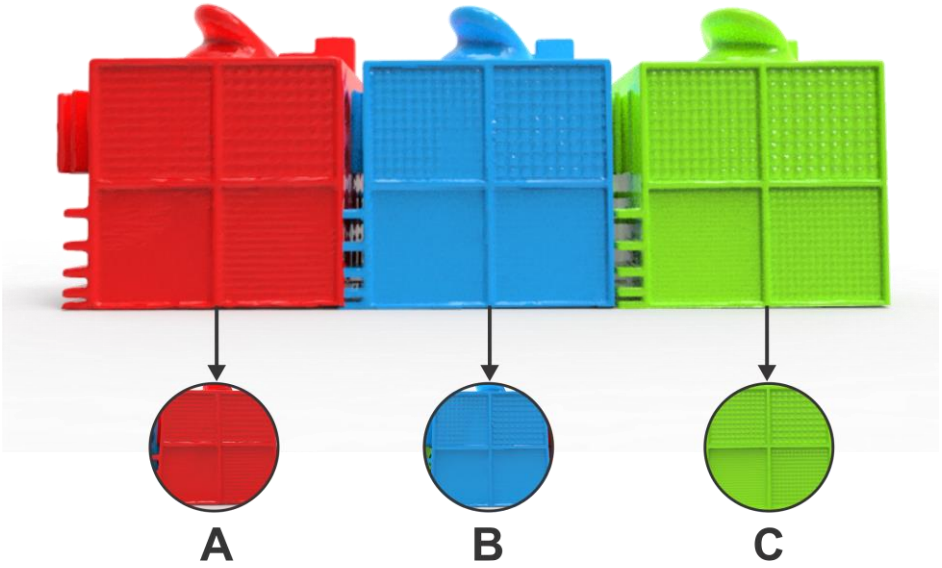

Figure 4.4 Pattern Test Geometry features translated from DICOM data

- The Angulation Test Geometry feature appeared to have been generated correctly in all software applications except the 3D Doctor® (Figure 4.5A) model. The 10° angled corner hypothetically representing the sagittal area behind the ear appeared to have been fused closed.

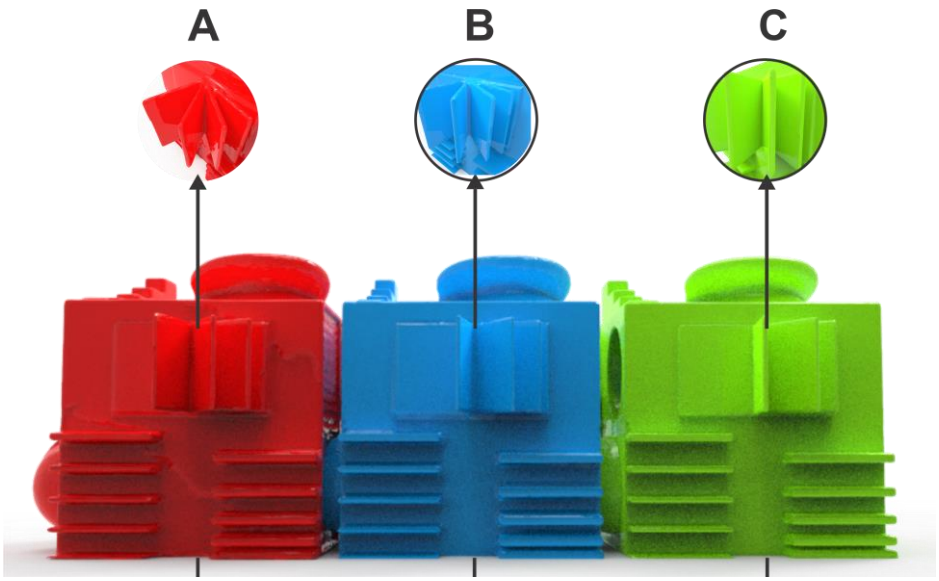

Figure 4.5 Angulation Test Geometry features translated from DICOM data

- The Elevation Test Geometry feature appeared to have been generated correctly in all three 3D models. The Anatomical test feature of an ear also seemed to have been translated

sufficiently without any visual deviations or errors due to undercuts, overhangs, or obstructions across all three software applications (Figure 4.6).

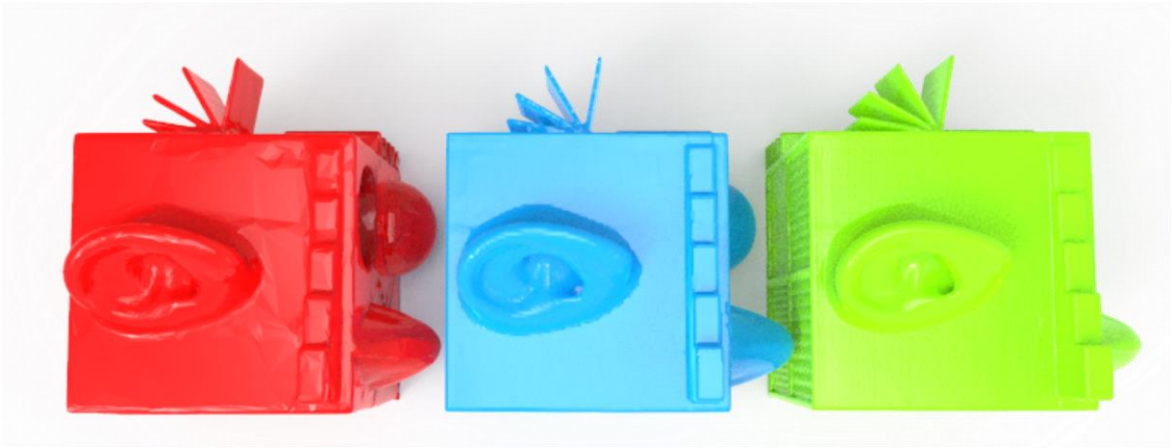

Figure 4.6 Elevation and Anatomical Test Geometries translated from DICOM data

- The Spacing and Thickness Test Geometries appeared to have been generated sufficiently except for some minor warping on the thinnest fin structure's edges. The Invesalius® model appeared to have the least deviation, followed by Mimics®, and lastly, the 3D Doctor® software package (Figure 4.7).

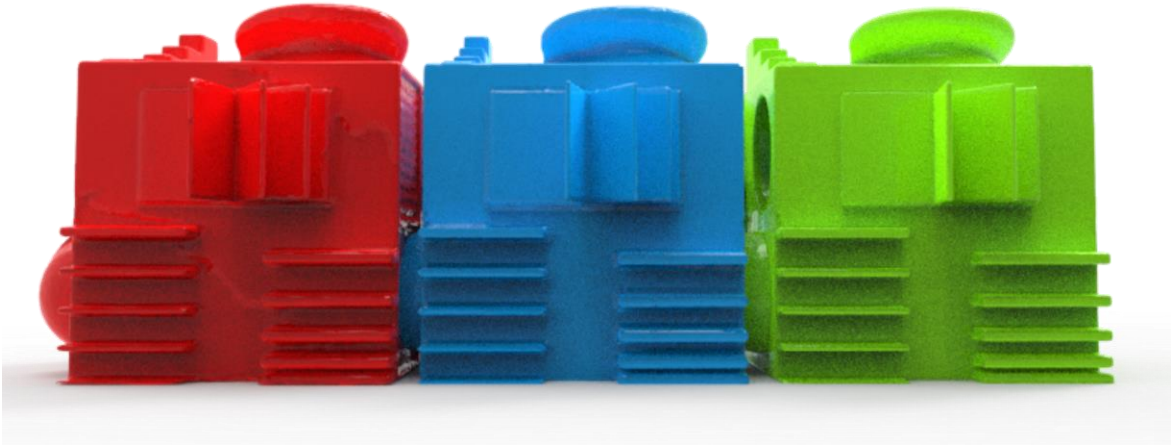

Figure 4.7 Thickness and Spacing Test Geometries translated from DICOM data.

After micro-CT scanning of the Second Test Model and producing a benchmark digital 3D model, the 3D models produced through the design, hand-held scanning, CT scanning, and micro-CT scanning were digitally readied by the Stellenbosch University's Central Analytical Facility (CAF) in order to make comparisons. The first comparison established the overall size difference between the various 3D models. These aim to highlight how the various forms of scanning and processing influenced the overall size of a processed digital model. The second method of comparison was through making use of a deviation analysis map. This aimed at highlighting how the different scanning modalities varied in capturing and producing specific areas of test model features.

4.4 Results of comparing digital 3D models

After completing all the scanning requirements for this study and producing digital 3D models from data, the models were uploaded to the MyVGL® software application. Here, the various digital 3D models were compared in terms of deviation to the dimensions of the micro-CT model.

4.4.1 MyVGL® software

MyVGL® is a free software application allowing for the viewing and documentation of either dimensional or volumetric analysis done on scanned models. The software is used in many diverse fields ranging from medical research to industrial CT scanning and animations. The data inputs could be derived from either X-Ray CAT, MRI, PET, SPECT, or Confocal Laser microscopy. The software generates image deviation maps based on differences of dimension and size between 3D models.

4.4.2 Comparing CAD design and micro-CT model

In order to determine how accurately the Second Test Model was fabricated through laser sintering, the CAD design was compared to the micro-CT scan of the model. After generating a digital model from the micro-CT image data, the CAD and micro-CT STL models were uploaded to the MyVGL® software application. After digitally superimposing the models and using a deviation analysis map, MyVGL® displayed that the model generated through the micro-CT scanning process was 3.31% greater in size (Figure 4.8). Since the Second Test Model was printed using thick walls, some shrinkage of the nylon model may have taken place while cooling after the printing process. The deviation map also indicates that these size differences are not unilateral and were more significant along the Y and Z axis (Figure 4.9).

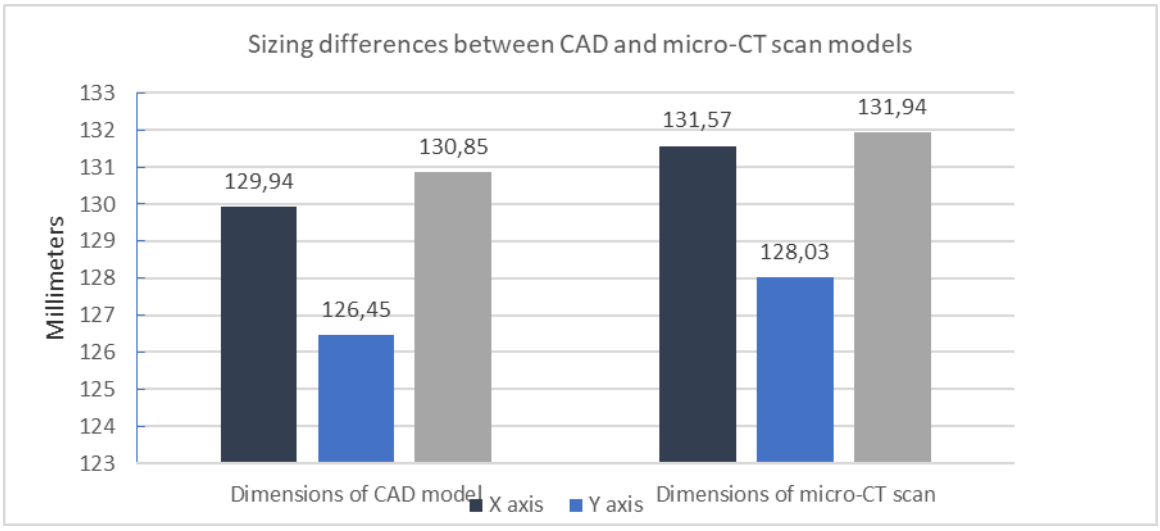

Figure 4.8 Sizing difference between CAD of Second Test Model and micro-CT.

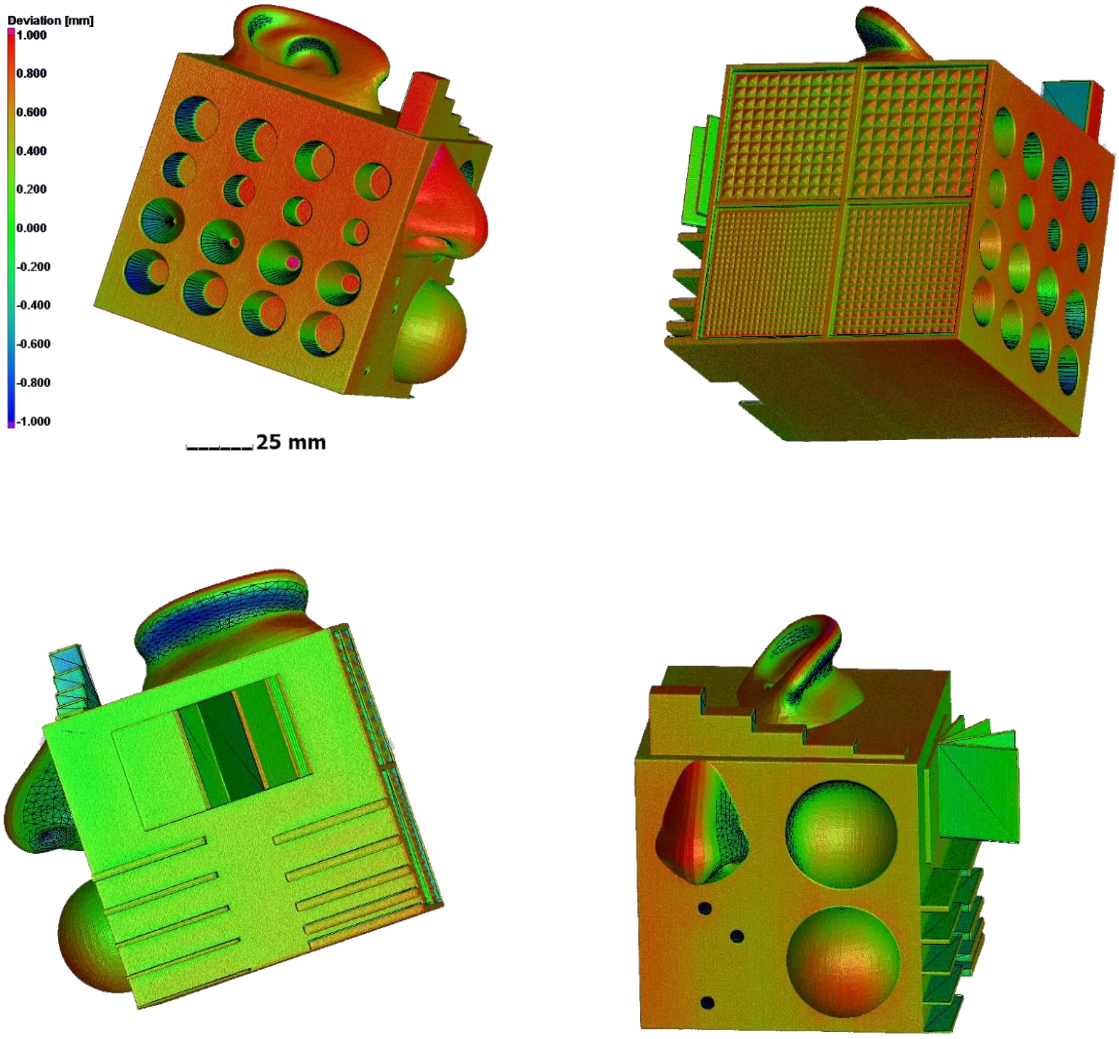

Figure 4.9 Deviation analysis map between CAD and micro-CT of Second Test Model.

The oversized printed model implies that the laser sintering process did not produce the model accurately according to the CAD. Since the nylon shrinks slightly after cooling down in the laser sintering machine, parts are printed oversized according to a scaling factor. In this case, the scaling may have been set slightly too high resulting in an oversized model.

4.4.3 Comparison between Artec® Spider® model and micro-CT model

The second comparison was between the STL model produced from the Artec® Spider® scanner and the micro-CT scan of the printed Second Test Model. It is important to note that the comparison was with the micro-CT scan of the actual printed model and not with the CAD of the model. The inaccuracy in printing the model was therefore taken into consideration since the hand-held and medical CT scans were also taken of the printed model. The software analysis showed that the STL model generated from the Artec® Spider® was slightly smaller than the micro-CT, having a difference of 0.42% in volume (Figure 4.10). Other variations in both the Depth, Angulation, and Distance test features were also observed. It is believed that these resulted from certain margins being too small or overhangs and undercuts, restricting the line of sight of the hand-held scanner. These differences are displayed in colours ranging from dark magenta to red glow in the deviation analysis image (Figure 4.11). Compared to all other STL models in which the metallic inserts were present, the Artec® Spider®'s digital model showed no disturbance surrounding these areas since the scanner uses projected light instead of X-rays such as with the CT scanner.

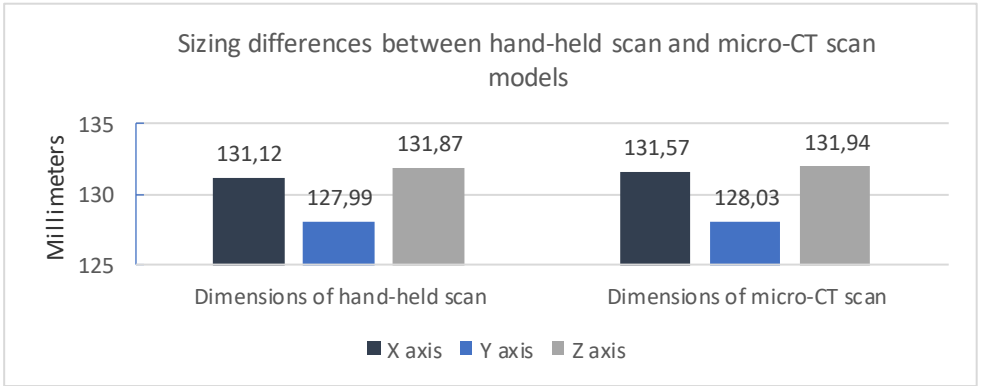

Figure 4.10 Size difference between Artec® Spider® and micro-CT.

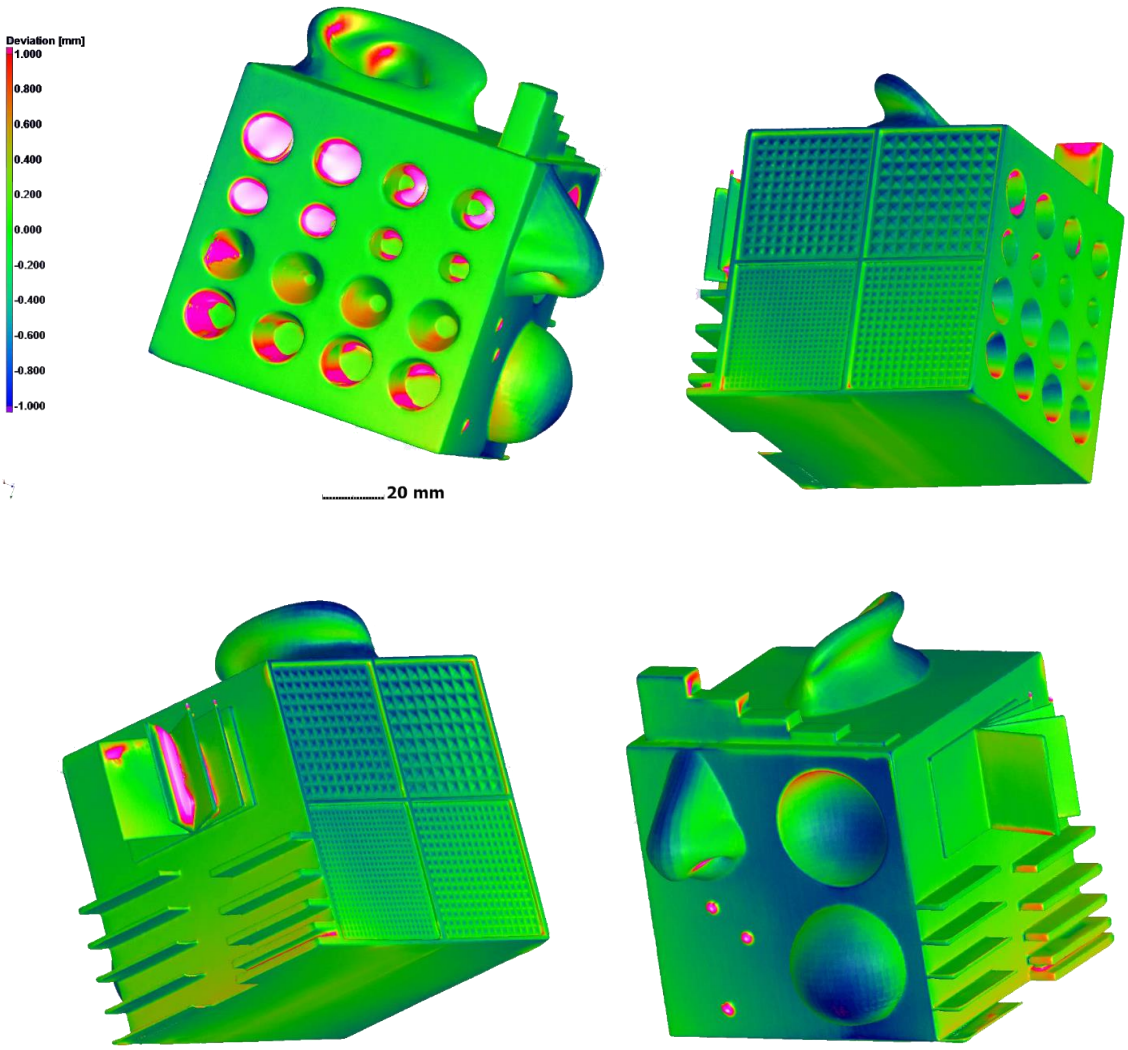

Figure 4.11 Deviation analysis map: Artec® Spider® and micro-CT.

4.4.4 Comparison between 3D Doctor® and micro-CT

For the third comparison, the STL model generated from medical image translation software application 3D Doctor®, was compared against the micro-CT model. Like the previous digital model comparison, the STL model's sizing appears smaller, with a volumetric difference of 4.05% (Figure 4.12). In the deviation analysis image map, the first apparent visual difference from the previous model is deformations around the metallic inserts' areas. It is believed that the scattering of X-rays causes disturbances in DICOM images leading to missing surface data when translation to the 3D model is applied. Another visual difference was the absence of more delicate details of the Pattern Test feature. The minor areas appear smoother than the larger patterns, with additional shrinkage indicated by the magenta colour (Figure 4.13). Additionally, no deviations were found with the Depth, Angulation, or Distance Test features, as with the Artec® Spider®'s model.

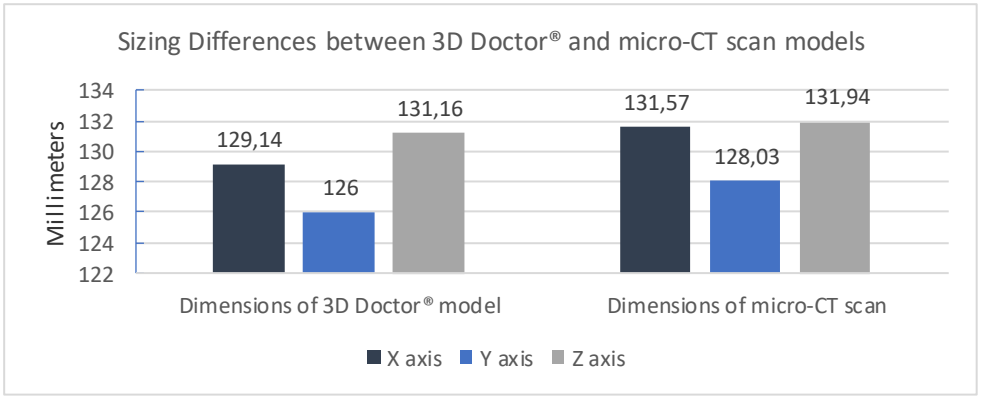

Figure 4.12 Sizing difference between 3D Doctor® and micro-CT

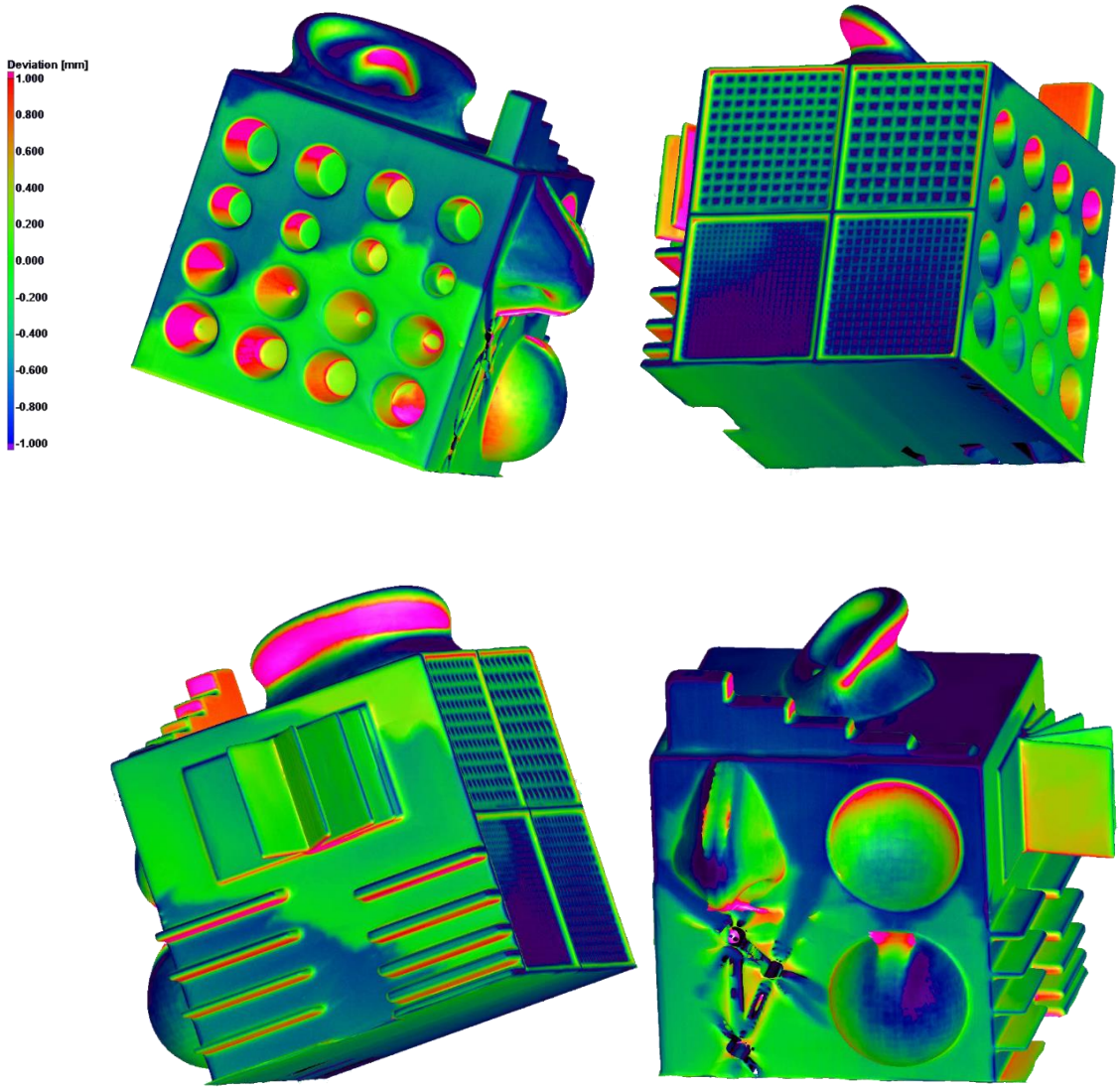

Figure 4.13 Deviation analysis map: 3D Doctor® and micro-CT.

4.4.5 Comparison between Invesalius® and micro-CT

In the third comparison, Invesalius® was the second software application, that used CT scanning and DICOM translation to produce a 3D model. As with the previously created STL models from both CT and hand-held scanning, the Invesalius® model appeared smaller, with a volumetric difference of 4.20% (Figure 4.14). Visually inspecting the deviation analysis image map, the first apparent difference was disturbances and missing mesh geometry surrounding areas that housed the metallic inserts in the Anchor Point Test Geometry (Figure 4.15). The reason for this is believed to be like those mentioned in the 3D Doctor®'s comparison. The Pattern Test features appear to be more prominent and clearly defined than the 3D Doctor® model, displaying all four grid pattern sizes, although slightly smaller in size, as indicated by the cyan to dark blue.

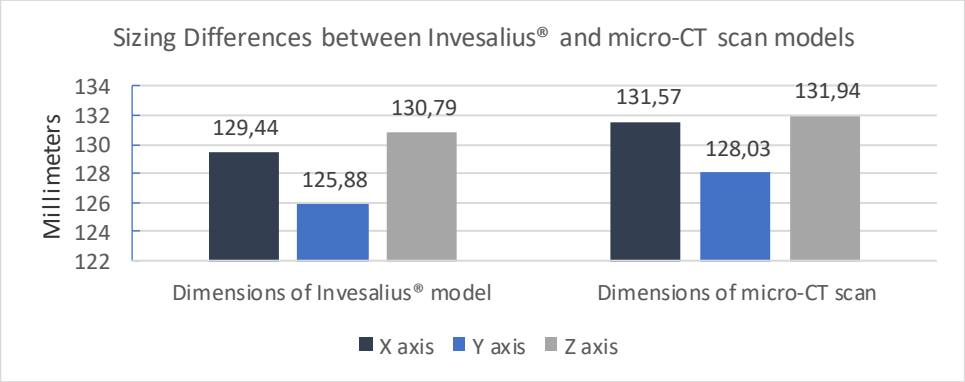

Figure 4.14 Sizing difference between Invesalius® and micro-CT.

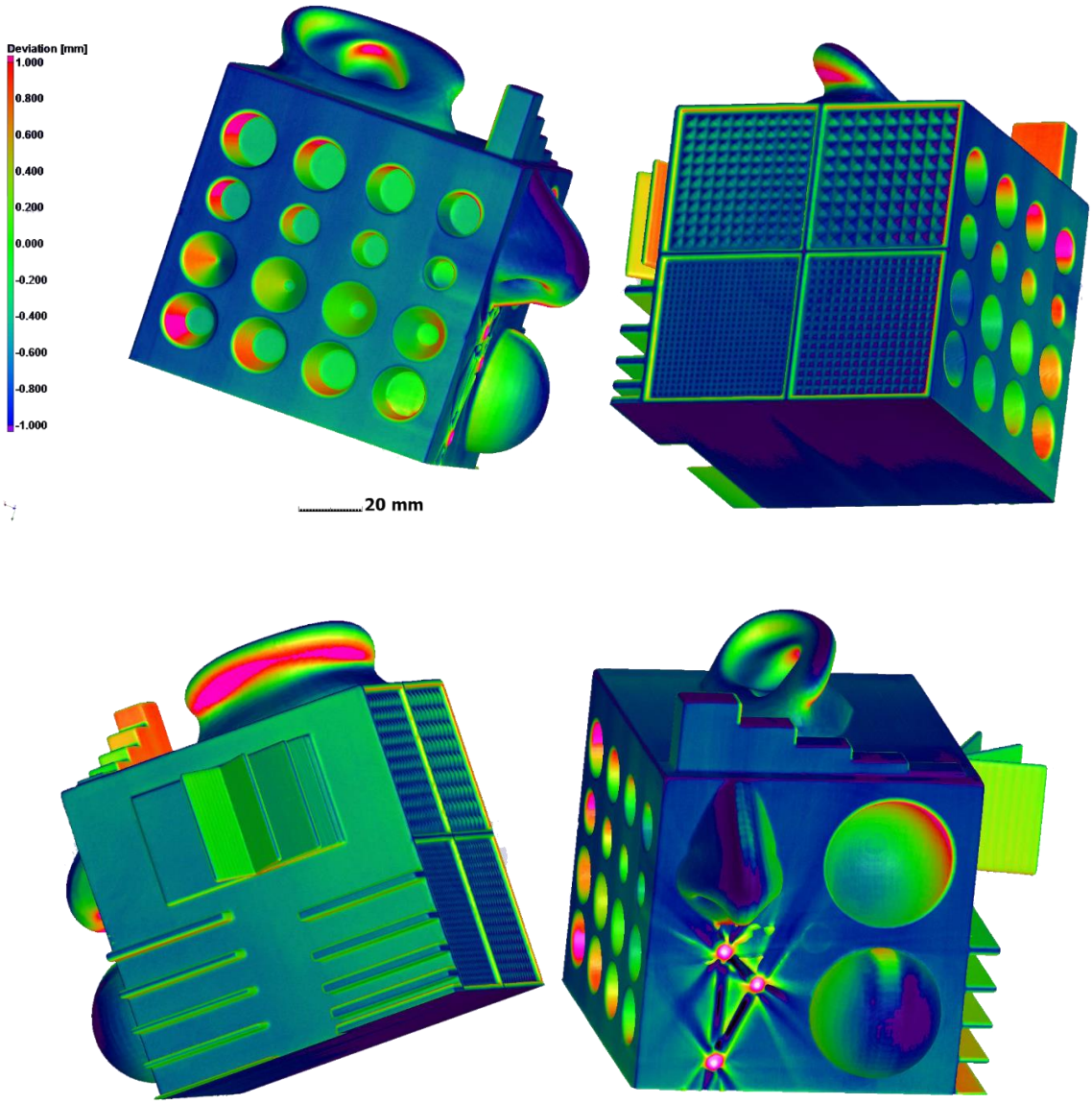

Figure 4.15 Deviation analysis map: Invesalius® and micro-CT.

4.4.6 Comparison between Materialise® Mimics® and micro-CT

The STL from the Materialize® Mimics® software package was compared against the micro-CT in the fifth comparison. As with all other compared STL models, this model appeared somewhat smaller, with a volumetric difference of 5.00% (Figure 4.16). Upon visual analysis, one could clearly distinguish all the finer geometries in the Pattern Test, to a greater extent than those shown in the 3D Doctor® model, although similarly undersized as the Invesalius® 3D model (Figure 4.17). Other features seemed to be very clearly defined, except for missing surface data around the Anchor Point Test feature similar to previous comparisons.

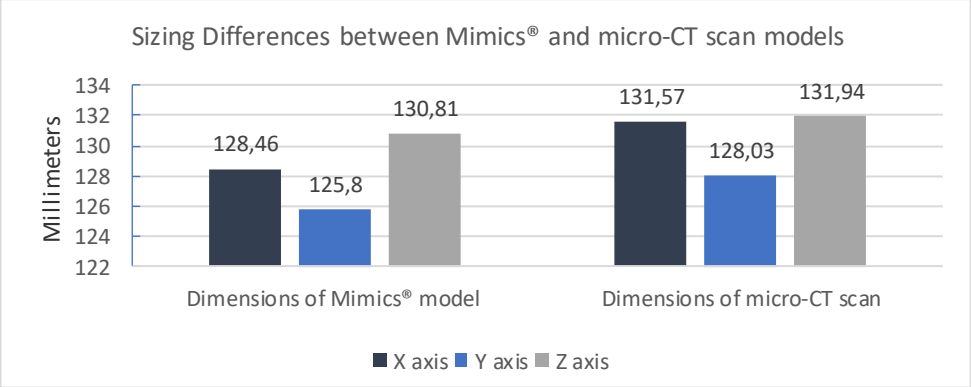

Figure 4.16 Sizing difference between Mimics® and micro-CT.

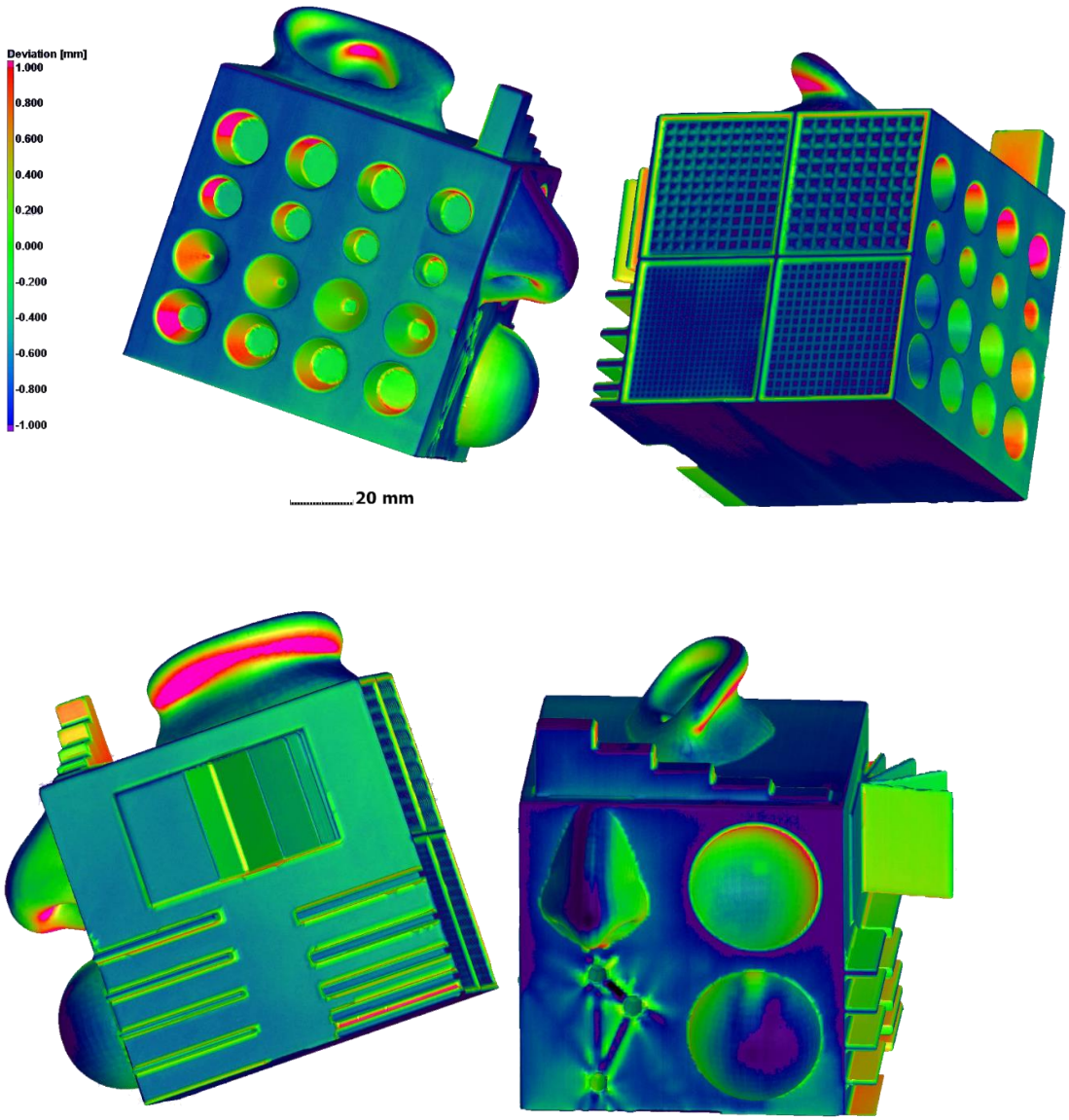

Figure 4.17 Deviation analysis map: Materialise® Mimics® and micro-CT.

Chapter 5

Conclusions and Future Work

5.1 Conclusion

This study aimed to investigate if a 3D hand-held scanner could generate sufficiently accurate digital data to make it suitable for the fabrication of maxillofacial prostheses. To achieve this aim, three objectives were set. The first objective was to determine what research has been performed by other researchers in this field of study. The second objective focussed on the design and fabrication of a Test Model to compare the accuracy of the digital data generated by the hand-held scanner with the digital data generated by a CT scanner. Under the third objective, the Test Model was to be scanned with the hand-held and CT scanners and compared to a scan of the same model taken with a micro-CT scanner. This comparison was then used to indicate the accuracy of the hand-held scanning and show its suitability for maxillofacial prosthesis fabrication.

In order to meet Objective 1, an extensive literature review was undertaken and was presented in Chapter 2. Various literary sources were reviewed to determine how maxillofacial prostheses were fabricated through traditional manual techniques and how this is improved on using modern CAD/CAM techniques. Different test geometries were developed to test the accuracy of AM processes; hand-held scanning and CT scanning were also presented. From this chapter, it was concluded that although CAD/CAM techniques present many advantages, CT scanning, which is most commonly used to determine facial geometry, is expensive, and patients in rural areas have limited access.

As a possible solution to this problem, 3D hand-held scanning was proposed as an alternative to CT scanning for determining facial geometry, as described in Chapter 3. In order to compare the accuracy of these scanners, a Test Model was designed and fabricated to highlight the strengths and weaknesses of the two scanning modalities, thereby meeting Objective 2 of the study. The designed Test Model consisted of various individual test features aimed at measuring accuracy. The first design iteration was based on determining specific numeric accuracy, while a later version (Second Test Model) included facial features to help demonstrate possible expected results from scanning an actual patient. Using laser sintering technology to fabricate the test models ensured

fewer design restrictions. No support structures are required in the printing process, making it possible to include undercuts and overhangs in the test model's geometry.

The Second Test Model was scanned using an Artec® Spider® hand-held scanner. The hand-held scanning process showed limitations in fully capturing areas obstructed by the device's "line of sight." This was evident in Depth, Spacing, and Angulation test features. The Depth test feature determined a correlation between the diameter and depth of a hole and the ability to fully capture it. This is believed due to the triangulation principle, which produced missing surface geometry due to smaller diameters at increased depths, restricting light reaching the bottom or the 3D camera from capturing any reflection. In capturing the Angled Test Model Feature, a similar problem was observed. This was seen between features of the test model where the corner of angulation ranged from between 0 and 15. Again in scanning the Spacing Test Model feature, this was observed where the spacing increments between features were too small to allow for the light patterns to penetrate between features, leading to unscanned areas of missing surface data. To compensate for this, the software would attempt to join or bridge any remaining data points together in an attempt to create a "watertight" STL mesh capable of fabrication; however, this may have some varying results.

However, all other features showed the minimum deviation from the Micro-CT's Golden Standard model, especially regarding the Pattern Test Model, which produced the most favoured results apart from that of the Micro-CT scan of the Second Test Model. The metallic inserts representing an area where a prosthesis could be attached showed no missing digital surface geometry due to exposure to radiation as seen in all other CT-produced models.

CT scanning was performed on the Second Test Model using a Toshiba® Aquilion® CT scanner. DICOM images from the CT scanner were translated using three differently priced DICOM image translation software applications from where a 3D model was generated from each. The CT scanning and processing of scan data through three chosen image translation software applications produce many similar and varying results. Test features housing metallic inserts lead to scattered pixels in DICOM image slices leading to missing digital 3D surface geometry in all 3D models from the various image translation software applications. There also appears to be varying accuracy in capturing finer surface detail. However, overhangs and undercuts did not present any problems in fully capturing the geometry of the Second Test Model.

The Second Test Model was next scanned with a Mediso® NanoScan® micro-CT scanner to obtain a highly accurate 3D model of the Test Model. The 3D model from the hand-held scanner and models translated from DICOM images were digitally compared to the micro-CT model through deviation maps, and results were presented in Chapter 4. This meets Objective 3 of the study. It was found that the deviation between the 3D model from the hand-held and the 3D model from the micro-CT was the least. In terms of comparing accuracy between the micro-CT 3D model and those produced through CT, it was found that the 3D Doctor® performed the best in terms of size accuracy but showed a significant amount of loss in displaying finer details. Materialise® Mimics® showed a slightly smaller 3D model, although displaying better ability in displaying finer details. The 3D model produced from the Invesalius® software application was also smaller than the micro-CT 3D model but to a lesser extent than the Mimics® 3D model. It also showed a similar level of detail in geometry to Mimics®. All 3D models produced from the CT scanning process showed a loss in digital surface geometry around areas that housed metallic inserts in the test model.

Learning how to operate the hand-held scanner and associated software is not difficult and is easily managed by most people. In comparison, a medical CT scanner can only be operated by a suitably trained radiographer, and patients are exposed to ionizing radiation during the scanning process. Patients are also required to lie down during CT scanning which deforms facial features to some extent, especially with obese patients. Hand-held scanning can be performed with the patient in a sitting position with facial features in a natural position resulting in a better fitting prosthesis. Hand-held scanners are also vastly less expensive than CT scanners. Since the hand-held scanners are portable, patients can be scanned at clinics in rural areas. The scan data can then be sent to central laboratories where the prosthesis can be produced and sent to the patient.

The three DICOM translation packages investigated in the study showed that the open-source software (Invesalius®) performed well compared to the commercial software (Materialise® Magics®) commonly used in maxillofacial prosthetic fabrication. Using the open-source software can reduce the cost of fabricating these prostheses in centres already equipped with a CT scanner.

5.2 Future Work

In future works, the researcher would like to explore the role that digital sculpting can play in developing maxillofacial prosthetics, which will potentially entail working with actual maxillofacial

cases. Such research would possibly include an additional focus on developing a scanning protocol for digitally recording areas needing maxillofacial prosthetic applications using hand-held scanning equipment. In addition, such a study would also assess the scanning devices' ability to capture various colours and eventually skin tones as their capabilities are constantly improving and could help contribute to overall better prosthetic making.

References

Ablesw.com. 2021. *3D-DOCTOR, Medical Modelling, 3D Medical Imaging, News*. [online] Available at: <https://www.ablesw.com/3d-doctor/news.html> [Accessed 9 November 2021].

Alqutaibi, A.Y. 2015. Materials of facial prosthesis: History and advance, *International Journal of Contemporary Dental and Medical Reviews*, pp. 1–4. doi: 10.15713/ins.ijcdmr.90

Amorim, P. Moraes, T., Silva, J., & Pedrini, H. 2015. InVesalius: An Interactive Rendering Framework for Health Care Support, 2, pp. 45–54. doi: 10.1007/978-3-319-27857-5.

Alsiyabi, A.S. and Minsley, G.E. 2006. Facial Moulage Fabrication Using a Two-Stage Polyvinyl siloxane Impression, *Journal of Prosthodontics*, 15(3), pp. 195–197. doi: 10.1111/j.1532-849X.

Artec3D, 2017. *Artec Spider scanning device*. [image] Available at: www.artec3d.com [Accessed 9 November 2021].

Avis, N.J., Kleinermann, F. and Mcclure, J. 2004. Soft Tissue Surface Scanning – A Comparison of Commercial 3D Object Scanners for Surgical Simulation Content Creation and Medical Education Applications, *Springer*, pp. 211–220.

Bakshi, K.R. and Mulay, A.V. 2016. A Review on Selective Laser Sintering: A Rapid Prototyping Technology, *5th National Conference RDME*, pp. 53–57. Available at: http://www.iosrjournals.org/iosr-jmce/papers/Conf15008/Vol-4/53-57.pdf.

Bennimahadeo, P. and Maharajh, J., 2016. The prevalence of abnormal findings in screening CT brains performed on patients admitted with psychiatric symptoms. *South African Journal of Radiology*, 20(1).

Bocchialini, G., Ambrosi, S., Castellani, A., Negrini, S., Zanetti, U. and Rossi, A., 2018. Six Years of Experience in Treating Facial Trauma in the Province of Brescia, Italy. *Craniomaxillofacial Trauma & Reconstruction Open*, 2(1), pp.s-0038-1675216.

Brown, A., De Beer, D. and Conradie, P. 2014. Development of a stereolithography (STL) input and computer numerical control (CNC) output algorithm for an entry-level 3D printer, *South African Journal of Industrial Engineering*, 25(2), pp. 39–47. DOI: https://doi.org/10.7166/25-2-675

Canon, 2021. *Toshiba Aquilion LB CT scanner*. [image] Available at: <https://global.medical.canon/products/computed-tomography/aquilion-lb> [Accessed 9 November 2021].

Champaneria, M., Workman, A. and Gupta, S. 2016. Sushruta: Father of Plastic Surgery, *International Journal of Science and Research*, 5(3), pp. 663–668

Childs, T. and Juster, N. 1994. Linear and Geometric Accuracies from Layer Manufacturing, *Annals of CIRP*, 43(2), pp. 163–166.

Childs, T. and Juster, N., 1994. Test model by Childs for testing various AM processese. Available at: https://www.sciencedirect.com/science/article/abs/pii/S0007850607621878?via%3Dihub> [Accessed 9 November 2021].

Ciobanu, O. and Rotariu, M., 2014. Photogrammetric Scanning and Applications in Medicine. *Applied Mechanics and Materials*, 657, pp.579-583.

Cooke, A & Soons, J. 2010. Variability in the Geometric Accuracy of Additively Manufactured Test Parts, *21st Annual International Solid Freeform Fabrication Symposium*, pp. 1–12. Available at: https://www.researchgate.net/publication/268060887_Variability_in_the_Geometric_Accuracy_of_Additively_Manufactured_Test_Parts. [Accessed 9 November 2021].

Cooke, A. and Soons, J., 2010. *Circular diamond test model for determining accuracy of AM part*. [image] Available at: <https://www.nist.gov/publications/variability-geometric-accuracy-additively-manufactured-test-parts> [Accessed 9 November 2021].

Cruz, R., Ross, M., Skewes, J., Allenby, M., Powell, S., and Woodruff, M. 2020. An advanced prosthetic manufacturing framework for economic personalised ear prostheses, *Scientific Reports*. Nature Publishing Group UK, pp. 1–12. doi: 10.1038/s41598-020-67945-z.

Demir, N. Cevik, P., Okutan, Y., Ozturk, A., & Colpan, B. 2019. Case Report A different wax sculpture technique for implant - retained auricular prosthesis, *European Journal of Dentistry*, pp. 433–437. doi: 10.4103/1305-7456.

Demir, N., Cevik, P., Okutan, Y., Ozturk, N. and Colpan, B., 2015. *Sculpting of an ear prosthesis out of wax*. [image] Available at: <https://www.ncbi.nlm.nih.gov/pmc/articles/PMC4569999/> [Accessed 9 November 2021].

Dincă, L.L., Banu, A. and Vişan, A. 2017. Additive manufacturing in maxillofacial reconstruction, *MATEC Web of Conferences*, 137, p. 02001. doi: 10.1051/matecconf/201713702001.

Eder, M., Brockmann, G., Zimmermann, A., Papadopoulos, M., Schwenzer-zimmerer, K., Zeilhofer, H., Sader, R., Papadopulos, N., and Kovacs, L. 2012. Evaluation of Precision and Accuracy Assessment of Different 3-D Surface Imaging Systems for Biomedical Purposes, *Journal of Digital Imaging*, 26, pp. 163–172. doi: 10.1007/s10278-012-9487-1.

Ehman, E., Yu, L., Manduca, A., Hara, A., Shiung, M., Jondal, D., Lake, D., Paden, R., Blezek, D., Bruesewitz, M., McCollough, C., Hough, D., and Fletcher, J., 2014. Methods for Clinical Evaluation of Noise Reduction Techniques in Abdominopelvic CT, *Radiographics*, 34(4), pp. 849–862. doi: https://doi.org/10.1148/rg.344135128.

Electro Optical Systems, 2021. *EOSINT P385*. [image] Available at: <https://www.eos.info/en/additive-manufacturing/3d-printing-plastic/eos-polymer-systems> [Accessed 11 November 2021].

Ford, J.M. and Decker, S.J. 2016. Journal of Forensic Radiology and Imaging Computed tomography slice thickness and its effects on three-dimensional reconstruction of anatomical structures, *Journal of Forensic Radiology and Imaging*. Elsevier, 4, pp. 43–46. doi: 10.1016/j.jofri.2015.10.004.

Ge, Q., Li, Z., Wang, Z., Kowsari, K., Zhang, W., He, X., Zhou, J. and Fang, N., 2020. Projection micro stereolithography based 3D printing and its applications. *International Journal of Extreme Manufacturing*, 2(2), p.022004.

Geierlehner, A., Malferrari, S. and Kalaskar, D.M. 2019. The optimization of a 3D scanning technique applied for 3D printing of bespoke medical devices, *Journal of 3D Printing in Medicine*, 3(2), pp. 71–82. doi: https://doi.org/10.2217/3dp-2018-0026

Gesine, G., Stoevesandt, D., Reising, A., Kielstein, T., Hiss, M., and Kielstein, H. 2013. Imaging in anatomy: A comparison of imaging techniques in embalmed human cadavers, *BMC Medical Education*, 13(1), p. 1. doi: 10.1186/1472-6920-13-143.

Goldman, L.W. 2007. Principles of CT: Radiation Dose and Image Quality, *Journal of Nuclear Medicine Technology*, 35(4), pp. 213–226. doi: 10.2967/jnmt.106.037846.

Golubev, A., Bogatencov, P. and Secrieru, G., 2018. DICOM data processing optimization in medical information systems. *Scalable Computing: Practice and Experience*, 19(2), pp.189-201.

Groenewald, A. 2017. Design of a universal phantom for quality assurance in diagnostic radiology X-ray imaging, *Acta Radiologica*, (December), pp. 1523–1531. doi: 10.1177/028418511983168.

Groenewald, A., 2017. *The TQR CDR phantom*. [image] Available at: <https://www.researchgate.net/publication/328577692_Design_of_a_universal_phantom_for_quality_assurance_in_diagnostic_radiology_x-ray_imaging> [Accessed 9 November 2021].

Gülcan, O., Günaydın, K. and Tamer, A., 2021. The State of the Art of Material Jetting—A Critical Review. *Polymers*, 13(16), p.2829.

Hayden, M. and Nacher, P.J. 2016. History and physical principles of MRI, *Magnetic Resonance Imaging Handbook*, pp. 1–26.

He, Y., Xue, G. and Fu, J. 2014. Fabrication of low-cost soft tissue prostheses with the desktop 3D printer, *Scientific Reports*, 4, pp. 1–7. https://doi.org/10.1038/srep06973

Hobson, M., Soisson, E., *Davis, S., and Parker, W.* 2014. Using the ACR CT accreditation phantom for routine image quality assurance on both CT and CBCT imaging systems in a radiotherapy environment, *Journal of Applied Clinical Medical Physics*, 15(4), pp. 226–239

Hofmann, M., Harris, J., Hudson, S., and Mankoff, J. 2016. Helping Hands: Requirements for a Prototyping Methodology for Upper-limb Prosthetics Users, *Proceedings of the SIGCHI Conference on Human Factors in Computing Systems (CHI '16)*, pp. 1769–1780. doi: 10.1145/2858036.2858340.

Hobson, M., Soisson, E., Davis, S. and Parker, W. 2014. *ACR Phantom*. [image] Available at: <https://www.ncbi.nlm.nih.gov/pmc/articles/PMC5875525/> [Accessed 10 November 2021]

Jack, R. and Schyns, P., 2015. The Human Face as a Dynamic Tool for Social Communication. *Current Biology*, 25(14), pp. 621-634.

Kersten, T.P., Lindstaedt, M. and Starosta, D. 2018. Comparative geometrical accuracy investigations of hand-held 3D scanning systems – An update. Int. Arch. Photogramm. Remote Sens. Spatial Inf. Sci., XLII-2, pp. 487–494

Keys, J., Dempster, M., Jackson, J., Williams, M. and Coyle, S., 2021. The psychosocial impact of losing an eye through traumatic injury and living with prosthetic restoration: A thematic analysis. *Acta Psychologica*, 219, p.103383.

Krupinski, E. 2000. The importance of perception research in medical imaging., *Radiation medicine*, 18(3), pp. 329–334. Available at: http://citeseerx.ist.psu.edu/viewdoc/download?doi=10.1.1.114.1045&rep=rep1&type=pdf.

Kruth, J. 1991. Material Incress Manufacturing by Rapid Prototyping Techniques, *Annals of the CIRP*, 40, pp. 603–614.

Kruth, J., 1991. *Test model by Kurth for determining material increase during AM*. [image] Available at: <https://www.sciencedirect.com/science/article/abs/pii/S0007850607611366> [Accessed 9 November 2021].

Li, X., Wagner, M., Wu, X., Tarasov, P., Zhang, Y., Schmidt, A., Goslar, T., and Gresky, J. 2013. Archaeological and palaeopathological study on the third / second century BC grave from Turfan, China : Individual health history and regional implications, *Quaternary International*. Elsevier Ltd and INQUA, 290–291, pp. 335–343. doi: 10.1016/j.quaint.2012.05.010

Liravi, F. and Toyserkani, E. 2018. A hybrid additive manufacturing method for the fabrication of silicone bio-structures: 3D printing optimization and surface characterization, *Materials & Design*. Elsevier Ltd, 138, pp. 46–61. doi: 10.1016/j.matdes.2017.10.051.

Mahesh, M., Wong, Y., Fuh, J., and Loh, H. 2004. Benchmarking for comparative evaluation of RP systems and processes, *Rapid Prototyping Journal*, 10(2), pp. 123–135. doi: 10.1108/13552540410526999.

Malard, O., Lanhouet, J., Michel, G., Dreno, B., Espitalier, F., and Rio, E. 2015. Full-thickness nasal defect: Place of prosthetic reconstruction, *European Annals of Otorhinolaryngology, Head and Neck diseases*. Elsevier Masson SAS, 132(2), pp. 85–89. doi: 10.1016/j.anorl.2014.02.007.2006.00100.x.

Mduzana, L., Tiwari, R., Lieketseng, N. and Chikte, U., 2020. Exploring national human resource profile and trends of Prosthetists/Orthotists in South Africa from 2002 to 2018. *Global Health Action*, 13(1), p.1792192.

Mildenberger, P., Eichelberg, M. and Martin, E. 2002. Introduction to the DICOM standard, *European Radiology*, 12(4), pp. 920–927. doi: 10.1007/s003300101100.

Mothopi, M., Owen, C., Howes, D., and Naidoo, L. 2012. The need for versatility in the prosthodontic treatment of maxillofacial defects, *South African Dental Jornal*, 67(August), pp. 420–423. Available at: https://www.researchgate.net/profile/Christopher_Owen5/publication/255972406_The_need_for_versatility_in_the_prosthodontic_treatment_of_maxillofacial_defects/links/586b640a08ae6eb871bb451d/The-need-for-versatility-in-the-prosthodontic-treatment-of-maxillofacial-defects.pdf.

Moylan, S., Slotwinski, J., Cooke, A., Jurrens, K., & Donmez, A., 2014. An Additive Manufacturing Test Artifact, *Journal of Research of the National Institute of Standards and Technology*, 119, pp. 429–459. doi: http://dx.doi.org/10.6028/jres.119.017.

Mahesh, M., Wong, Y., Fuh, J. and Loh, H., 2004. *Test Model by Mahesh, Wong, Fuh and Loh for evaluating AM processes*. [image] Available at: <https://www.emerald.com/insight/content/doi/10.1108/13552540410526999/full/html> [Accessed 9 November 2021].

Mediso, 2017. *Mediso NanoScan micro-CT scanner*. [image] Available at: <https://mediso.com/global/en/product/pre-clinical-products/nanoscanr-petct> [Accessed 10 November 2021].

Mohammed, M., Cadd, B., Pearl, G. and Gibson, I. 2018. *Plaster mould for casting the prosthesis*. [image] Available at: <https://www.researchgate.net/publication/323754623_Augmented_patient-specific_facial_prosthesis_production_using_medical_imaging_modelling_and_3D_printing_technologies_for_improved_patient_outcomes> [Accessed 9 November 2021].

Moylan, S., Slotwinski, J., Cooke, A., Jurrens, K. and Donmez, A. 2014. *Test model by Moylan*. [image] Available at: <https://pubmed.ncbi.nlm.nih.gov/26601039/> [Accessed 9 November 2021].

Neel, S., Gibson, R., Daniels, C. and Klosterman, E. 1998. Dimensional Accuracy in X-Ray Computed Tomography Imaging, *Review of Progress in Quantitative Nondestructive Evaluation*, 17(937), pp. 411–418.

Neel, S., Gibson, R., Daniels, C. and Klosterman, E., 1998. *CT scanning test model*. [image] Available at: <https://link.springer.com/chapter/10.1007/978-1-4615-5339-7_52> [Accessed 9 November 2021].

Keys, J., Dempster, M., Jackson, J., Williams, M. and Coyle, S., 2021. The psychosocial impact of losing an eye through traumatic injury and living with prosthetic restoration: A thematic analysis. *Acta Psychologica*, 219, p.103383.

Ott, K., and Serlin, D. 2002. *Artificial Parts, Practical Lives: Modern Histories of Prosthetics*. NYU Press Available at: https://books.google.co.za/books/about/Artificial_Parts_Practical_Lives.html?id=cJm2qZw3CdAC&printsec=frontcover&source=kp_read_button&redir_esc=y#v=onepage&q&f=false.

Padmanabhan, T., Mohamed, K. and Parameswari, D. 2012. Prosthetic Rehabilitation of an Orbital and Facial Defect: A Clinical Report Prosthetic Rehabilitation of an Orbital and Facial Defect:, *Journal of Prosthodontics*, 21(August 2019), pp. 200–203. doi: 10.1111/j.1532-849X.2011.00817.x.*Prosthodontics*, (June 2012), pp. 561–567. doi: 10.1111/j.1532-849X.2012.00869.x.163231.

Prasad, K., Swaminathan, A. and Prasad, A. 2021. *Final prosthesis with pigments added*. [image] Available at: <https://www.researchgate.net/publication/340855701_Fabrication_of_a_Silicone_Auricular_Prosthesis_-_A_Case_Report> [Accessed 11 November 2021].

Porter, D., Cohen, A., Krueger, P., and Son, D. 2017. Additive Manufacturing Utilizing Stock Ultraviolet Curable Silicone, *Solid Freeform Fabrication Symposium*, pp. 1771–1783.

Prasad, K., Swaminathan, A. and Prasad, A. 2016. Fabrication of a Silicone Auricular Prosthesis – A Case Report, *Nitte University Journal of Health Science*, 6(1).

Ravuri, R., Tella, S. and Thola, K., Bheemalingeshwarrao., 2014. *Taking an impression using polyvinyl siloxane*. [image] Available at: <https://www.ncbi.nlm.nih.gov/pmc/articles/PMC3939511/> [Accessed 9 November 2021].

Riverside Imaging Specialists, 2021. *Example of DICOM image slices*. [image] Available at: <https://www.riversideimagingspecialists.com/mri-ct-scans/> [Accessed 9 November 2021].

Schmid, M., and Wegener, K. 2016. Additive manufacturing: polymers applicable for laser sintering (LS). *Procedia Engineering*, Vol.149, No.2016, pp.457-464.

Schramek, G., Stoevesandt, D., Reising, A., Kielstein, J., Hiss, M., and Kielstein, H. 2013. Imaging in anatomy: a comparison of imaging techniques in embalmed human cadavers, *BMC Medical Education*, 13(1), p. 1. doi: 10.1186/1472-6920-13-143.

Seminati, E., Talamas, D., Young, M., Twiste, M., Dhokia, V., and Bilzon, J. 2017. Validity and reliability of a novel 3D scanner for assessment of the shape and volume of amputees' residual limb models, *PLos One*, 12(9), pp. 1–16. doi: https://doi.org/10.1371/journal.pone.0184498.

Sercombe, T. and Hopkinson, N. 2006. Process Shrinkage and Accuracy during Indirect Laser Sintering of Aluminium, *Advanced Engineering Materials*, 8(4), pp. 260–264. doi: 10.1002/adem.200500265.

Secrombe A. and Hopkins, J. 2006. *Test model by Sercombe and Hopkins for determining shrinkage of aluminium during sintering*. [image] Available at:

<https://www.researchgate.net/publication/43454115_Process_Shrinkage_and_Accuracy_during_Indirect_Laser_Sintering_of_Aluminium> [Accessed 9 November 2021].

Sing, S., An, J., Yeong, W., and Wiria, F. 2016. Laser and electron-beam powder-bed additive manufacturing of metallic implants: A review on processes, materials and designs, *Journal of Orthopaedic Research*, 34(3), pp. 369–385. doi: 10.1002/jor.23075.

Taicher, S., Sela, M., Tubiana, L., and Peled, I. 1983. A technique for making a facial moulage under general anaesthesia, *THE JOURNAL OF PROSTHETIC DENTISTRY*, 50(5), pp. 677–680. doi: https://doi.org/10.1016/0022-3913(83)90209-3.

Ter-Pogossian, M. 1977. Basic Principles of Computed Axial Tomography, *Seminars in Nuclear Medicine*, 7(2), pp. 109–126.

Tetteh, S., Bibb, R. and Martin, S., 2017. Maxillofacial prostheses challenges in resource constrained regions. *Disability and Rehabilitation*, 41(3), pp.348-356.

Van Zyl, B., Barnard, M., Cloete, K., Fernandez, A., Mukosi, M. and Pitcher, R., 2021. Towards equity: a retrospective analysis of public sector radiological resources and utilization patterns in the metropolitan and rural areas of the Western Cape Province of South Africa in 2017. BMC Health ServicesResearch, 21(1).

Veerareddy, C., Nair, K.C. and Reddy, G.R. 2012. Simplified Technique for Orbital Prosthesis Fabrication: A Clinical Report, *Journal of Prosthodontics,* 21(7):561-8. doi: 10.1111/j.1532-849X.2012.00869.x

Unkovskiy, A., Spintzyk, S., Brom, J., Huettig, F., and Keutel, C. 2018. Direct 3D printing of silicone facial prostheses: A preliminary experience in digital work flow, *The Journal of Prosthetic Dentistry*. Editorial Council for the Journal of Prosthetic Dentistry, 120(2), pp. 303–308. doi: 10.1016/j.prosdent.2017.11.007.1038/srep06973.

Voros, S. 2009. What are the potential advantages and disadvantages of volumetric CT scanning?, *Journal of Cardiovascular Computed Tomography*. Mosby, Inc, 3(2), pp. 67–70. doi: 10.1016/j.jcct.2008.12.010.

Wang, J., Leng, S., Schmidt B., Allmendinger, T., Grant, K., Flohr, T. and McCollough, C. 2013. Electronic Noise in CT Detectors: Impact on Image, *American Journal of Roentgenology*, 201(4), pp. 626–632. doi: 10.2214/AJR.12.10234.

Wang, Y., Xu, Z., Wu, D., and Bai, J. 2020. Current status and prospects of polymer powder 3D printing technologies. *Materials*, Vol.13, No.10, pp.2406-2425.

Winkler, G., Aurich, V., Hahn, K., Martin, A. and Rodenacker, K., 1999. Noise Reduction in Images: Some Recent Edge-Preserving Methods. [online] pp.3-33. Available at: <https://www.researchgate.net/publication/33027830_Noise_Reduction_in_Images_Some_Recent_Edge-Preserving_Methods> [Accessed 10 November 2021].

Yadav, S. and Balakrishnan, D. 2017. CAD / CAM-Assisted Auricular Prosthesis Fabrication for a Quick, Precise, and More Retentive Outcome, *Journal of Prosthodontics*, pp. 1–6. doi: 10.1111/jopr.1258

Yadav, S.K. & Shrestha, S. 2017. A study on posttraumatic experience of road traffic accident afflicted maxillofacial trauma patient at tertiary hospital, Journal of Natural Science, Biology and Medicine, 8(1) ,pp 40–45.

Annexure A